STRUCTURE AND FUNCTION STUDIES OF VESICLE-ASSOCIATED MEMBRANE PROTEIN-ASSOCIATED PROTEIN B ASSOCIATED WITH AMYOTROPHIC LATERAL SCLEROSIS

Lua Shixiong

NATIONAL UNIVERSITY OF SINGAPORE

2011/2012

STRUCTURE AND FUNCTION STUDIES OF VESICLE-ASSOCIATED MEMBRANE PROTEIN-ASSOCIATED PROTEIN B ASSOCIATED WITH AMYOTROPHIC LATERAL SCLEROSIS

Lua Shixiong
B.Sc. (Hons.), NUS

A THESIS SUBMITTED FOR

THE DEGREE OF MASTER OF SCIENCE

DEPARTMENT OF BIOLOGICAL SCIENCES

NATIONAL UNIVERSITY OF SINGAPORE

2011/2012

ACKNOWLEDGMENTS

SUMMARY

The process of protein folding is remarkably efficient, but sometimes it can go wrong. This can have harmful consequences, as the incorrect folding of proteins is thought to be the cause of diseases. Amyotrophic lateral sclerosis 8 (ALS8) caused by the missense Thr46Ile and Pro56Ser mutation in the MSP domain of Vesicle-associated membrane protein-associated protein B (VAPB) is one example of such " misfolding diseases", and also the main focus of my research. In this thesis, the first structural investigation on both wild-type, Thr46Ile and Pro56Ser mutated MSP domains is presented.

The results revealed that the wild-type MSP domain is well-folded at neutral pH but can undergo acid-induced unfolding reversibly. It has thermodynamic stability energy (G^0_{N-U}) of 7.40kcal/mol and is also active in binding to a Nir2 peptide with a K_d of 0.65μM. Further determination of its crystal structure reveals that it adopts a seven-stranded immunoglobulin-like β sandwich.

By contrast, the Pro56Ser mutation renders the MSP domain to be insoluble in buffer. Nevertheless, as facilitated by the discovery that "insoluble proteins" can be solubilized in salt-free water (Li *et al*., 2006), we have successfully characterized the residue-specific conformation of the Pro56Ser mutant by CD and heteronuclear NMR spectroscopy. Surprisingly, the Pro56Ser mutant remains highly-unstructured under various conditions, lacking of tight tertiary packing and well-formed secondary structure, only with non-native helical conformation weakly-populated over the sequence. As such, the abolishment of native MSP structure consequently leads to aggregation and loss of functions under the physiological condition.

Unexpectedly, unlike the Pro56Ser MSP domain mutant, the Thr46Ile mutation did not eliminate the native secondary and tertiary structures, as demonstrated by its far-UV CD spectrum, as well as Cα and Cβ NMR chemical shifts. However, the Thr46Ile mutation did result in a reduced thermodynamic stability and loss of the cooperative urea-unfolding transition which consequently causes it to be prone to aggregation at high protein concentrations and temperatures *in vitro*. The same mutation also causes a 3 fold reduction in its ability to bind to the Nir2 peptide and significantly eliminate its ability to bind to EphA4. We have also provided evidence that the EphA4 and Nir2 peptide appear to have overlapped binding interfaces on the MSP domain, which strongly implies that two signalling networks may have a functional interplay *in vivo*.

Our study provides the first molecular basis for understanding the Pro56Ser and Thr46Ile ALS-causing mutations. We have also shown that by introducing additional Proline residues in the right context, the MSP domain could gain resistant to the Pro56Ser mutation. Lastly, we hypothesized that the interplay of two signalling networks mediated by the FFAT-containing proteins and Eph receptors respectively may play a key role in ALS pathogenesis.

TABLE OF CONTENTS

LIST OF TABLES

LIST OF FIGURES

NOTATIONS AND ABBREVAIATIONS

1, 8-ANS	1-anilinonaphthalene-8-sulfonic acid
1D/2D/3D	One-/Two-/Three-dimensional
ALS	Amyotrophic lateral sclerosis
BiP	Binding Ig protein
CCD	Coiled coil domain
cDNA	Complementary DNA
CD	Circular Dichroism
Da (kDa)	Dalton (kilodalton)
DNA	Deoxyribonucleic Acid
DTT	Dithiothreitol
dVAP	Drosophila VAP
E. coli	*Escherichia coli*
ER	Endoplasmic reticulum
Eph	Erythropoietin-producing hepatocellular carcinoma
FALS	Familiar ALS
FPLC	Fast Protein Liquid Chromatography
g/ mg /µg	Gram/Milligram/Microgram
GPI	Glycosylphosphatidylinositol
HSQC	Heteronuclear Single Quantum Coherence
hVAP	Human vesicle-associated membrane protein-associated protein
ITC	Isothermal titration calorimetry
IPTG	Isopropyl β-D-1-thiogalactopyranoside
l/ml/µl	Liter/Milliter/Microliter
LB	Luria Bertani
Min	Minute
M (mM)	Mole/L (Milimole/L)
MND	Motor neuron disease
MR	Molecular Replacement

MSP	Major Sperm Protein
MW	Molecular Weight
NMR	Nuclear Magnetic Resonance
NOE	Nuclear Overhauser Effect
PBS	Phosphate-buffered Saline
PCR	Polymerase Chain Reaction
PDB	Protein Data Bank
ppm	Parts Per Million
RP-HPLC	Reversed-Phase High Performance Liquid Chromatography
SALS	Sporadic ALS
SDS-PAGE	Sodium Dodecyl Sulfate Polyacrylamide Gel Eletrophoresis
SMA	Spinal muscular atrophy
TM	Transmembrane
TMD	TM domain
TFA	Trifluoroacetic acid
Tris	2-amino-2-hydroxymethyl-1,3-propanediol
UPR	Unfolded protein response
UPS	ubiquitin-proteasome system
VAMP	Vesiclee-associated membrane protein
VAP	VAMP-associated protein
VAPA/B/C	VAMP-associated protein A/B/C
VAPB-2	VAMP-associated protein B protein lacking exon 2
VAPB-4, 5	VAMP-associated protein B protein exons 4 and 5
VAPB-3	VAMP-associated protein B protein exon 3
VAPB-3, 4	VAMP-associated protein B protein exons 3 and 4
VCS	VAP consensus sequence
wt	wild-type

Chapter 1
Introduction

Proteins are polymers of amino acids. There are 20 different types of amino acids, and by controlling the order and the number in which they are assembled into a polypeptide chain, a vast array of different macromolecules can be efficiently constructed by a single type of factory in the cell, the ribosome, using information encoded within the DNA. In order to function, however, the synthesized polypeptide chain must fold into the three-dimensional shapes that are critical to their function, their native conformation. While it might take an eternity for the protein to explore the huge number of accessible conformations before finding the native state (Levinthal, 1968), most of the time, proteins can spontaneously seek out their native conformation (Anfinsen, 1973). Sometimes folding is also assisted or even made possible by cellular enzyme complexes called chaparones which protects the protein while it is folding. However, certain circumstances can also cause proteins to misfold or unfold leading to various diseases.

1.1 Protein folding diseases

As mentioned, proteins need its fold to be functional. So unsurprisingly diseases exist due to the inability of proteins to adopt, or remain in, it's native functional conformational state. Protein folding diseases can be divided into two groups: in the first, a small error in the genetic blueprint leads to incomplete folding of a protein, which affects its physiological function. This might, for instance, happen to p53, the malfunctioning of this central tumor suppressor could cause cancer. In the other, excessive quantities of wrongly folded or unfolded proteins aggregates, leading to proteinaceous deposits that are pathogenic features of the disease. Systems such as the unfolded protein response (UPR) and ubiquitin-proteasome complex are in place in the cell to target misfolded proteins for degradation and clearance. However these systems

maybe overwhelmed in the diseased state and the misfolded proteins accumulate as either extracellular deposits (eg. senile plaques in Alzheimer's disease) or intracellular inclusions (eg. Lewy bodies in Parkinson's disease). These deposits may be the direct cause of the particular pathology associated with the diseases or they may be inert "packages" designed to protect the cell from toxic insult.

In this thesis, I focused on two point mutations in the MSP domain of VAPB that result in a form of protein folding disease that are characterized by the specific death of nerves cells that control muscles. Several biophysical methods such as NMR, ITC and CD was routinely used to investigate the structural characteristics of the wild type MSP domain of VAPB and the assessment of the consequences of several key mutations. It is hope that the knowledge provided in this thesis would contribute to the understanding of the molecular mechanism underlying the mutation-causing disease.

1.2   What is Amyotrophic lateral sclerosis?

Amyotrophic lateral sclerosis (ALS) also known as Lou Gehrig's disease, motor neuron disease (MND) or Charcot's disease was first described by French neurologist Jean-Martin Charcot in 1869 (Meininger, 2011). It is the most common adult-onset motor neuron neurodegenerative disease characterized by the selective dysfunction and death of upper and lower motor neurons projecting from the brainstem, spinal cord, corticospinal tracts and primary motor cortex (Nassif *et al*., 2010). This lethal, progressive disorder causes patients to suffer from a spectrum of symptoms which includes muscle weakness, atrophy, paralysis and bulbar symptoms which eventually leads to death due to respiratory muscle failure.

1.2.1   Disease forms – Sporadic and Familiar ALS

ALS is divided into two forms, sporadic ALS (SALS) and familiar ALS (FALS). SALS constitute the majority of ALS cases and the disease occurs apparently at random with no clear associated risk factors. FALS patients on the other hand, carry an inheritable pathogenic gene mutation and make up 5 to 10% of the diseased population.

1.2.2   Genetic risk factors

Despite the difference in genetic components, both SALS and FALS cases are clinically indistinguishable and share the same pathological features (Chen *et al*., 2010). It is therefore thought that knowledge gained from studying the pathogenic genes identified in FALS patients may eventually elucidate the potential mechanisms that lead to the death of motor neurons in ALS and provide insights for an efficient treatment for both disease forms (Bruijn *et al*., 2004 and Pasinelli *et al*., 2006). To date, multiple genes that are causative or closely linked to the onset of FALS have been identified through genetic screening of FALS kindred. These genes include: *ang* on chromosome (Greenway *et al*., 2004 and Greenway *et al*., 2006), *sod1* on chromosome 2 (Rosen *et al*., 1993 and Shaw, 2005), *als2* on chromosome 2 (Hadano *et al*., 2001; Yang *et al*., *2001* Hadano *et al*., 2006), *setx* on chromosome 9 (Chen *et al*., 2004), *fus* on chromosome 16 (Kwiatkowski *et al*., 2009 and Vance *et al*., 2009), *vapb* on chromosome 20 (Nishimura *et al*., 2010; Chen *et al*., 2010 and Hamamoto *et al*., 2005), *tardbp* on chromosome 1 (Yokoseki *et al*., 2008; Sreedharan *et al*., 2008 and Kabashi *et al*., 2008), *chmp2b* on chromosome 3 (Momeni *et al*., 2006 and Parkinson *et al*., 2006) and *dctn1* on chromosome 2 (Puls *et al*., 2003 and Munch *et al*., 2004)   which encodes for Angiogenin, Cu/Zn superoxide dismutase 1, Alsin, Senataxin, Fused in sarcoma protein (FUS), VAMP (vesicle-associated membrane protein)-associated protein B (VAPB), TAR

DNA binding protein 43 (TDP-43), charged multi-vesicular body protein 2b, and dynactin 1 respectively (table 1).

1.2.3 Environment risk factors

Although several genetic risk factors have been identified to cause FALS, the cause of SALS remains largely unknown. Numerous researches have also focused on studying various aspects of our lifestyle that could possibly interact with genes to cause or contribute to SALS. A large number of environment risk factors have been studied in recent years and to name a few, these includes: exposure to agricultural chemicals or contact with animals linked to agricultural work (Furby *et al*., 2010); pesticide exposure (Sutedja *et al*., 2009) and smoking (Armon, 2009). However, there is still insufficient evidence to implicate any environment risk factor as being responsible for the cause of SALS.

1.3 The human VAP (hVAP) family of proteins

The Vesicle-associated membrane protein (VAMP)-associated protein (VAP) family were initially identified as orthologues of VAP-33, a 33Kda protein in *Aplysia californica* through its ability to bind to the vesicle - soluble N-ethylmaleimide-sensitive factor attachment protein receptor (v-SNARE), VAMP1 and VAMP2, in a yeast two-hybrid screen (Skehel *et al*., 1995). The VAP family of proteins is highly conserved among Eukaryotics. Humans have two VAPs (hVAPs), VAPA and VAPB (Nishimura *et al*., 1999) and share ~60% sequence identity. Alternatively spliced variants of the VAPB gene exists and lacked specific exons of VAPB, i.e. exon 2 (VAPB-2), exons 4 and 5 (VAPB-4, 5), exon 3 (VAPB-3), and exons 3 and 4 (VAPB-3, 4) and exons 3 to 5 VAPC (Nishimura *et al*., 1999 and Nachreiner *et al*,., 2010).

Table 1
Main Genes linked to Familial ALS

Familial ALS type	MIM ID	Gene	Locus	Protein	Normal Function	Inheritance	Mutations	Cause sporadic ALS
ALS	105850	*ang*	14q11.2	Angiogenin	Involved in Angiogenesis and regulates protein synthesis	AD	6	Yes
ALS1	147450	*sod1*	21q22.1	Cu/Zn superoxide dismutase 1	Provides defense against oxygen toxicity	AD	> 120	Yes
ALS2	606352	*als2*	2q33	Alsin	Plays a role in intracellular endosomal trafficking	AR	10	No
ALS4	608465	*setx*	9q34	Senataxin	Involved in DNA repair and the production of RNA	AD	3	Probably not
ALS6	137070	*fus*	16p11.2	Fused in sarcoma protein (FUS)	DNA repair, regulation of transcription, RNA splicing	AR	18	Yes
ALS8	605704	*vapb*	20q13.3	Vesicle-associated membrane protein - associated protein B	Involved in lipid metabolism and transfer, unfolded protein response, hepatitis C virus replication	AD	2	No
ALS10	605078	*tardbp*	1p36.2	TAR DNA binding protein 43 (TDP-43)	Biogenesis of microRNA, exon skipping, regulation of transcription	AD	14	Yes
ALS-FTD	609512	*chmp2b*	3p11.2	Charged multi-vesicular body protein 2b	Involved in vesicles trafficking and formation of endocytic multi-vesicular bodies	AD	2	Not known
LMND	601143	*dctn1*	2p13	Dynactin 1	Axonal transport of vesicles and organelles	AD	6	Yes

AD = autosomal dominant; AR = autosomal recessive; LMND = lower motor neuron disease; FTD = frontotemporal lobe dementia.

1.3.1 Expression and subcellular localization

VAPA and VAPB are ubiquitously expressed in various mammalian tissues and organs (Weir *et al*., 1998; Nishimura *et al*., 1999 and Skehel *et al*., 2000), including the heart, placenta, lung, liver, skeletal muscle, and pancreas. Both hVAPs are also found in a wide range of intracellular membranes, including the Endoplasmic reticulum (ER) (Skehel *et al*, 2000), the Golgi, the ER–Golgi intermediate compartment (Soussan *et al*., 1999), recycling endosomes, tight junctions (Lapierre *et al*., 1999), the neuromuscular junctions (Pennetta *et al*., 2002), and the plasma membrane (Foster and Klip, 2000). Because of this broad distribution, the hVAP family of proteins is suggested to be involved in diverse cellular functions.

Other than VAPC, the expression of the alternative splice variants of the VAPB gene has never been demonstrated in mammalian tissues or organs. They were, however, detected by Nachreiner *et al*., (2010) only at the mRNA level in various tissues of the nervous system such as the muscle, cerebellum, cortex and spinal cord. In *vitro,* two of the variants (VAPB-2 and VAPB-4, 5) were detectable on the protein level in transfected over expressing 293 cells. Two other variants (VAPB-3 and VAPB-3, 4) became detectable only after inhibition of the ubiquitin/proteasomal pathway, a condition commonly found in neurodegenerative diseases such as Alzheimer's disease and Parkinson's disease (Hoozemans *et al*., 2006). The expression of VAPB-2, 3, 4 was never detected in *vitro*. It was then hypothesized that these splice variants of VAPB might become highly expressed under pathological conditions and contribute to ALS pathogenicity as with other splice variants of ALS-associated proteins such as SOD1 (Hirano *et al*, 2000) or the glutamate transporter EAAT2 (Honig *et al*., 2000).

The tissue distribution of VAPC remains largely unknown but kukihara *et al*., (2009) had shown through immunoblotting of pool lysates of various organs prepared from several people that several bands detected by Anti-VAPC antibody despite being smaller than the expected size of VAPC were observed in the stomach, duodenum, small intestine, uterus, vagina, prostate, and bladder. However, VAPC was not detected in liver tissues in which the Hepatitis C Virus replicates.

1.3.2 Domains of hVAPs

The hVAP proteins are composed of three conserved domains, namely an N-terminal Major Sperm Protein (MSP) domain, a central coiled-coil domain, and a C-terminal transmembrane (TM) domain (Figure 1a).

1.3.2.1 The MSP domain

The hVAPs possess an amino (N)-terminal, cytoplasmic facing domain of about 125 residues. It was named the MSP domain because of its similarity (22% sequence identity) with the nematode major sperm protein (MSP), a protein that mediates the amoeba-like crawling motion in nematode sperms by forming an extensive fibrous network at the leading edge of the sperm's pseudopod. The MSP and VAP MSP domain share an evolutionary conserved immunoglobulin-like seven-stranded β sheet domain fold (Baker *et al*., 2002 and Kaiser *et al*., 2005) but unlike VAPs, the MSP does not contain a coiled-coil motif or a transmembrane domain. Thus, the VAP MSP domain, like the MSP may function to facilitate the oligomerisation of VAPs. Indeed, Haaf *et al*., (1998) had demonstrated that the MSP dimerizes spontaneously in solution. In *vivo*, the MSP dimer form helical long chains which further associate with each other to form filaments, which in turn forms supercoils to produce bundles. But contrary to the

proposed function of VAPs MSP domain, the isolated VAPA MSP domain remains monomeric (Kaiser *et al*., 2005). Kim *et al*., (2010) also further provided clear evidences that the MSP domain of VAPB does not contribute to VAPB oligomerisation.

The hVAP MSP domain also harbors a particularly conserved 16 amino acid segment – the VAP consensus sequence (VCS) (Nishimura *at al*., 1999) (figure 1b). It is also interesting to note that while most VAPs have three prolines within the VCS, VAPB and a nematode VAP, VPR-1, have only two prolines in this region. The distribution of the Proline residues in the VCS as proposed by Nakamichi *et al*., (2011) is critical for the proper MSP structure, and hence any alterations will affect the cellular localization, substrate specificity and ultimately the function of VAPs. The Pro56Ser mutation on VAPB which causes ALS8 leaves only a single Proline residue within the VCS. Based on this hypothesis, Nakamichi *et al*., (2011) further showed that when Scs2p and VAPA were mutated to be similar to VAPB (P56S) leaving only a single Proline in the VCS region, Scs2p became inactive and aggregated, and VAPA became localized to membranous aggregates indistinguishable from those induced by VAPB (P56S). However contrary to the believe that the inclusion of an additional Proline at position 63 of VAPB will render it resistance to the Pro56Ser alike VAPA (P56S), the localization of VAPB (P56S, A63P) was similar to that of VAPB (P56S) and different from that of VAPA (P56S). Henceforth, this suggests that another factor(s) other than the distribution or three Proline residues in the VCS is required for proper cellular localization of VAPB.

Interestingly, the VCS was lacking in the splice variants VAPB-2 and VAPB-2,3,4 due to the loss of exon 2. The other spice variants VAPC, VAPB-3, VAPB-3,4 and VAPB-4,5 on the other hand contain the Pro56 residue that is mutated to a Serine residue in

ALS8 patients despite having a reorganized MSP domain. This thus indicates a relevance of these splice variants to ALS8 as they can also contribute to pathogenesis due to the inability to interact with FFAT-motif containing protein or because of the pathogenic P56S mutation.

1.3.2.2   The coiled coil domain

The hVAPs also possesses a variable central coiled coil domain (CCD) of ~50 amino acids that resembles the CCD repertoire found in VAMPs and other SNARE proteins (Nishimura *et al*., 1999). By using chemical cross-linking and co-immunoprecipitation experiments, Kim *et al*., (2010) had shown that the deletion of the CCD domain from the wild type VAPB abolished dimerization of VAPB without affecting its ability to interact with the FFAT motif-containing protein Nir2. This has provided clear evidences that CCD is critical for VAPB oligomerisation.

1.3.2.3   The TM domain

Finally, the hVAPs possess a single carboxyl (C)-terminal hydrophobic stretch which anchors the hVAPs to the Endoplasmic reticulum (ER) membrane. This membrane topology defines the VAPs as C-tail-anchored (C-TA) protein (Borgese *et al*, 2007). As seen in figure 1c, the TM domain (TMD) contains a GXXXG motif and is recognized as a "dimerization motif," which mediates the assembly of two TM helices (Brosig *et al*, 1998; Russ *et al*, 2000 and Senes *et al*, 2004). Indeed, Nishimura, *et al* (1999) had demonstrated that the VAPB undergoes homo- dimerization with itself and also hetero-dimerization with VAPA, VAMP1 and VAMP2 through the TM domain. In another study, Kim *et al.,* (2010) further showed that by replacing the two glycines in the "dimerization motif" with isoleucine, the dimerization of TM helices is abolished but has no effect on

the oligomerization of full length VAPB. Henceforth, the GXXXG motif contributes only

to the oligomerisation of the TM domain but not of the full length protein.
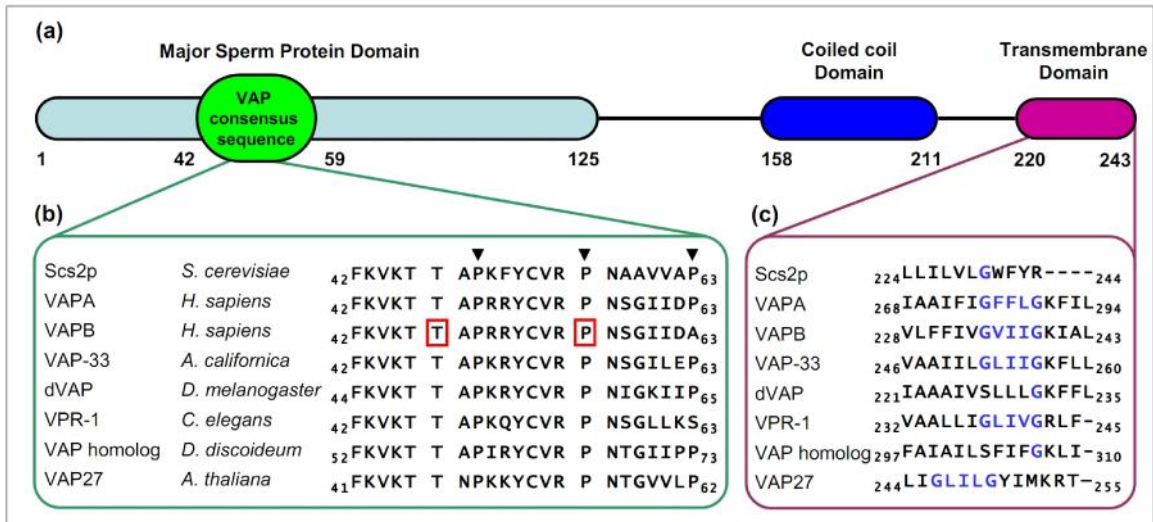
Figure 1. Primary organization of VAP homologues. (a) Domain organization of VAPs. All VAP homologues consist of an N-terminal major sperm protein (MSP) domain which contains the VAP consensus sequence (amino acid residue 42 to 59); a C-terminal transmembrane domain (TMD) and a predicted coiled-coil domain (CCD) which resembles the CCD of numerous SNARE proteins. (B) Alignment of amino acid sequences around the VCS of VAPs. Protein sequence positions are presented according to the human VAPB protein. The 3 conserved Proline residues in the VCS are indicated by closed triangles. The conserved Proline residue (boxed) at position 56 and Threonine residue (boxed) at position 46 of human VAPB is substituted by a Serine and Isoleucine residue respectively in ALS8. (c) Alignment of amino acid sequences around the TMD of VAPs. The GXXXG (blue) motif which mediates the assembly of two TM helices is shown. The database accession numbers: Scs2p (*Saccharomyces cerevisiae*), BBA07936; VAPA (*Homo sapiens*), NP_003565; VAPB (*Homo sapiens*), NP_004729; VAP-33 (*Aplysia calfornica*), Q16943; dVAP33A (*Drosophila melanogaster*), NP_996348; VPR-1 (*Caenorhabditis elegans*), NP_491704; VAP homolog (*Dictyostelium discoideum*), XP_641953; VAP27 (*Arabidopsis thaliana*), NP_567101.

1.3.3   Cellular functions of hVAPs

The VAPs interacts with a plethora of other proteins and their known interactors are

summarized in Table 2 (taken and modified from (Lev *et al*., 2008). The array of

interactions is diverse and broad, henceforth in this chapter; I will focus only on the

cellular functions of hVAPs that might have a relation to ALS pathogenesis.

1.3.3.1   Interactions with FFAT-motif containing proteins.

The hVAP proteins have been shown to interact with proteins carrying a short motif

consisting of two phenylalanines in an acidic tract (Wyles *et al*., 2002, Wyles and

Ridgway, 2004). This short motif is termed the FFAT motif and corresponds to the

consensus sequence EFFDAxE. Through the FFAT motif, hVAPs interact with a

multitude of lipid-binding, lipid sensing or lipid-transport proteins (Table 2) and mediates the transfer of lipids between the ER and other organelles, such as the Golgi, endosomes, and plasma membrane (Olkkonen, 2004; Holthuis and Levine, 2005; Levine and Loewen, 2006; Kawano *et al*., 2006; Perry and Ridgway, 2006). The hVAPs also interact with intracellular proteins (Wyles *et al*., 2002 and *Weir et al*., 2001) including Nir1, Nir2, and Nir3 via the FFAT motif which differentially affects the organization of the ER (Amarilio *et al*., 2005). The hVAPs also interact with the ceramide transporter CERT via the FFAT motif and target it to the Golgi apparatus (Hanada *et al*., 2007, Kawano et al., 2006). CERT mediates the transport of Ceramide from the ER where it was synthesized to the Golgi where it is being converted to sphingomyelin, a major component of cellular membranes.

The FFAT motif interacts with VAPs via a highly conserved region in the N-terminal MSP domain. Co-crystallization of rat VAPA MSP domain and rat ORP1 fragment containing the FFAT motif (EFYDALS) revealed a 2:2 complex (PDB ID: 1Z90) in which the FFAT motif binds to a positive surface of VAPA (Kaiser *et al*., 2005). The crystal complex together with mutagenic screens (Loewen *et al*., 2005 and Kaiser *et al*., 2005) on hVAPs revealed several key residues which are crucial for FFAT binding: Lys45, Thr47, Lys87, Met89 and Lys118. Most recently, Furuita *et al*., (2010) also revealed the NMR solution structure (PDB: 2RR3) of human VAPA MSP domain and a FFAT motif (EFFDAPE) containing fragment of OSBP in a 1:1 complex.

Table 2
VAP interacting proteins

Interacting protein	VAP protein	Interacting domain	References
SNAREs			
VAMP	aVAP33	-	(Skehel *et al.*, 1995)
VAMP-1	VAPA	MSPD, TMD	(Weir *et al.*, 1998, 2001)
VAMP-2	VAPA	-	(Weir *et al.*, 2001)
Syntaxin 1A	VAPA	-	(Weir *et al.*, 2001)
bet1	VAPA	-	(Weir *et al.*, 2001)
sec22	VAPA	-	(Weir *et al.*, 2001)
αSNAP	VAPA	-	(Weir *et al.*, 2001)
NSF	VAPA	-	(Weir *et al.*, 2001)
Viral Proteins			
P48 Norwalk virus non-structural protein	VAPA	-	(Ettayebi and Hardy, 2003)
HCV NS5A	VAPB	CCD	(Hamamoto *et al.*, 2005)
HCV NS5A	VAPA	CCD, TMD	(Tu *et al.*, 1999)
HCV NS5B	VAPA	MSP	(Hamamoto *et al.*, 2005 and Tu *et al.*, 1999)
60K cowpea mosaic virus	VAP27	CCD	(Carette *et al.*, 2002)
FFAT- motif containing Protein (FFAT motif: EFFDAxE)			
Opi1p	SCS2p	MSP	Loewen *et al.*,2003, 2005)
Osh1, Osh2, Osh3	SCS2p	-	(Loewen *et al.*, 2003)
OSBP	VAPA	MSP	(Wyles *et al.*, 2002 and Furita *et al.*, 2010)
ORP1-4, 6, 7, 9	VAPA, VAPB	-	(Wyles and Ridgway, 2004)
CERT	VAPA, VAPB	-	(Kawano *et al.*, 2006)
Nir1, Nir2, Nir3	VAPA, VAPB	-	(Amarilio *et al.*, 2005)
Other proteins			
VAPA, VAPB	VAPA, VAPB	CCD > TMD > MSP	(Nishimura *et al.*, 1999 and kim *et al.*, 2009)
Occludin	VAPA	-	(Lapierre *et al.*, 1999)
Insig1, Insig2	VAPA, VAPB	-	(Gong *et al.*, 2006)
Tubulin	dVAP33	-	(Pennetta *et al.*, 2002
PRA2	VAPA	-	(Gougeon and Ngsee, 2005)
PP2Cε	VAPA	TMD	(Saito *et al.*, 2008)
Stt4p, Fks1p, Num1p, Rpn10p, YGR086Cp	SCS2p	-	(Gavin *et al.*, 2002)

MSP = Major sperm protein domain, CCD = Coiled coil domain, TMD = Transmembrane domain

1.3.3.2 Involvement of VAPB in the Unfolded Protein Response

1.3.3.2.1 The Unfolded Protein Response (UPR)

The endoplasmic reticulum (ER) is a reticular membranous network throughout the cytoplasm of eukaryotic cells in which proteins are synthesized and post-translationally modified for proper folding and function. However, not all newly synthesized proteins are folded correctly and the percentage of misfolded protein was estimated to be at 30% in normal cells (Schubert *et al*., 2000). With the help of ER chaperones such as Binding Ig protein (BiP), a fraction of these misfolded proteins are refolded to have correct structures, whereas the rest remain misfolded and accumulate in the ER lumen. This causes ER stress (Ellgaard *et al*., 1999) that alerted the ER-resident stress sensors which transduce the signals from the ER lumen to trigger an adaptive self-defense response called the unfolding protein response (UPR) to decrease the load of misfolded proteins. In addition to the UPR, the ubiquitin–proteasome systems (Werner *et al*., 1996) also play a role to reduce the stress on ER, by degrading misfolded proteins that are transported to the cytosol via the translocon.

In mammals, there are three main types of ER-resident stress sensors, IRE1 (a transmembrane serine/threonine kinase and an endoribonuclease), PERK (an ER-resident type I transmembrane protein kinase) and ATF6 (an ER-localized leucine zipper transcription factor) (Kohno 2007). Under the normal conditions, the ER luminal domains of these sensor proteins and of the ER chaperone, BiP associates to keep the sensor proteins inactive. Once ER stress occurs, BiP dissociates from the sensor proteins to be engaged in refolding the accumulated misfolded protein. The sensor proteins are then freed and are activated to initiate the UPR by regulating a number of pathways.

After dissociation from BiP, free IRE1 oligomerize and autophosphorylate, which results in its activation (Bertolotti *et al*., 2000). Under normal ER stress condition, the activated IRE1 initiates splicing of XBP1 mRNA to generate an active XBP1 which work as a transcription factor to upregulate the expression of ER chaperons such as BiP and GRP94. The increased level of ER chaperone caused refolding (Harding *et al*., 2000) of accumulated misfolded proteins in ER. Under a severe ER stress condition, the activated IRE1 interacts with TRAF2 and activates an apoptosis-stimulating kinase 1 (ASK1)/c-*jun* N-terminal kinase (JNK) cascade that triggers apoptosis (Urano *et al*., 2000).

PERK (PKR-like ER protein kinase) also oligomerize, autophosphorylate and become activated after dissociation from BiP (Bertolotti *et al*., 2000). Activated PERK phosphorylates and inactivates eukaryotic translation-initiation factor 2α (eIF2α) to suppress global protein translation thereby reducing the load on the ER (Harding *et al*., 1999). In addition, phosphorylated eIF2α also enhances translation of ATF4 (Harding *et al*., 1999 and Vattem *et al*., 2004) which in turn upregulates the expression of key genes important for recovery from ER stress. Under a severe ER stress condition, expression of apoptosis-related transcription factor, CHOP (Zinszner *et al*., 1998) is also induced via the PERK pathway.

Unlike IRE1 and PERK which autophosphorylates upon dissociation from BiP, ATF6 (activating transcription factor 6) translocates to the Golgi apparatus and is cleaved by site 1 protease (S1P) and site 2 protease (S2P). This result in the release of its cytoplasmic basic leucine zipper (bZIP) domain from the membrane and its translocation to the nucleus where it functions as a transcriptional factor to activate genes encoding molecular chaperones and proteins involved in ER-associated degradation (Ye *et al*.,

2000).

Some cells are particularly sensitive to ER stress such as the neurons cells (Oyadomari and Mori., 2004) which has a large cell body with slow/no turnover and pancreatic β cells (Lipson *et al*., 2006) which are actively producing secretary proteins and. Through these well-organized self-defense systems, cells try to escape from ER stress. Unfortunately there is a limit to this homeostatic response and in several cellular conditions such as an elevated demand for protein secretion (Lipson *et al*., 2006 and Gass *et al*., 2002); presence of pathogenic missense mutations (Bartoszewski *et al*., 2008 and Ito *et al*., 2009); viral infection (Isler *et al*., 2005) and deprivation of nutrient/oxygen (Lee, 1992 and Feldman *et al*., 2005), protein misfolding are enhanced and/or UPR are misregulated, resulting in an overwhelming ER stress that results in the fatal outcome of cells.

1.3.3.2.2 VAPB is involved in the activation of UPR

Kanekura *et al*., (2006) had demonstrated that over expression of wild-type (wt)-hVAPs (VAPA and VAPB) but not other synaptic vesicular proteins, VAMP1 or VAMP2 induces the IRE1-mediated XBP1 splicing reaction which activates UPR. Also, by reducing the level of endogenous VAPB using small interfering RNA, the group provided further evidences that activation of UPR due to ER stress caused by DTT or thapsigargin can be attenuated. In addition, Suzuki *et al*., (2009) also showed that VAPB mutants (K87D/M89D-VAPB and T46A/T47A-VAPB) that localize normally to the ER like wt-VAPB but do not interact with FFAT motif-containing protein are unable to trigger UPR as well. In another experiment, Suzuki *et al*., (2009) further showed that VAPB mutants with a truncated MSP domain or a deleted TM domain were also unable to trigger UPR.

Taken together, these observations have suggested that the MSP domain of wt-VAPB with proper ER localization and maybe a FFAT motif-containing protein is physiologically involved in activation of the IRE1/XBP1 signaling pathway. The involvement of VAPB on UPR was also confirmed by Chen *at al*., (2010).

VAPB is also involved in the ATF6 dependent pathway of UPR by interacting directly with the ER-localized transcription factor ATF6 via its cytosolic MSP domain. But in contrast to the study by Kanekura *et al*., (2006) showing that VAPB is a positive regulator of UPR, Gkogkas *et al*., (2008) in their studies established that over expression of VAPB attenuates the activity of ATF6, and reducing VAPB levels enhance ATF6-dependent transcription.

The involvement of VAPB in the PERK pathway of UPR was also investigated by Chen *at al*., (2010). However, phosphorylation of eIF2α was not significantly enhanced or reduced in cells over expressing VAPB.

In conclusion, the work by the three independent groups showed that VAPB could influence UPR by acting through the IRE1/XBP1 or the ATF6 pathway. Henceforth the effect of the ALS8 causing mutation − Pro56Ser and Thr46Ile on UPR is worthy of attention.

1.3.3.3 Interactions with Eph receptors.

The erythropoietin-producing hepatocellular carcinoma (Eph) receptors are transmembrane receptors tyrosine kinases that have been implicated in numerous cellular functions such as cell signaling and development. In the human genome there are nine EphA receptors, which promiscuously bind five glycosylphosphatidylinositol (GPI) linked ephrin-A ligands; and five EphB receptors, which promiscuously bind three

transmembrane ephrin-B ligands (Elena, 2010). Exceptions are the EphA4 and EphB2 receptors, which can also bind ephrin-Bs and ephrin-A5, respectively, and EphB4, which preferentially binds ephrin-B2 only (Elena, 2010).

Multiple Ephrins and Eph receptors including EphA4 and A7 are can be found throughout the adult nervous system and in skeletal muscle of vertebrate species (Iwamasa *et al*., 1999 and Lai *et al*., 2001). Eph receptors are implicated in the regulation of the survival of cultured spinal cord motor neurons (Magal *et al*., 1996) and influence proliferation and apoptosis in the adult mammalian CNS (Ricard *et al*., 2006)). Additionally, binding to Eph receptors expressed by neurons could stabilize synapses (Calò *et al*., 2006). Thus, it is possible that Eph receptors signaling in expressing cell might be crucial in mediating the susceptibility of motor neurons in ALS patients.

Indeed, in 2008, Tsuda *et al*., demonstrated that cleavage of the full length drosophila VAP (dVAP) releases the N-terminal MSP domain which although lack an N-terminal signal sequence, are secreted from cells by an as yet unidentified unconventional mechanism (Kosinski *et al*., 2005). This finding is further supported by an earlier study by Omenn *et al*., (2005) whom discovered the presence of hVAP MSP domain in the blood serum using mass spectrometry. Tsuda *et al*., (2008) also showed that the hVAP MSP domain is able to bind the extracellular ligand binding domain of EphA4 in a pull-down assay; and also competes with mouse EphrinB2 for EphA4. Their work revealed a testable novel pathway in which VAP fragments present in the blood serum may act as diffusible hormones for Eph receptors present on neuron cells and may be crucial for motor neuron survival or muscle functions.

1.4 ALS8-causing mutations in VAPB

A form of FALS classified as amyotrophic lateral sclerosis type 8 (ALS8) is caused by a mis-sense point mutation in the MSP domain of hVAPs. This disease-associated mutation first identified by Nishimura *et al*., (2004) substitutes a highly conserved Proline residue at position 56 with a Serine (P56S) in the VCS of VAPB. The same mutation was also identified in patients with different clinical courses, such as late-onset spinal muscular atrophy (SMA), and typical severe ALS with rapid progression (Nishimura *et al* 2005). Nevertheless, all of these neurodegenerative disorders are characterized by the death of motor neurons. A second disease-associated mutation also in the VCS of VAPB with similar effects substitutes a highly conserved Threonine residue at position 46 with an Isoleucine (T46I) has also recently been reported by Chen *et al*., (2010). It is believed that the P56S and T46I mutations have the same effect in ALS pathogenesis.

In 2008, two additional mutations in a non-conserved region of VAPB were also reported (Landers *et al*., 2008): D130E (aspartic acid to glutamic acid at position 130) and del160 (deletion of amino acid at position 160, which is a serine). However, the D130E mutant were found to be in the same ratio between ALS patients and healthy individuals by a study in southern Italy (Conforti *et al*., 2006) and therefore suggested that it might not be an ALS causative gene. Also the del160 mutant was an isolated case and is identified in only one individual of a family. Finally, both D130E and del160 mutants do not form cytoplasmic aggregates like the P56S and T46I mutant which further suggests that if they are causative genes for ALS8, they might act via a mechanism which may be distinctly different form P56S and T46I.

So far no diseases associated mutation has been identified in the VAPB

homologue, VAPA. Also, it has been demonstrated experimentally that while the P56S mutation dramatically influences the activity of VAPB, it does not have a significant effect on VAPA.

1.4.1 Functional consequences of mutations

To elucidate the possible mechanism that leads to ALS8, several groups had biochemically and biologically characterized ALS-linked VAPB (P56S), VAPA (P56S) and recently VAPB (T46I) by Chen *et al*., (2010) and compared with wt-hVAPs, and have found clear differences between them.

First of all, both VAPB (P56S) (Nishimura *et al*, 2004; Teuling *et al*, 2007 and Kanekura *et al*, 2006) and VAPB (T46I) (Chen *et al*, 2010) formed large membranous aggregates and causes ER structural change when expressed in cultured cells. In contrast, wt-hVAP and VAPA (P56S) showed a reticulated subcellular distribution, colocalized with ER. Both VAPB (P56S) and VAPB (T46I) mutants, unlike wt-hVAPs and VAPA (P56S) are also resistant to solubilisation in buffers containing nonionic detergents such as Triton X-100. In addition, the Triton X-100-insoluble VAPB mutants displayed a smeared ladder mobility when analyzed with SDS-PAGE. These observations of VAPB mutants together, suggested that P56S and T46I probably caused misfolding of wt-VAPB and triggered VAPB protein aggregation (Kanekura *et al*, 2006 and Chen *et al*, 2010).

Another distinct difference between wt-VAPB and the VAPB mutants is the ability to interact with FFAT motif-containing proteins. Using pull-down assays combined with mass spectrometry, Teuling *et al*., (2007) had demonstrated that this interaction is disrupted by the P56S mutation. The mechanism of which is elucidated by the work of Kim *et al*., (2010) whom demonstrated that P56S obstructs FFAT binding through

enhancing VAPB oligomerization and thus decreases accessibility to the VAPB binding domain. The disruption of FFAT to VAP interaction causes a dysfunction in lipid metabolism resulting in hyperlipidemia and increased cholesterol and triglyceride levels in ALS8 patients (Marques *et al*., 2006 and Dupuis *et al*., 2008). These data together suggest that VAPB (P56S) might manifest its pathogenicity because of its "loss of function" mutation.

Overexpression of wt-hVAPs and related mutants also yielded different effects on protein trafficking and further suggest that VAPB (P56S) might instead be a gain of function mutant. In their study, Prosser *et a*l., (2008) had experimentally shown that the transport of membrane proteins from the ER to the Golgi is inhibited by over-expressed wt-VAPA and VAPB (P56S) in CHO cells but not wt-VAPB. Additionally, they also showed that such inhibition can be alleviated by over expressing FFAT containing peptide. Intriguingly their studies also showed that the P56S aggregates could be dissolved by FFAT overexpression. This however was contrary to another similar study conducted by Teuling *et al*., (2007) which showed a lack of effect of FFAT containing peptides to dissolve the membranous aggregates. This may reflect differences in the FFAT constructs or the presence of a purification tag which might hinder interactions. Indeed the construct used by Prosser *et a*l., (2008) was a fragment from OSBP1 with a small Myc tag at the N-terminus while Teuling *et al*., (2007) used a FFAT containing fragment from Nir2 with a larger N-terminal GFP moiety. Since wt-VAPB has no effect on protein trafficking, VAPB (P56S) is thought to gain a novel negative function which could be rescued by the introduction of FFAT containing peptides.

In addition to such "loss or gain of function" phenotypes, VAPB (P56S) and VAPB

(T46I) also have a unique dominant negative effect. To begin with, it was observed that both VAPB (P56S) and VAPB (T46I) cause a redistribution of co-expressed wt-VAPB from its normal localization and traps it into VAPB inclusions in mammalian cells and *Drosophila* (Chai *et a*l., 2008; Tsuda *et a*l., 2008 and Chen *et al*., 2010) and prevent wt-VAPB from fulfilling its role in any cellular function. Intriguingly, such co-aggregating activity induced by the P56S mutation affects only VAPB but not VAPA and specifically occurs only when P56S-VAPB is co-expressed with wt-VAPB, but not VAPA, VAMP1, or VAMP2 (Kanekura *et al.* 2006). Later, Suzuki *et al*., (2009) further demonstrated that this specific co-aggregating property of VAPB (P56S) is due to the development of an aberrantly strong affinity for the MSP domain of wt-VAPB. In addition, the pathogenic effect due to the mis-sense mutation in the MSP domain of VAPB is not limited to cultured cells expressing them. In fact Chen *et al*., (2010) have shown that VAPB (T46I) expressing cells have the ability to affect cells in an unclear mechanism that, although not producing the mutant protein, they too become stressed and eventually undergo cell death. Collectively, these observations support the hypothesis that VAPB (P56S) specifically exerts a dominant-negative effect on co-expressed wt-VAPB or normal cells expressing wt-VAPB.

Another striking difference observed by Chen *et al*., (2010) is that ubiquitinated aggregates were abundant in both VAPB (P56S) and VAPB (T46I) expressing cells as compared to wt-VAPB-expressing cells. The group further went on to investigate this abnormality and discovered that the ubiquitin-proteasome system (UPS) was impaired by an unknown mechanism in cells expressing VAPB (T46I). Again, untransfected cells co-cultured with mutant VAPB transfected cells are also observed to be more likely to

contain ubiquitinated aggregates than controls. The way damaged cells expressing a pathogenic protein affect neighboring cells is intriguing and suggests that a non-cell-autonomous mechanism may play a role in the pathogenesis of the disease (Ilieva *et al*, 2009).

Additional lines of evidences which suggested the presence of a non-cell-autonomous mechanism at play comes from the work of Tsuda *et al*., (2008), Teuling *et al*. (2007) and Mitne-Neto *et al*., (2011). First, Tsuda *et al*., (2008) proposed that the P56S mutation inhibits the ability of the wt-VAPB MSP domain to be secreted and thus prevented its interaction with Eph receptors. Reduced signaling due to VAP-Eph interaction could also come from the down regulation of wt-VAPB expression. Indeed, it is reported that the level of wt-VAPB is significantly reduced in the spinal cord of SOD1 mutants and SALS patient (Teuling *et al*., 2007) and also motor neurons derived from induced pluripotent stem-cells of ALS8 patients (Mitne-Neto *et al*., (2011). It is therefore possible that such reduced signaling may be responsible for some non-autonomous defects leading to ALS pathogenesis. In contrast to the idea that MSP domain of wt-VAPB is secreted from cells, Chen *et al*., (2010) was unsuccessful in recovering any VAPB fragments from the culture medium. The group further suggests that wt-VAPB may be released within exosomes, as has been shown for the secretion of α-synuclein related to the pathology of Parkinson's disease (Emmanouilidou *et al*., 2010).

Finally, the ALS-associated T46I and P56S mutations in VAPB, also prevents wt-VAPB from fulfilling its role in UPR. This was demonstrated by Kanekura *et al*., (2006) and Chen *at al*., (2010) as they observed that the P56S and T46I mutations abolish the ability of wt-VAPB to trigger UPR via the IRE1/XBP1 pathway. Their finding is

consistent with the hypothesis that VAPB (P56S) and VAPB (T46I) is a loss-of-function and dominant-negative mutant. On the contrary, Gkogkas *et al*., (2008) had proposed that P56S-VAPB is instead a "toxic gain-of-function mutation. In his study, he has demonstrated that VAPB (P56S) has an enhanced inhibitory activity towards ATF6-dependent activation of UPR as compared to the wt-VAPB. Although further investigations are required, the malfunctioning of UPR caused by VAPB (P56S) and VAPB (T46I) is certainly worthy of attention.

In summary, we now have a plethora of knowledge about the pathogenic effects of the ALS-associated VAPB mutations. Based on these results, several models of diseases pathogenesis have been proposed and they can be broadly divided into three groups. First, the ALS-associated mutant inhibits the UPR-associated activity of wt-VAPB. Cells harboring the mutant thus become exposed to ER stress, making it vulnerable and thereby resulting in motor neuron degeneration. Secondly, the ALS-associated mutant disrupts the binding of wt-VAPB to FFAT-motif-containing proteins, leading to abnormal lipid transport and biosynthesis and, eventually, to slow motor neuron degeneration. Lastly, the ALS-associated mutant impaired the secretion or release of hVAP MSP domain or other factors triggered by VAPB respectively, to illicit a yet undetermined non-cell-autonomous defect which affects the viability of motor neurons due to decreases signaling by Eph receptors and other receptors. The motor neurons are especially vulnerable to VAPB mutations because wt-VAPB is highly expressed in the cell where it supports the high rate of lipid metabolism and transport that upkeep its exceptionally large size and complex morphology. Perhaps, all these proposed mechanisms and factors may also work in tandem to produce the key features of ALS pathology resulting in specific death of motor

neurons.

1.4.2 Structural consequences of mutations

The first examination of the effect of the P56S mutation on the structure of VAPB was done by Nishimura *et al*., (2004) using a 3D model of VAPB based on the nematode MSP dimer structure (PDB: 1MSP). As shown in figure 2, the Proline residue at position 56 of VAPB creates an S-shaped loop between two short stretches of β-strand and splits half of the β strands in VAPB into the top part of the β-sandwich and the other half of the β-strand into the bottom part. The P56S mutation is then proposed to disrupt the S-shaped loop to favor a new hydrogen-bond pattern that moves the short stretch of B stand that lies in the bottom half of the β sandwich to the opposite side. This misfolding of VAPB is thus proposed to cause the pathogenic effects observed.

Figure 2. VAPB models (taken from Nishimura *et al*., (2004) . The top part of the β sandwich is made of green β strands, and the bottom part is made of red strands. Wild type induces a kink and splits half of the strand into the top part of the sandwich (green) and the other half of the strand into the bottom part (red). The P56S mutation disrupts the hydrogen bonds between strands on the same sheet of the β sandwich, favoring new hydrogen bonds that move the bottom half to the opposite side of the β sandwich.
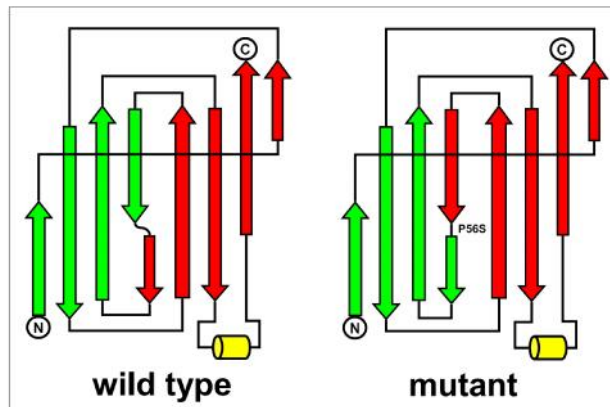
Furuita *et al*., (2010) had also inferred the effects of the P56S mutation on the MSP domain of VAPB from VAPA (P56S). As judged by the ^{1}H, ^{15}N HSQC spectra of P56S and wt-VAPA MSP domain, the structure of P56S VAPA was not observed to differ greatly from that of wt-VAPA. The author then suggested that since the MSP domain of VAPA and VAPB share 82% amino acid sequence identity, their structures are probably similar and hence the effects of the P56S mutation on the MSP domain of VAPA should

be similar on VAPB. Their work further supports the proposal by Nishimura *et al*., (2004) that the P56S mutation induces conformational changes within the MSP domain.

In a more direct examination, Kim *et al*., (2010) had utilized Far-UV CD spectroscopy and the fluorophore 1-anilinonaphthalene-8-sulfonic acid (1, 8-ANS) to probe for the effects of P56S on the MSP domain on VAPB. Their results indicated that the P56S mutation induces conformational changes within the MSP domain causing an exposure of hydrophobic patches that enhances the propensity of the mutated domain to oligomerize.

1.5 A challenge to study misfolded proteins

Possible treatment of misfolding diseases such as ALS could exploit detailed knowledge of protein folding and the prevention of abnormal folding. But it is particularly challenging to study these misfolded proteins experimentally due to their tendency to aggregate into amyloids. This is especially true for VAPB (P56S) which formed large membranous aggregate when are over expressed in cultured cells. Furthermore, these aggregates cannot be characterized in detail at the molecular level because they are not crystalline and are too large to be studied by solution NMR spectroscopy. The situation has improved dramatically as a result of recent progress in the application of solid-state NMR spectroscopy and of successes in growing nano- or microcrystals of small peptide fragments that have characteristics of amyloid fibrils yet is amenable to single crystal X-ray diffraction analysis. Also, with our recent discovery that "insoluble proteins" can be solubilized in salt-free water (Song, 2009) we have successfully for the first time, characterized the residue-specific conformation of VAPB(P56S) that caused Amyotrophic lateral sclerosis (ALS) by CD and heteronuclear

NMR spectroscopy.

1.6   Objectives

To fully understand the molecular mechanism underlying the VAPB mutation-causing ALS, one essential step is to structurally characterize the wild-type VAPB MSP domain, followed by the assessment of the consequence of the Pro56Ser and Thr46Ile mutation. Here I investigated the structure, thermodynamic stability, activity and has also used heteronuclear NMR spectroscopy to gain residue-specific conformational properties of wt-VAPB and its related T46I and P56S mutant. It is hoped that the results gathered in this study will provide a structural rationale on how the P56S mutation may lead to ALS8.

In this thesis, we also found a difference in the distribution of conserved prolines between VAPA and VAPB. Other than Pro-63 in the VCS of VAPA MSP domain which has been studied by Nakamichi *et al*., (2011), two other prolines at position 13 and 97 were also substituted in wt-VAPB. Here, I investigated whether the substitutions of Gln-13, Ala-63 and Thr-97 to a Proline residue affected the structural characteristics of VAPB (P56S). It is hoped that by having a deeper understanding of the effect of the different Proline mutation, we can better understand why VAPA but not VAPB is resistant to the P56S mutation.

Chapter 2

Methods and Materials

2.1 Cloning of the MSP domain of hVAPs

To obtain the gene which encodes for the MSP domain (residues 1−125) of hVAPs (VAPB and VAPA), 2 sets of primers (referring to table S1, VAPA and VAPA _ANTI; VAPB and VAPB _ANTI) were designed based on the sequence of the VAPA (GenBank: NM_003574.5) and VAPB gene (GenBank: NM_004738.4) The DNA fragment was then amplified from a HeLa cell cDNA library by performing a PCR reaction [95°C for 5 min, 30x (95°C for 30 sec, 55°C for 30sec, 72°C for 40sec) 72°C 10min, 4°C ∞].

The PCR product and a pET-32a vector (Novagen) were then double digested with the restriction enzymes, BamHI and Xho1 (New England Biolab) for 6hrs at 37°C and then gel purified using QIAquick gel extraction kit (QIAGEN), following the manufacturer's protocol. The digested PCR product containing the coding sequence of the MSP domain of hVAP was then ligated into the digested vector in an overnight reaction at 4°C using T4 DNA ligase (New England Biolab). By performing this cloning strategy, the MSP domain of hVAP was fused to an N-terminal 6x histidyl tag linked with a thrombin cleavage site (LVPRGS) both provided in frame by the pET-32a vector.

DH5-α *E.coli* (Novagen) competent cell was then transformed with the recombinant plasmids and plated onto LB plates with Ampicillin (Sigma). Single colonies were picked and grown overnight at 37°C in 3 ml of LB media with Ampicillin. Overnight cultures were centrifuged to harvest the bacterial cells and plasmids were subsequently isolated and purified with the GENEALL™ plasmid quick purification kit (General Biosystem). Plasmids were screened by double digestion using BamH1 and Xho1 and monitored in agarose electrophoresis gel. The entire nucleotide sequence of the

recombinant VAPB MSP domain gene was verified by sequencing. Sequencing results were analyzed with GeneRunner (Hastings Software, USA) and DNAMAN (Lynnon Corporation, Canada). Correct clones were transformed into BL21 (DE3) *E. coli* (Novagen) strain for expression.

2.2 Site directed mutagenesis

The point mutations: P12S, P56S, T46I, Q13P, A63P and T97P on MSP domain of VAPB and P56S on VAPA were synthesized according to the QuikChange site-directed mutagenesis kit (Stratagene). Briefly, two synthetic oligonucleotide primers (table S2) containing the desired mutation were designed using the QuikChange® Primer Design Program. A mutated plasmid containing the desired mutation is generated by performing a PCR reaction [95°C for 5 min, 12x (95°C for 30 sec, 55°C for 60sec, 68°C for 13min) 4°C ∞] using a high fidelity DNA polymerase.   Following temperature cycling, the 50ul reaction product is treated with 2 units of DpnI (New England Biolabs). The DpnI endonuclease (target sequence: 5´-Gm^6 ATC-3´) is specific for methylated and hemimethylated DNA and is used to digest the parental DNA template and to select for the mutant plasmid. Following digestion, the mutant plasmid containing the desired mutation is then transformed into DH5-α competent cell and plated onto LB plates with Ampicillin. Single colonies were picked and grown overnight at 37°C in 3 ml of LB media with Ampicillin. Overnight cultures were centrifuged to harvest the bacterial cells and plasmids were subsequently isolated and purified with the GENEALL™ plasmid quick purification kit (General Biosystem). The entire nucleotide sequence of the mutated VAPB MSP domain gene was verified by sequencing. Sequencing results were analyzed with GeneRunner (Hastings Software, USA) and DNAMAN (Lynnon Corporation,

Canada). Correct clones were transformed into BL21 (DE3) *E. coli* (Novagen) strain for expression.

2.3 Expression of recombinant protein

A single colony of *E.coli* BL21 (DE3) cells harboring the expression plasmid was grown overnight at 37°C with shaking in 5ml of LB medium containing Ampicillin (0.1 mg/ml). A 5ml aliquot of this culture was diluted into 1L of the same medium and grown at 37°C with shaking. When cell growth reaches the mid-log phase (OD_{600} of 0.6-0.8), expression from the T7promoter was induced by adding IPTG (Sigma) to a final concentration of 0.3mM. After growth was continued for another 16hrs at 20°C, cells were harvested by centrifugation at 6000 rpm for 30 min at 4°C. The cell pellet was frozen and kept at -20°C.

2.4 Extraction

The cell pellet from each 1L culture (2-3g wet weight) was thawed and resuspended in 30ml lysis buffer (150mM NaCl, 50mM NaH_2PO_4, pH 7.4) with one cØmplete protease inhibitor cocktail tablet (Roche) and sonicated on ice (Sonics VibraCell) at 30% amplitude for 10 min (pulse: 1" on and 1" off). The suspension was centrifuged at 18,000 rpm at 4°C for 20min. The supernatant containing soluble proteins and pellet representing the insoluble cell fraction was then appropriately used for subsequent purification or are discarded.

2.5 Purification under the native condition

The MSP domain of VAPB, EphA4 and the respective mutants of the MSP domains: VAPA (P56S), VAPB (T46I), VAPB (P56S, Q13P), VAPB (P56S, A63P), VAPB (P56S, T97P) and VAPB (P56S, Q13P, A63P, T97P) were purified under the

native condition. The supernatant representing the fraction of soluble recombinant proteins was first purified with immobilized metal affinity chromatography (IMAC). 30ml of the supernatant were applied onto 0.8ml (0.5ml for VAPB (T46I) and VAPA (P56S); and 0.2ml for VAPB (P56S, Q13P), VAPB (P56S, A63P), VAPB (P56S, T97P) and VAPB (P56S, Q13P, A63P, T97P) Ni^{2+}-NTA agarose (QIAGEN) equilibrated with equilibration buffer (150mM NaCl, 50mM NaH_2PO_4, pH 7.4). After the protein-Ni^{2+}-NTA mix was incubated for at least 1 hour with shaking at 4^oC, the slurry was poured into an empty column and the flow through was discarded.

For the MSP domain of VAPB, EphA4, VAPA (P56S) and VAPB (T46I), the column with the slurry was washed with 10 column volumes (CV) of wash buffer (150mM NaCl, 50mM NaH_2PO_4, 20mM Imidazole, pH 8.0) and 40 units of thrombin was subsequently added to achieve in-gel cleavage of the 6x Histidyl tag.

For VAPB (P56S, Q13P), VAPB (P56S, A63P), VAPB (P56S, T97P) and VAPB (P56S, Q13P, A63P, T97P), the column with the slurry was washed with 10 column volumes (CV) of wash buffer (150mM NaCl, 50mM NaH_2PO_4, 20mM Imidazole, pH 8.0) and eluted with 5 CV of elution buffer (150mM NaCl, 50mM NaH_2PO_4, 250mM Imidazole, pH 8.0).

Dithiothreitol (DTT) was subsequently added to the released recombinant protein to make up a final concentration of 100mM. DTT was not added to the released recombinant EphA4 protein.

Recombinant proteins were further purified by an AKTA fast protein liquid chromatography (FPLC) machine on a HiLoad™ 16/60 Superdex™ 200 prep grade Column. For purification of Recombinant EphA4, the gel filtration column was

equilibrated with PBS (300mM NaCl, 50mM NaH_2PO_4, pH 7.4). For the purification of all VAPB related recombinant protein, 20mM β-mercaptoethanol was additionally added to the equilibration buffer. The length of each run was 1.5CV. Fractions of 1ml were collected and each peak fraction was analyzed by SDS-PAGE. Recombinant proteins were pooled and concentrated using an Amicon Ultra-15 centrifugal filter device (Millipore) with a 5kDa cut off.

The samples at each purification step were collected and analyzed by SDS-PAGE with 4% stacking gel and 12% separating gel. The identities of all recombinant proteins were verified by MALDI-TOF mass spectrometry.

2.6   Purification under the denaturing condition

VAPB (P56S) and VAPB (P12S) were found in the inclusion body and hence purified under the denaturing condition. The pellet representing the fraction of insoluble recombinant proteins was first dissolved in the denaturing buffer (50mM NaH_2PO_4, 8M urea, pH 8.0) and enriched using 1ml of Ni^{2+}-NTA agarose equilibrated with denaturing buffer. After the protein-Ni^{2+}-NTA mix was incubated for at least 1 hour with shaking at room temperature, the slurry was poured into an empty column and the flow through was discarded. 10 column volumes (CV) of wash buffer (50mM NaH_2PO_4, 8M urea, 20mM Imidazole, pH 8.0) and eluted with 5 CV of elution buffer (50mM NaH_2PO_4, 8M urea, 250mM Imidazole, pH 8.0). 100mM of DTT was subsequently added to the eluted fraction before it was further purified by reverse-phase HPLC on a C4 column (Vydac).

Elution and separation was achieved using a gradient of 0.5% (v/v) /min of acetonitrile, containing 0.1% Trifluoroacetic acid (TFA) at a flow rate of 6ml/min. The chromatography was monitored at both 215nm and 280nm. All the peaks were collected

and lyophilized. The identities of all recombinant proteins purified by HPLC were also verified by MALDI-TOF mass spectrometry.

The Pro56Ser and Pro12Ser samples precipitated upon addition of thrombin, thus the 6x Histidyl tag was not removed.

2.7 Isotope labeling

The generation of the isotope-labeled proteins for NMR studies, followed a similar procedure except that the bacteria were grown in M9 medium (171.g/L Na_2HPO_4, 3g/L K_2HPO_4, 0.5g/L NaCl, 1g/L $(NH_4)_2SO_4$, 4g/L glucose, 1mM $MgSO_4$ 2mg/L Thiamine (VB1) and 75mg/L Amplicilin) with the addition of $(^{15}NH_4)_2SO_4$ for ^{15}N labeling and $(^{15}NH_4)_2SO_4/[^{13}C]$glucose for ^{15}N-/ ^{13}C-double labeling.

2.8 Purification of Peptides used in binding assay

The Nir2 peptide (EEEFFDAHE) was purchased from Genesis Biotech Inc. and further purified by HPLC on a reverse-phase C18 column (Vydac) before lyophilization. The powder of the peptide following lyophilization were weighed and then dissolved in 10 mm phosphate buffer. The pH was adjusted to pH 6.5 before it was used for binding studies.

2.9 Measurement of protein concentration

Protein concentrations were calculated with the extinction coefficient of the Tryptophan and Tyrosine residues. All VAPB related recombinant proteins have an Ext. coefficient of $8855cm^{-1}M^{-1}$(assuming ALL Cys residues appear as half cysteines). EphA4 has an Ext. coefficient of $32930cm^{-1}M^{-1}$ (assuming ALL Cys residues appear as half cysteines). With the absorbance at 280nm in the presence of 6M guanidine hydrochloride (Sigma) and the extinction coefficient, the protein concentration was

calculated with the formula A=ε*c*l [A= absorbance, ε=extinction coefficient ($M^{-1}cm^{-1}$), l =path length of cuvette (cm) and c= protein concentration (M)].

2.10 Circular Dichroism (CD) spectroscopy

The secondary structure of all the recombinant proteins were determined with a Far UV (190-260 nm) circular Dichroism (CD) of a 20μM protein solution in 10mM phosphate buffer, pH 6.5. Measurements were carried out in a Jasco J-810 spectropolarimeter (Jasco Corporation, Tokyo, Japan) at 25°C using 0.1 cm path length stoppered cuvettes. The spectra correspond to the average of three scans. Each scan was recorded using a scan speed of 50 nm /min, resolution 0.1nm, and band width 2nm. For data processing, the baseline was subtracted.

To study the effects of pH on the secondary structure of the recombinant proteins, far UV spectrums were collected in the pH range of 3.0 to 9.0. The pH was adjusted by addition of microliter amounts of dilute Hydrochloric acid or sodium hydroxide. For data processing, the spectrum was multiplied with a dilution factor that results from the additional volume during pH adjustments.

2.11 Urea unfolding

To measure the thermodynamic stability of the VAPB MSP domain and of its mutants, we varied the urea concentration from 0 to 8 M and monitored the change in the ellipticity at 222 nm of a 50uM protein sample by collecting a series of far-UV CD. The unfolding curve was constructed by plotting the ellipticity values at 222 nm versus the molar concentration of urea. By assuming a two-state unfolding process, the stability free energy (ΔG^{o}_{N-U}) was determined using the two equations (Gupta et al, 1996) below. The values of the Gibbs energy change (kcal mol-1) determined from the measurements were

plotted and analyzed using LEM, the linear free energy model.

$$\Delta G_{\text{N-U}} = -RT \ln \frac{y - y_{\text{N}}}{y_{\text{D}} - y}$$

Where:
R = molar gas constant 1.9858775 cal K^{-1} mol^{-1}
T = Temperature = 20°C + 273.15 = 293.15 K
y = measured optical property in a particular denaturing condition
y_{N} = optical properties of the protein in the fully <u>native</u> states under the same condition
y_{D} = optical properties of the protein in the fully <u>denatured</u> states under the same condition

$$\Delta G_{\text{N-U}} = \Delta G^0_{\text{N-U}} - m[\text{denaturant}]$$

Where:
m = the slope of the $\Delta G_{\text{N-U}}$ versus [denaturant] plot
$\Delta G^0_{\text{N-U}}$ = value of $\Delta G_{\text{N-U}}$ at [denaturant] = 0 M

2.12 ITC Characterization of Binding Activity

Isothermal titration calorimetry (ITC) experiments were performed using a Microcal VP-ITC machine. All titrations were conducted in 10mm phosphate buffer, pH 6.5, at 25 °C. All samples were degassed for 15 min to remove bubbles before the titrations to prevent the formation of bubbles. The Nir2 peptide was loaded into a 300ul syringe, while all recombinant VAPB related MSP protein was placed in a 1.8ml sample cell. The concentration of sample in the syringe is typically 20-fold that of the sample in the cell. To subtract the effects due to sample dilution, control experiments with the same parameter settings were also performed for the peptide and buffer. To obtain thermodynamic binding parameters, the titration data after subtraction of the blank values were fitted to a single-binding site model using the built-in software ORIGIN version 5.0 (Microcal Software Inc.).

2.13 NMR Spectroscopy

All NMR data were collected at 25 °C on an 800 MHz Bruker Avance spectrometer equipped with a shielded cryoprobe. For ^{1}H, ^{15}N HSQC characterization, the wild-type VAPB MSP sample and all related MSP mutants except P56S and P12S were prepared in 10 mM phosphate buffer (pH 6.5) with an addition of 10% D2O for the deuterium lock for the NMR spectrometers. In contrast, the Pro56Ser and Pro12Ser mutants were dissolved in salt-free water and 10% D20.

For achieving sequential assignments, triple-resonance experiments, including HNCACB, CBCA(CO)NH, and HNCO, were conducted for both wild-type, Pro56Ser and T46I MSP domains on doubly labeled samples at a protein concentration of 800μM (for wt-VAPB and P56S) and 300μM for T46I.

For NOE analysis, ^{15}N-edited HSQC-TOCSY and HSQC-NOESY spectra were recorded for the ^{15}N-labeled Pro56Ser mutant.

The ^{1}H chemical shift was referenced directly to 2,2-dimethyl-2-silapentanesulfonic acid (DSS), whereas the ^{15}N and ^{13}C chemical shifts were indirectly referenced to DSS (Wishart *et al*., 1995). The secondary structure mapping based on N, HN, CA, CB, CO, and HA chemical shifts were performed using DANGLE in CCPNMR (Vranken *et al*., 2005 and Cheung *et al*., 2010).

Chapter 3

Studies on the MSP domain of VAPB, VAPB (P56S) and VAPB (T46I)

3   Results

3.1   Studies on the wt-VAPB MSP domain

The wt-VAPB MSP domain (1-125) has been successfully cloned, expressed and purified the recombinant the using a prokaryotic system under the native condition. The purified wt-VAPB MSP domain is highly soluble in the buffer systems used. CD and NMR spectroscopy was utilized to study its structural properties.

3.1.1   Structural properties of the wt-VAPB MSP Domain

As shown in Figure 3a, at pH 6.5, the wt-VAPB MSP domain has a far-UV CD spectrum typical of a β-dominant secondary structure, with the maximal negative signal at ~218 nm and positive signal at ~199 nm. Upon lowering the pH value, the intensity of the positive signal at ~199 nm reduces gradually and eventually disappeared at pH 3.5. In addition, at pH 3.5, the maximal negative signal shifted from ~218 nm to ~212 nm, implying that the wt-VAPB MSP domain may be unfolded to some degree.

To gain detailed knowledge about the acid-induced unfolding, a series of two-dimensional ^{1}H-^{15}N HSQC spectra on the ^{15}N-labeled wt-VAPB MSP domain was collected with pH values varying from 6.5 to 2.5. Consistent with the CD results, at neutral pH the wild-type MSP domain has a HSQC spectrum typical of a well-folded protein (Figure 3b). When the pH was lowered down to 5.5 and 4.5, slight shifts of the HSQC peaks was observed (Figure 3c). This indicates that no large conformational change occurs which is also consistent with the CD results. However, upon lowering the pH value to 3.5, two sets of peaks can be observed in the HSQC spectrum (Figure 3d). One set of the HSQC peaks is very similar to those at pH 6.5 with very large spectral dispersions while another newly appeared set of peaks have a dramatically-reduced

dispersion which resembles that of an unfolded species. When the sample was further acidified, the intensity of the peaks from the unfolded population increased, and at pH 2.5 only the peaks set from the unfolded species could be observed. When the sample pH value was adjusted back to 6.5, the unfolded state could fold back to the well-folded state, indicating that the acid-induced unfolding is reversible for the wt-VAPB MSP domain.
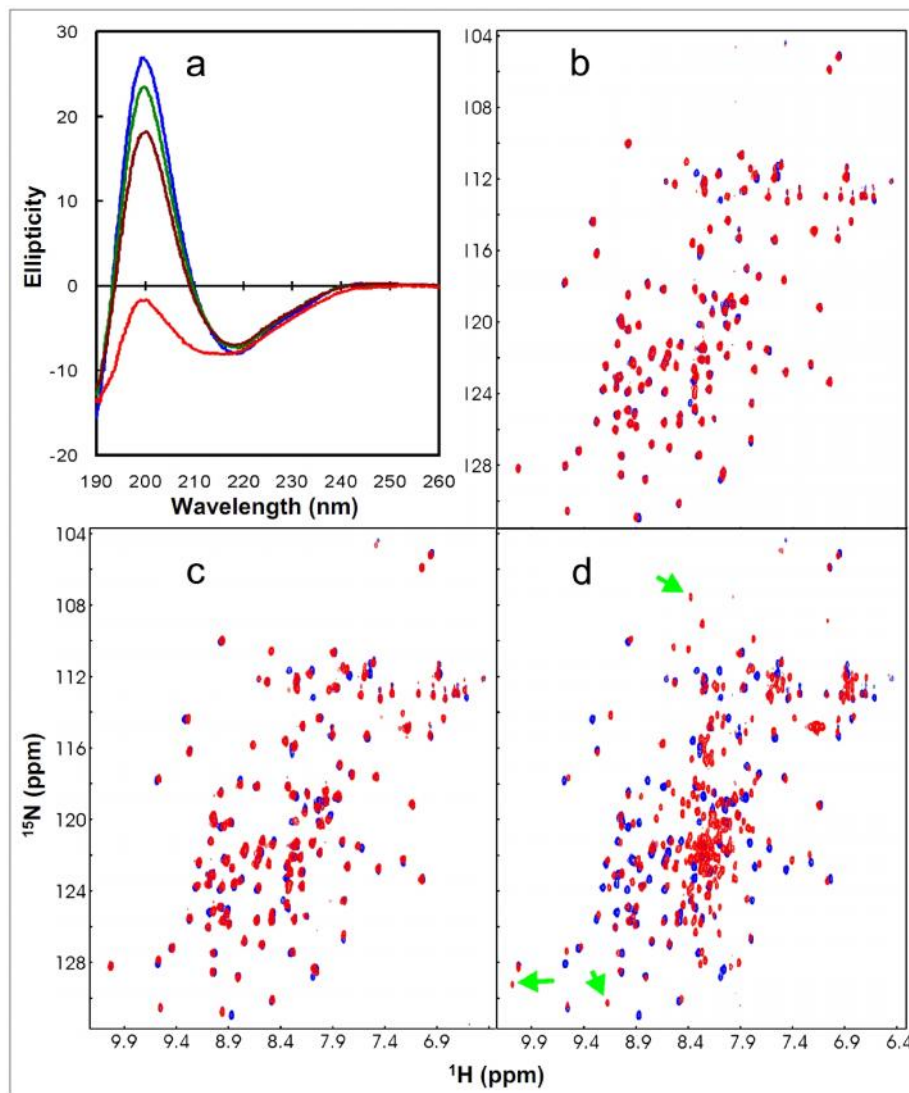
Figure 3. Structural characterization of the wild-type MSP domain
a. Far UV CD spectra of the wild-type MSP domain at a protein concentration of ~20 μM at pH 6.5 (blue), 5.5 (green), 4.5 (brown) and 3.5 (red). b. Superimposition of the two dimensional 1H-15N NMR HSQC spectra at a protein concentration of ~50 μM at pH 6.5 (blue) and 5.5 (red). c. Superimposition of the HSQC spectra at pH 6.5 (blue) and 4.5 (red). d. Superimposition of the HSQC spectra at pH 6.5 (blue) and 3.5 (red). Green arrows are used to indicate some HSQC peaks newly manifested at pH 3.5.

3.1.2   Stability of the wt-VAPB MSP Domain

Next, Dr Shi Jiahai had measured the thermodynamic stability energy by monitoring the ellipticity change at 222nm during urea-unfolding. As seen in Figure 4, the unfolding process appears highly cooperative, starting at the urea concentration of ~3.5 M and ending at ~5.1 M. Fitting of the unfolding data yields the free energy of the conformational stability (ΔG^0_{N-U}) to be 7.40 ± 0.41 kcal/mol. In general, thermodynamic stability energy for most proteins ranges from 5 to 20 kcal/mol under physiological conditions. This implies that the thermodynamic stability of the wild-type MSP domain is not very high.

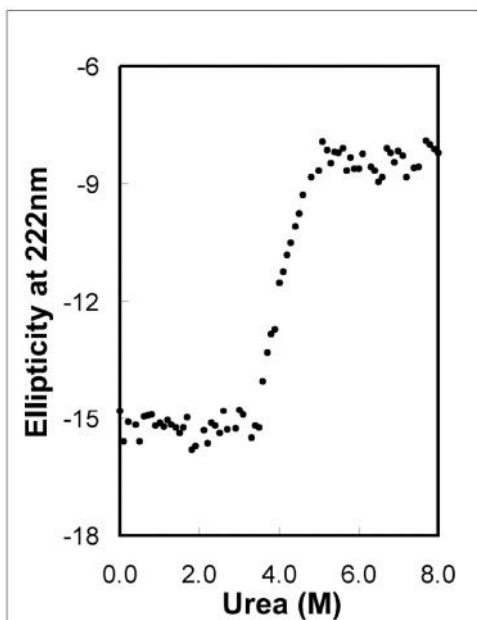**Figure 4. Thermodynamic stability of the wild-type MSP domain**
The urea-induced unfolding curve as reflected by change of the ellipticity at 222 nm with urea concentrations ranging from 0 to 8 M.

3.1.3   Binding Activity of the wt-VAPB MSP Domain

The thermodynamic parameters for the binding between the wt-VAPB MSP domain and the FFAT-containing motif of the Nir2 protein were also measured by ITC (Figure 5).

The wt-VAPB MSP domain is able to bind tightly to the FFAT-motif containing peptide EEEFFDAHE derived from the human Nir2 protein, with a dissociation constant (K_D) of 0.65 µM. As such, the CD and ITC results together clearly demonstrate that at neutral pH, the wild-type MSP domain is both structurally well-folded and functionally active.
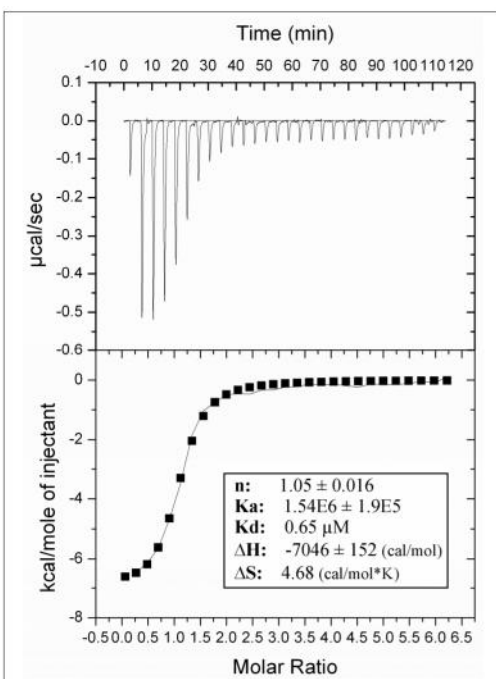
Figure 5. Activity of the wild-type MSP domain.
The ITC titration profiles of the binding reaction of the wild-type MSP domain to the FFAT-motif containing peptide derived from Nir2 (upper panel); and integrated values for reaction heats with subtraction of the corresponding blank results normalized by the amount of ligand injected versus molar ratio of MSP/FFAT (lower panel). The thermodynamic binding parameters obtained from fitting the data are shown in the box.

3.1.4 Crystal Structure of the wt-VAPB MSP Domain

I have also succeeded in optimizing the conditions required to obtain crystals of wt-VAPB MSP domain with good diffraction qualities. The crystal structure at 2.5 Å resolution with a final R-factor of 0.2068 (R_{free}=0.2655) was solved by Dr Shi jiahai. The wt-VAPB MSP domain adopts a seven-stranded immunoglobulin-like β sandwiches with

s-type topology. In the final model, one asymmetric unit contains two MSP molecules which form a dimer linked through an intermolecular disulfide bridge between two Cys53 residues (Figure 6a). On the other hand, based on the FPLC and DLS characterization, the wt-VAPB MSP domain was shown to be a monomer in solution. Henceforth, the dimer observed here in the wt-VAPB MSP domain structure is probably an artifact arising due to crystallization at a very high protein concentration (10 mg/ml). The two individual molecules in the dimeric wt-VAPB MSP structure are very similar, with a RMS deviation of only 0.41 Å for the backbone atoms.
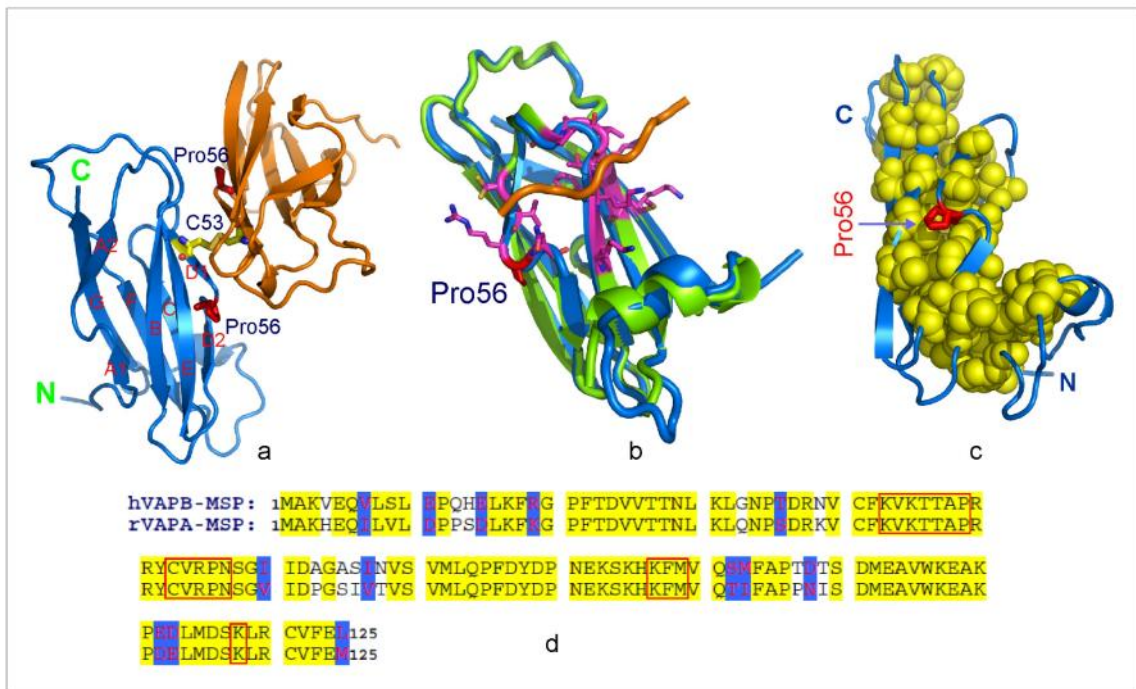

Figure 6. Crystal structure of the wild-type MSP domain
a. Dimeric crystal structure of the wild-type hVAPB MSP domain (3IKK) linked by an intermolecular disulfidge bridge between two Cys53 residues. It shares the same fold as the rVAPA MSP domain (1Z9L), composed of seven-stranded immunoglobulin-like β sand-wiches with s-type topology. The b-strands are labeled in one molecule and Pro56 side chains are displayed as sticks. b. Structural superimposition of the hVAPB MSP and rVAPA MSP (1Z9O) in complex with an ORP1 peptide containing the FFAT motif. The rVAPA residues involved in direct contacting with the peptide are displayed as sticks. Pro56 located at one end of the binding pocket is also shown as red sticks. c. The hVAPB MSP structure in blue ribbon, with hydrophobic residues displayed as yellow spheres and Pro56 as red sticks. d. Sequence alignment of the hVAPB and rVAPA MSP domains, with residues on the binding interface with the peptide boxed.

The wt-VAPB MSP domain also possess two unique S-shape loops over residues Gln11-Pro12-Gln13-His14 and Arg55-Pro56-Asn57-Ser58, which appear to be stabilized

43

by the cis-peptide bond conformation constrained by Pro12 and Pro56 respectively (Figure 6c). The first S-shape loop connects the β-strands Ser9-Leu10 and Glu15-Arg19 whereas the second S-shape loop connects the β-strands Cys53-Val54 and Gly59-Ile61 (Figure 6d). In particular, it has been speculated that because of being critically located in the S-shape loop, Pro56 might play a key role in stabilizing the MSP domain and consequently its mutation would result in insolubility.

3.2   Studies on the Pro56Ser Mutation

To address the consequence of the ALS8-causing P56S mutation, the P56S mutant of the wt-VAPB MSP domain was generated by using site-directed mutagenesis. The recombinant VAPB (P56S) protein was found in the inclusion body when expressed using a prokaryotic system. All attempts to refold it had failed due to severe precipitation. However, we recently discovered these "insoluble proteins" could be in fact solubilized in salt-free water and now this approach has also been used by other groups to characterize insoluble proteins (Amos *et al*., 2009 and Delak *et al*., 2009). Therefore, P56S-VAPB was purified under the denaturing conditions in the presence of 8M urea using affinity chromatography followed by RP-HPLC on a C4 column. The lyophilized VAPB (P56S) protein is then dissolved in salt free water.

The purified VAPB (P56S) protein is highly soluble in salt free water and has an acidic pH due to the remaining TFA from the HPLC solvent. Far-UV CD and NMR spectroscopy was then utilized to study its structural properties.

3.2.1   Structural Consequences of the Pro56Ser Mutation

As shown in Figure 7a, at pH 3.5 the VAPB (P56S) MSP domain has a far-UV CD spectrum characteristic of a predominantly-unstructured protein, with its maximal

negative signal at ~199 nm and without any positive signal. The mutant remains highly unstructured up to a pH of 5.5 and further attempts to neutralize the pH causes it to precipitate.

Next, the effect of salt on the conformational properties of VAPB (P56S) was explored by far-UV CD. As shown in Figure 7b, the overall shapes of the CD spectra are still similar at various pH and salt concentrations up to 10mM, indicating that the mutant remains similarly disordered under these conditions. However, when the pH value reached 6.5 for the sample containing 10mM salt, the protein precipitated immediately and consequently the CD signal disappeared.

NMR spectroscopy was also utilized to study the effect of pH and salt on the VAPB (P56S) MSP domain. As seen in figure 7c, and also consistent with the above CD results, at pH 3.5, the mutant has a HSQC spectrum characteristic of an unfolded protein without any tight tertiary packing, with only 0.8 and 11 ppm dispersions over ^{1}H and ^{15}N dimensions respectively. Interestingly, at pH 3.5 many HSQC peaks of the mutant are superimposable to those from the unfolded population of the wild-type at pH 3.5 (Figure 7c), implying that the mutant might have a conformational ensemble similar to that of the unfolded population of the wild-type at pH 3.5. However, unlike the wt-VAPB MSP domain which could reversibly fold back at pH above 4.5, VAPB (P56S) at pH 4.5 and 5.5 still remains highly unstructured as no significant dispersion change is observed for their HSQC spectra (Figures 7d and 7e). At pH 6.5, the protein completely aggregated and consequently no HSQC peaks could be detected. Also consistent with the CD results, at pH 3.5, upon adding varying amount of salt, no significant change of spectral dispersions occurs and only some peaks undergo slight shifts probably due to the non-

specific interactions with the salt ions. This thus suggests that the salt has no considerable effect on the conformation of VAPB (P56S).
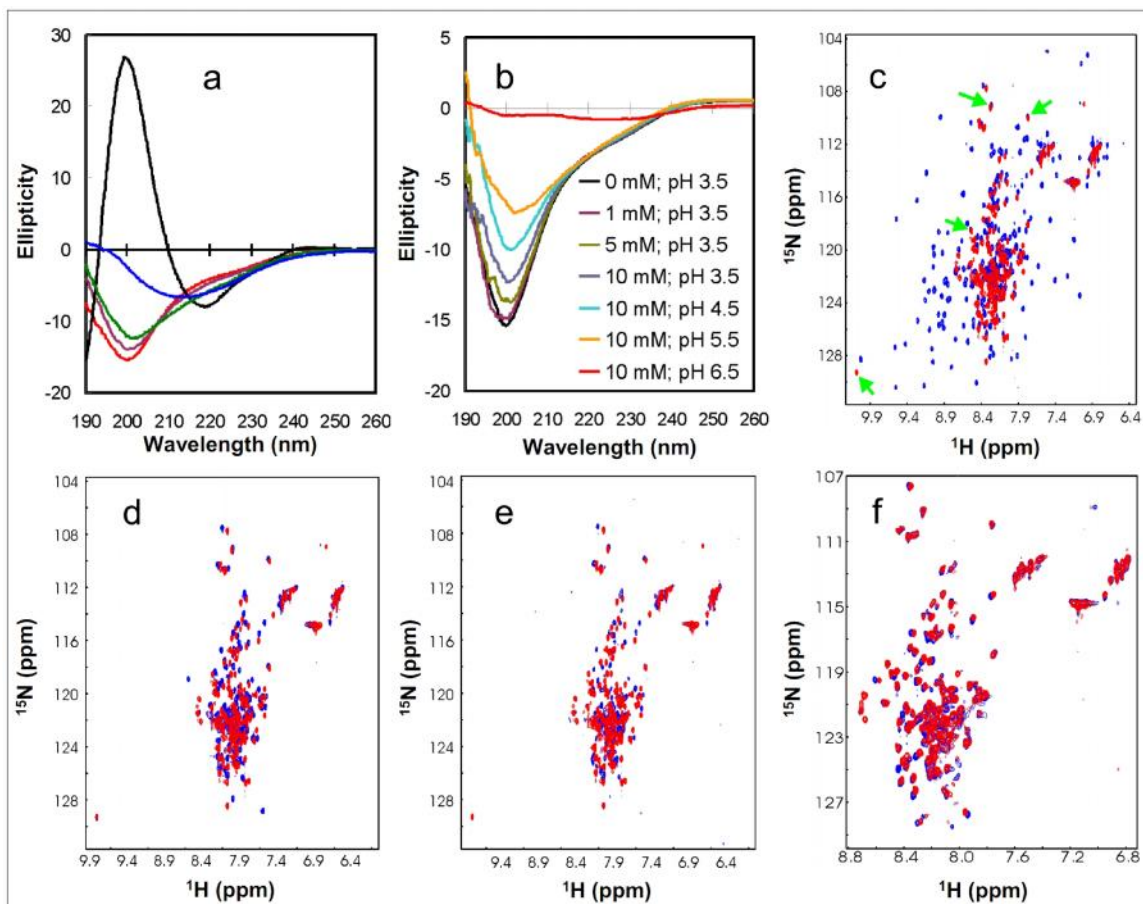

Figure 7. Structural consequence of the Pro56Ser mutation
a. Far UV CD spectra of the wild-type MSP (black) and Pro56Ser mutant at pH 3.5 (red), 4.5 (brown), 5.5 (green) and 6.5 (blue). b. Far UV CD spectra of the Pro56Ser mutant at different pH values and salt concentrations. c. Superimposition of the HSQC spectra of the wild-type MSP domain at pH 3.5 (blue) and Pro56Ser mutant at pH 3.5 (red). Green arrows are used to indicate some superimposable HSQC peaks. d. Superimposition of the HSQC spectra of the Pro56Ser mutant at pH 4.5 (blue) and 3.5 (red). e. Superimposition of the HSQC spectra of the Pro56Ser mutant at pH 5.5 (blue) and 3.5 (red). f. Superimposition of the HSQC spectra of the Pro56Ser mutant at pH 3.5 in the absence (red) and presence of 20 mM salt (blue).

3.2.2 Residue specific Conformational Properties of VAPB (P56S)

In order to gain knowledge about the residue-specific conformational properties of VAPB MSP domain, both wild-type and VAPB (P56S) MSP domains were isotope-labeled and a series of three-dimensional heteronuclear NMR experiments were collected. For the wild-type MSP domain, NMR HSQC resonance peaks were detected

and assigned for almost all residues except for several short stretches over Gln11-His14, Ser84-Lys87 and Lys110-Glu112. For the Pro56Ser mutant, probably due to more severe conformational exchanges on the μs-ms time scale or/and dynamic aggregation in the unfolded state, more NMR HSQC resonance peaks were invisible, including fragments Ala48-Arg51, Met72-Gln74, Pro80-Phe94, Pro111-Ser117 and Val122-Leu125.

With the CA, CO and HA chemical shift of each resonance peak, the chemical shift deviations from their random coil values was calculated for both native and P56S MSP domains. As seen in Figure 8, the wild-type MSP domain has very large CA and CO deviations typical of a fully-folded protein, while the P56S mutant has dramatically reduced deviations characteristic of an unfolded protein. It also appears that in the P56S mutant, the native β-sheet secondary structure is totally eliminated. Instead, based on the negative HA chemical shift deviations (Figure 8c), it appears that non-native helical conformation is weakly populated over the sequence. In addition, the software DANGLE in CCPNMR was used to map the secondary structures based on chemical shift deviations. The results indicate that in solution the wild-type wt-VAPB MSP domain has secondary structure patterns completely consistent with those in the crystal structure. By contrast, the VAPB (P56S) mutant has random coil conformation almost over the whole sequence except for the presence of a weakly-populated helix over residues Thr97 to Glu108 (Figure 8c). Interestingly, in the wild-type MSP structure, a helix is also found but much shorter, only spanning over residues Ala104 to Glu108.

The ^{15}N-edited HSQC-NOESY spectrum was also analyzed, but no long-range NOEs could be identified, strongly suggesting the absence of any stable tertiary packing in the VAPB (P56S) mutant. As shown in Figure 9, except for the missing residues,

sequential $d_{NN}(i, i + 1)$ and medium-range $d_{\alpha N}(i, i + 2)$ NOEs could be observed over the majority of the sequence, suggesting that the non-helical conformation is indeed populated to some degree. However, $d_{NN}(i, i + 2)$ NOEs could be found only over two segments (Gly33−Thr46 and Thr97−Glu108), while only two $d_{\alpha N}(i, i + 3)$ NOEs could be identified between Ala104 and Lys107 and between Val105 and Glu108. These results, together with a complete lack of any $d_{\alpha N}(i, i + 4)$ NOE, imply that the non-native helical conformation is very dynamic and only weakly populated in the P56S-VAPB (Delak *et al*., 2009).
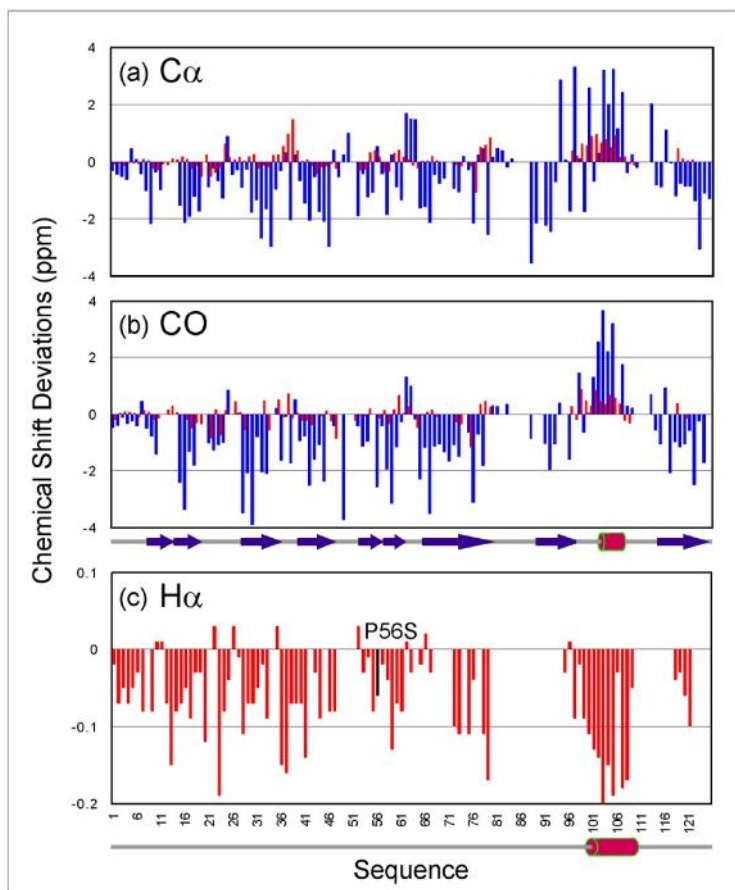
Figure 8. Residue-specific conformational properties
Bar plot of chemical-shift deviations (Dd = dobs – dcoil) of Ca (a), CO (b) and Ha (c) from their random-coil values for the wild-type (blue) and Pro56Ser (red) domains. The black bar is used to indicate Pro56Ser mutation. The secondary structures of the Pro56Ser mutant are mapped out by DANGLE to be predominantly random coil for almost all the sequence except for the presence a weakly-populated helix (red cylinder) over residues Thr97 to Glu108.
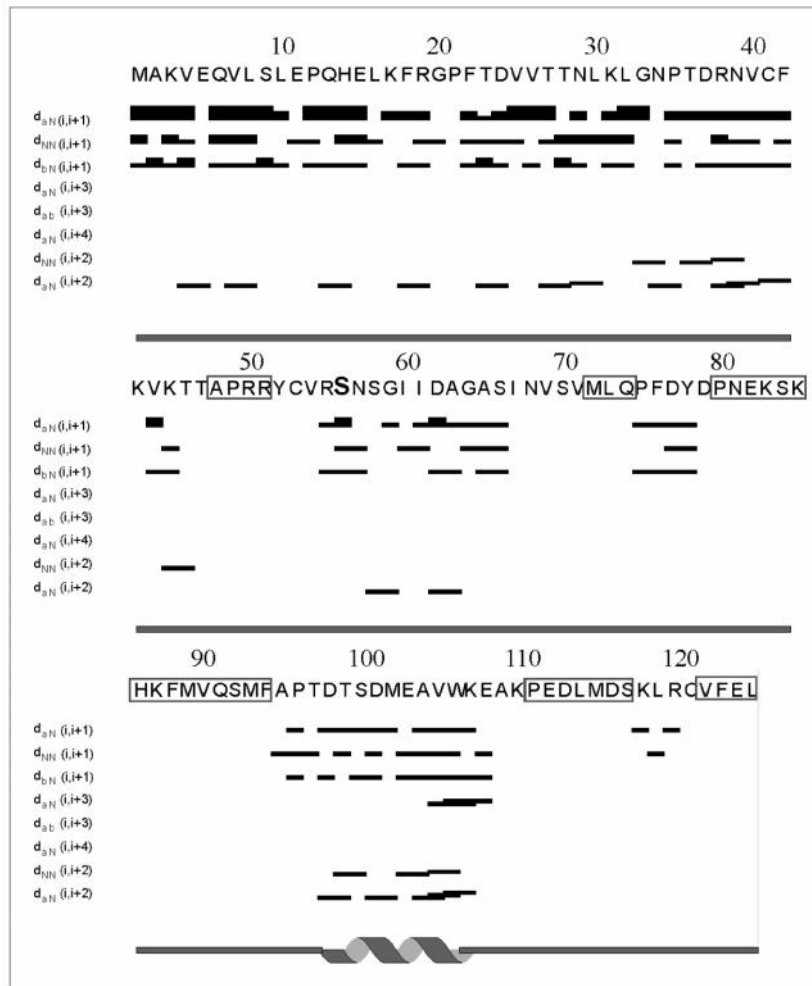
Figure 9. Characteristic NOEs defining secondary-structure
NOE connectivities identified for the Pro56Ser mutant. Plots were generated by CCPNMR. The boxed residues are not detectable in the HSQC spectrum and thus not assigned.

3.2.3. Binding activity VAPB (P56S)

NMR HSQC titrations were also utilized to examine whether the P56S-VAPB mutant is still able to bind to the Nir2 peptide in solution. However, the obtained result demonstrates that there is no detectable binding at pH 3.5 even in the presence of 10mM salt, at a molar ratio even up to 1:50 (data not shown). Unfortunately, further attempts to detect the binding interaction at a physiologically relevant pH failed because of severe aggregation of the protein upon neutralizing the pH.

3.2.4. Structural Consequences of the Pro12Ser Mutation

As mentioned above, there are two characteristic S-shape loops present in the wt-VAPB MSP domain. To investigate if Proline 12 also plays a similar role as Proline 56, Proline 12 was mutated to Serine by using site-directed mutagenesis. Interestingly, the P12S mutant indeed became insoluble and was only found in the inclusion body. As such, we purified the recombinant VAPB (P12S) protein as described above and dissolve it in salt free water. As judged by the CD results, in salt-free water (Figure 10a), VAPB (P12S) is highly unstructured at pH values below 5.5 but becomes severely aggregated at pH 6.5. This is further supported by the HSQC spectra at different pH values. At pH 6.5, no HSQC peaks could be detected even with the spectral contour down to the noise level (Figure 10e), suggesting a drastic aggregation at this pH. In addition, many HSQC peaks of the Pro12Ser mutant are also superimposable to those of the Pro56Ser mutant (Figure 10b). This implies that the VAPB (P12S) and VAPB (P56S) mutants might have similar conformational properties over a large portion of the molecules.

3.3. Studies on the Thr46Ile Mutation

In addition to the P56S mutation, T46I was also recently identified to cause ALS8 (Chen *et al*., 2010). To address the consequence of the ALS8-causing T46I mutation, the T46I mutant of wt-VAPB MSP domain was generated by using site-directed mutagenesis. Although like VAPB (P56S), when expressed in a prokaryotic system, a large portion of the recombinant protein still existed in inclusion bodies, there was also a significant portion of soluble VAPB (T46I). Subsequently, VAPB (T46I) was purified under the native condition similar to wt-VAPB. The purified VAPB (T46I) mutant was soluble in the buffer systems used but tends to aggregate at high concentration (~10mg/ml) and high temperature. CD and NMR spectroscopy was utilized to study its structural properties.
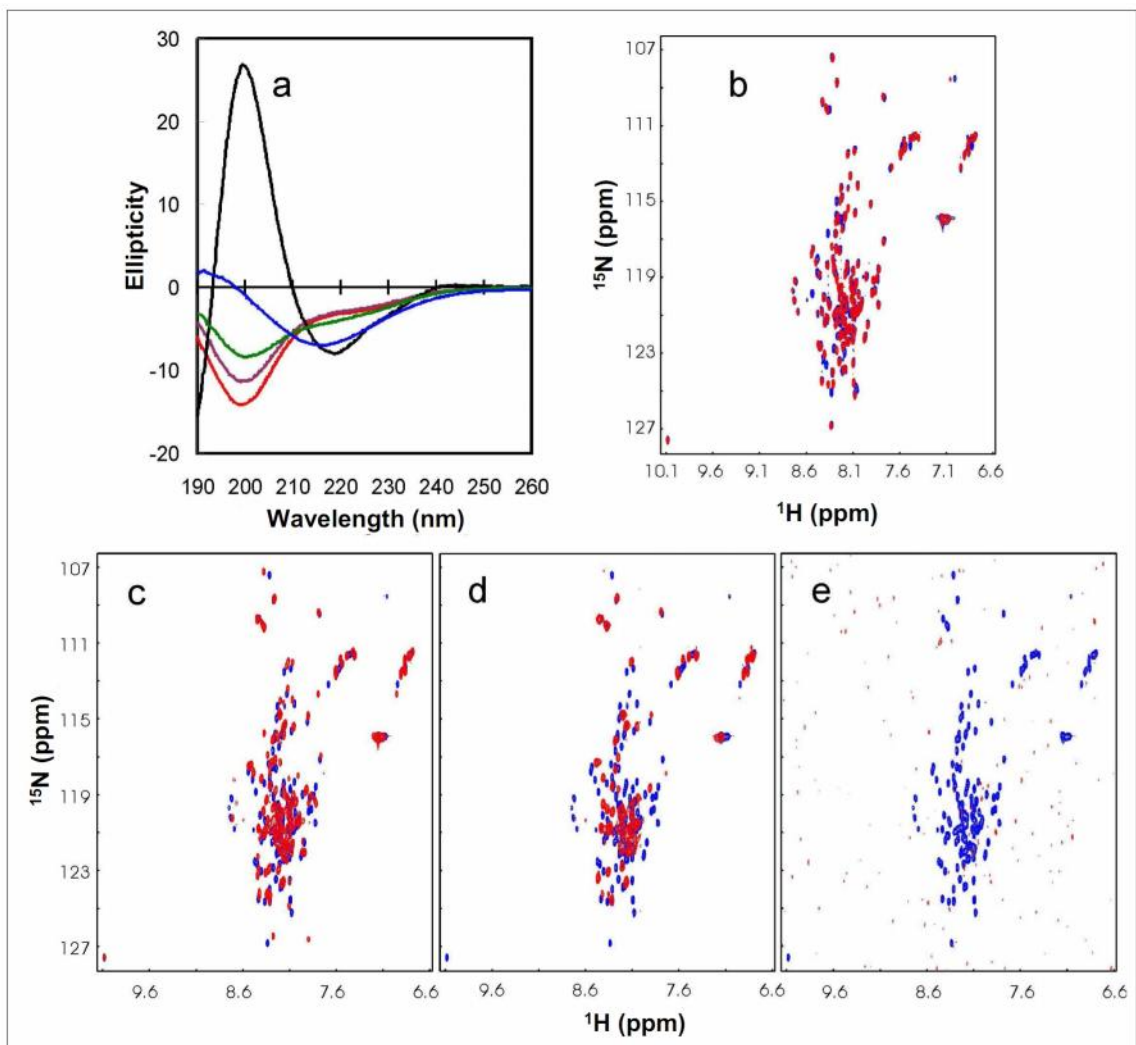
Figure 10. Structural consequence of the Pro12Ser mutation
a. Far UV CD spectra of the wild-type MSP (black) and Pro12Ser mutant in salt-free water at pH 3.5 (red), 4.5 (brown), 5.5 (green) and 6.5 (blue). b. Superimposition of the HSQC spectra of the Pro56Ser (blue) and Pro12Ser mutants in salt-free water at pH 3.5 (red). c. Superimposition of the HSQC spectra of the Pro12Ser mutant in salt-free water at pH 3.5 (blue) and 4.5 (red). d. Superimposition of the HSQC spectra of the Pro56Ser mutant in salt-free water at pH 3.5 (blue) and 5.5 (red). e. Superimposition of the HSQC spectra of the Pro12Ser mutant in salt-free water at pH 3.5 (blue) and 6.5 (red).

3.3.1.   Structural Consequences of the Thr46Ile Mutation

As shown in Figure 11a, at pH 6.5, the VAPB (T46I) MSP domain has a far-UV CD spectrum typical of a β-dominant secondary structure, with the maximal negative signal at ~218 nm and positive signal at ~199 nm. The overall shape of the CD spectra is also highly similar to that of the structured wt-VAPB but completely different from the unstructured VAPB (P56S). This implies that VAPB (T46I) has a native-like secondary structure and that this mutation, unlike P56S did not result in the elimination of the native structure of wt-VAPB nor cause aggregation at neutral pH.

Next, a two-dimensional ^{1}H-^{15}N HSQC spectra of the ^{15}N-labeled VAPB (T46I) MSP domain was collected at pH 6.5. As seen in figure 11b, and also consistent with the above CD results, at pH 6.5, the mutant has a HSQC spectrum characteristic of a well-folded protein, with very large spectral dispersions that extends 3.5 ppm and 25 ppm over the ^{1}H and ^{15}N dimensions respectively. Many HSQC peaks of the VAPB (T46I) mutant are also superimposable to the wt-VAPB at pH 6.5, implying similar conformational properties over a large portion of the molecules.

3.3.2.   Residue-Specific Conformational Properties of VAPB (T46I)

In order to gain knowledge about its residue-specific conformational properties, the MSP domain of VAPB (T46I) was double isotope-labeled (^{15}N and ^{13}C) and a pair of triple-resonance NMR spectra, namely HNCACB and CBCA(CO)NH was acquired. For the VAPB (T46I) MSP domain, NMR HSQC resonance peaks were detected and assigned for almost all residues except for several short stretches over Glu11-His14,   Ile46-Tyr52, Glu82-Ser84 and C-terminal Phe123- Leu125. Probably due to more severe conformational exchanges, more NMR HSQC resonance peaks were invisible over the
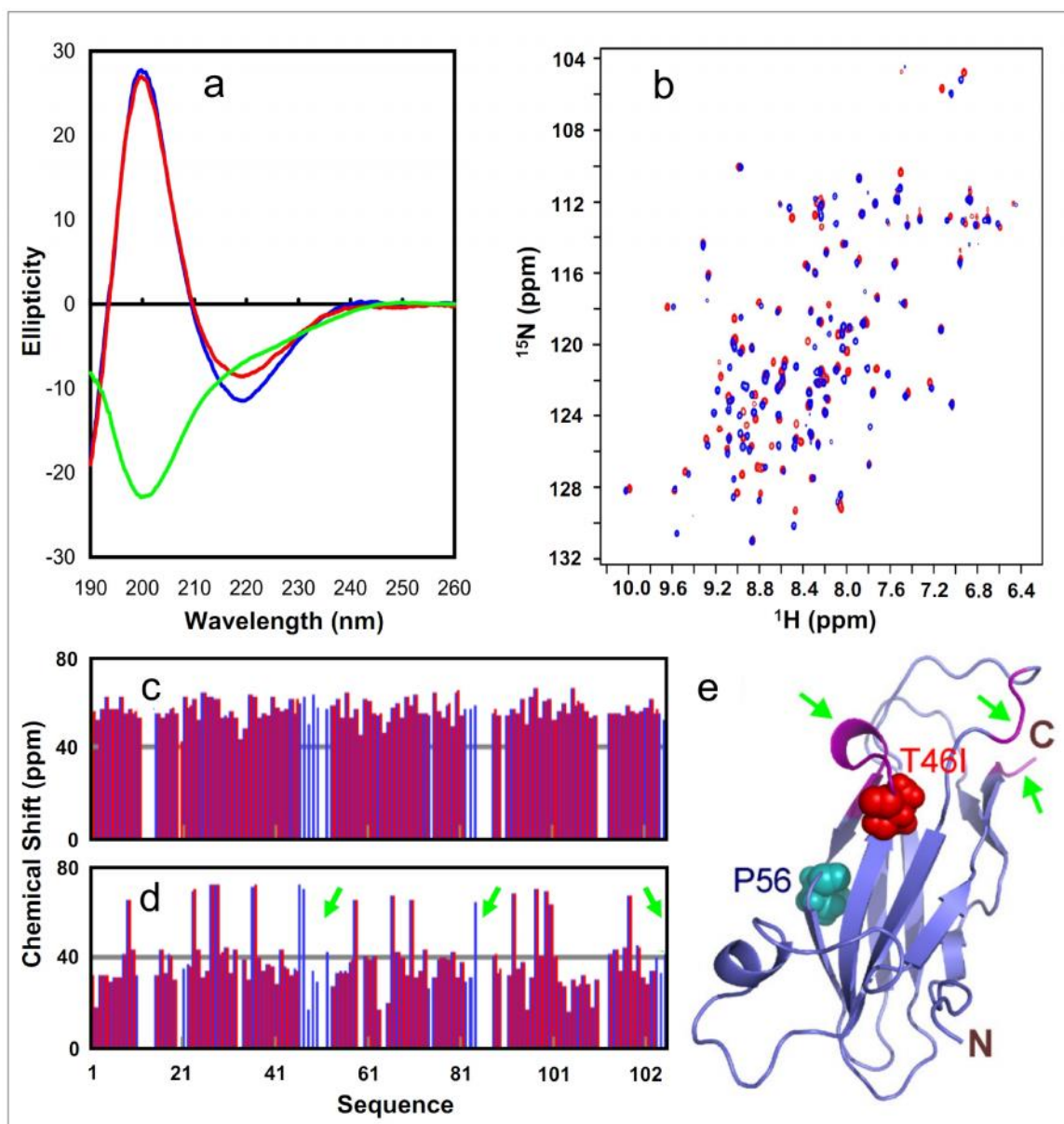
Figure 11. Structural Characterization of VAPB (T46I) MSP domain
a. Far UV CD spectra of the wild-type MSP (pH6.5) (blue) and VAPB (T46I) (pH6.5) (red) mutant and P56S (pH3.5) (green) at a protein concentration of ~20 μM. b. Superimposition of the two-dimensional NMR HSQC spectra of the wt-VAPB MSP domain (blue) and VAPB (T46I) MSP domain (red) at protein concentrations of 100 μM at pH 6.5. Cα (c) and Cβ (d) chemical shifts of the WT- (blue) and T46I- (red) MSP domains. The residues with the disappeared HSQC peaks are indicated by green arrows. (e). The crystal structure of the wt-VAPB MSP domain to which the T46I residues with their HSQC peaks undetected were mapped. The two mutation residues causing ALS, P56S and T46I, were displayed as spheres.

stretch of Ile46-Ala50 as compared to wt-VAPB. As compared to wt-VAPB, several HSQC peaks have also shifted dramatically. Together these data suggests that the T46I mutations causes part of the MSP domain to become more flexible or are more exposed as compared to wt-VAPB.

Next, the Cα and Cβ chemical shift of each resonance peak for VAPB (T46I) was compared with wt-VAPB MSP domain. As seen in figure 11c, d, e the VAPB (T46I) has very large and similar Cα, and Cβ deviations typical of a fully-folded protein and are almost identical to those of wt-VAPB. To sum up, these results provides the strongest evidence that the T46I mutant assumes a three-dimensional structure highly similar to that of wt-VAPB, and intriguingly, the short regions which harbors the Thr46 seems to become more flexible as well.

3.3.3. Stability of the VAPB(T46I) MSP Domain

The thermodynamic stability energy of VAPB (T46I) was also measured by monitoring the ellipticity change at 222nm during urea-unfolding. As seen in Figure 12a, unlike wt-VAPB with a cooperative unfolding transition, VAPB (T46I) shows a non-cooperative transition as well as reduced stability. VAPB (T46I) starts unfolding at a urea concentration of ~1.6 M and shows no ending even at 8 M, while WT starts at ~3.5 M and ends at ~5.1 M. As a result of losing the cooperative unfolding transition, the precise energy of thermodynamic stability could not be fitted out from the VAPB (T46I) unfolding curve.

The loss of a cooperative unfolding transition of VAPB (T46I) implies that its tight tertiary packing is disrupted to some degree (Song *et al*., 1999 and Wei *et al*., 2005) and consequently the T46I molecule may be more accessible to partially- or highly
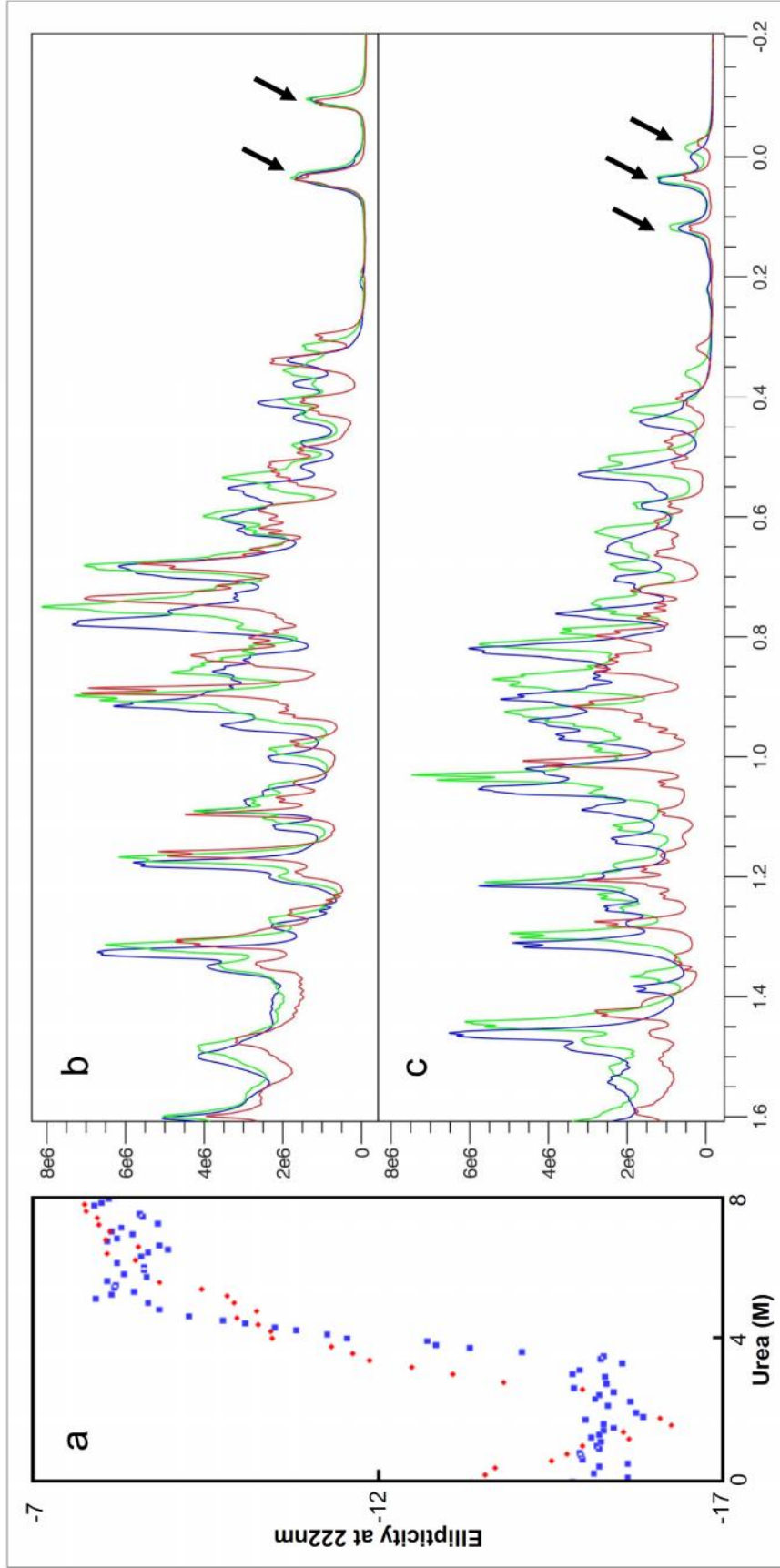
Figure 12. Stability of wt-VAPB and VAPB (T46I) MSP domain

(a). The urea-induced unfolding curves of the WT- (blue) and T46I- (red) MSP domains as reflected by changes of the ellipticity at 222 nm with urea concentrations ranging from 0 to 8 M. One-dimensional NMR spectra of wt-VAPB - (b) and VAPB (T46I) - (c) MSP domains at 25°C (Blue) , 35° (Green) and 45°C (Red)

unfolded states prone to aggregation. Indeed, we have observed that VAPB (T46I) is prone to aggregation at high protein concentrations and temperatures. For example, while at 45°C the et-VAPB MSP domain showed no precipitation and has almost no change of the upfield peaks in the one-dimensional NMR proton spectra (Figure 12b), a large portion of the VAPB (T46I) mutant precipitated at ~42°C and the remaining protein has a dramatic structural alteration as evidenced from the changes of the upfield peaks (Figure 12c).

3.3.4. Binding Activity of VAPB (T46I) MSP Domain

The thermodynamic parameters for the binding between the VAPB (T46I) MSP domain and the FFAT-containing motif of the Nir2 protein were also measured by ITC (Figure 13a). The VAPB (T46I) MSP domain is still able to bind to the FFAT-motif containing Nir2 peptide EEEFFDAHE with a dissociation constant (K_D) of 2.20 µM. Thus, unlike P56S which abolishes the ability of VAPB to interact with FFAT-motif containing proteins, the T46I mutation merely causes a reduction in affinity by ~3 times as compared to wt-VAPB.

HSQC titrations were also utilized to visualize the binding of the wt-VAPB and VAPB (T46I) MSP domain to the Nir2 peptide. As shown in Figures 13b and 13d, in wt-VAPB, for the residues directly contacting the peptide (Kaiser *et al*., 2005 and Shi *et al*., 2010), their HSQC peaks mostly disappeared at a molar ratio of 1:2 (wt-VAPB/Nir2), while for the residues not directly contacting but close to the binding interface, their HSQC peaks shifted. Intriguingly, due to the reduced affinity, the addition of the Nir2 peptide only induced the shift, but not disappearance of the VAPB (T46I) HSQC peaks (Figure 13d).
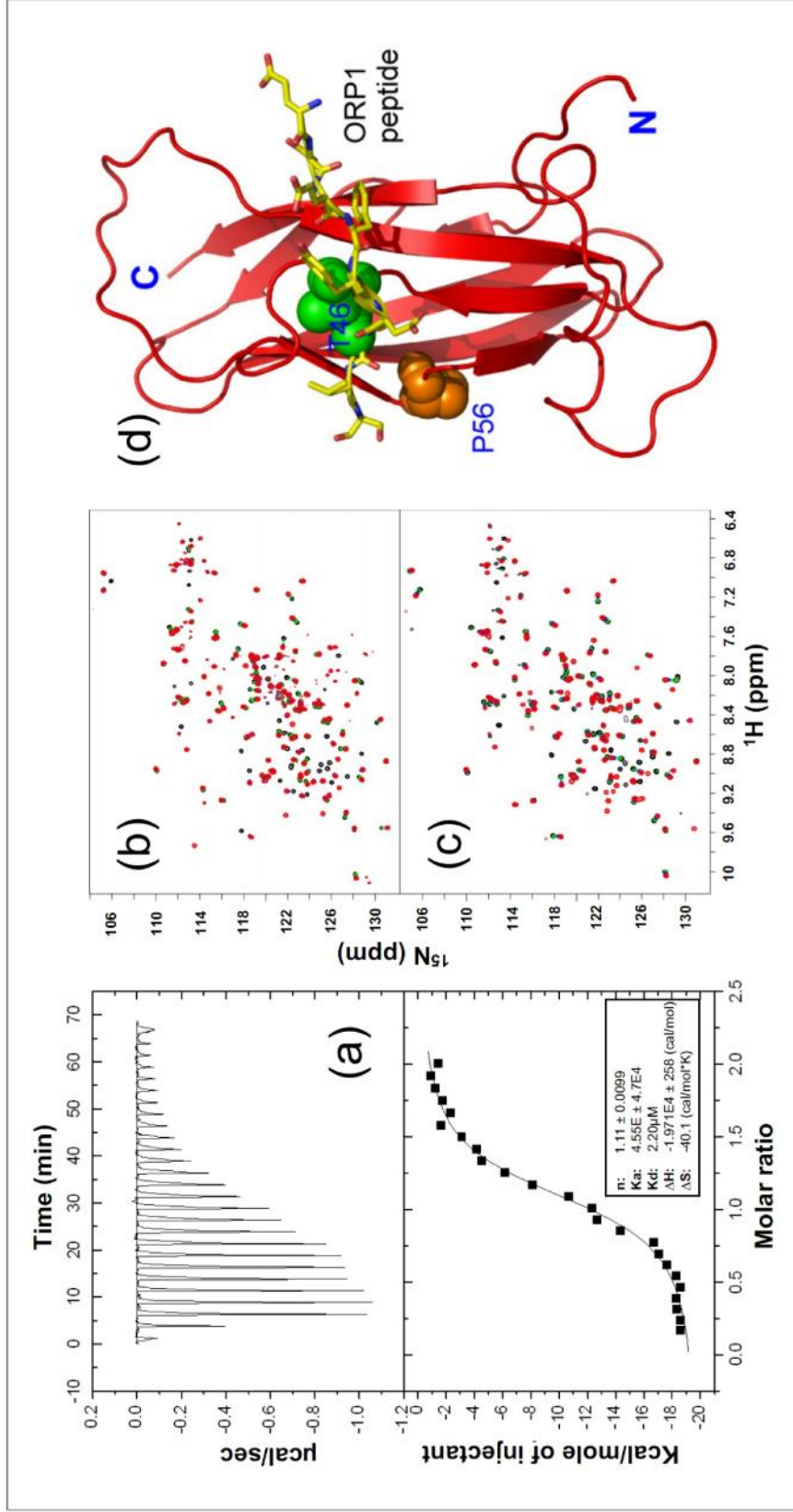
Figure 13. Interaction between the T46I-MSP domain and the Nir2 peptide.
(a). The ITC titration profile of the binding reaction of the T46I-MSP domain to the Nir2 peptide (upper panel); and integrated values for reaction heats with subtraction of the corresponding blank results normalized by the amount of ligand injected versus molar ratio of MSP/Nir2 (lower panel). Thermodynamic binding parameters obtained from fitting the data are shown in the box. Superimposition of the two-dimensional NMR HSQC spectra of the wt-VAPB (T46I) - (c) MSP domains in the absence (black) and presence of the Nir2 peptide at molar ratios 1:0.5 (green), 1:1 (blue) and 1:2 (red). (d). Crystal structure of the VAPA MSP-ORP1 complex to illustrate the MSP-peptide binding interface (Kaiser *et al.*, 2005).

3.3.1. Interactions of VAPB MSP domain with the EphA4 receptor

As mentioned in section 1.3.3.3, the MSP domain was identified by Tsuda *et al.,* (2008) to be a novel ligand for the EphA4 ligand binding domain. To gain insights into the underlying structural basis, I attempted to gain thermodynamic parameters for the EphA4-wt-VAPB-MSP binding by ITC but unfortunately a complex ITC profile was obtained. This implied that the binding may be involved in muti-sites or/and multi-steps. The EphA4-wt-VAPB-MSP complex also failed to crystallize after extensively screened a variety of buffer conditions. As such, NMR HSQC titrations were utilized to further gain molecular details for the binding interaction between EphA4 and the MSP domain.

First we monitored the change of the HSQC spectra of ^{15}N labeled wt-VAPB - and VAPB (T46I) - MSP domain upon the gradual addition of the unlabeled EphA4 ligand binding domain. Because the EphA4 ligand binding domain was intolerable to reducing agents, DTT which was used in the buffer solubilizing wt-VAPB and VAPB (T46I) has to be removed. In addition, the titration was done at pH 8.0 to match the pH used in the in *vitro* study by Tsuda *et al.,* (2008). The removal of the reducing agent produced striking differences in the HSQC spectra of ^{15}N labeled wt-VAPB but not ^{15}N labeled VAPB (T46I). As seen in figure 14a, many of the HSQC resonance peaks of wt-VAPB showed line broadening. This implies that in an oxidizing environment, the wt-VAPB MSP domain may undergo conformational exchanges in the μs-ms time scale possibly due to aggregation. It is unlikely that wt-VAPB formed a tight oligomer as it was purified as a monomer even in the oxiding environment. In addition, as mentioned, Kim *et al.,* (2010)
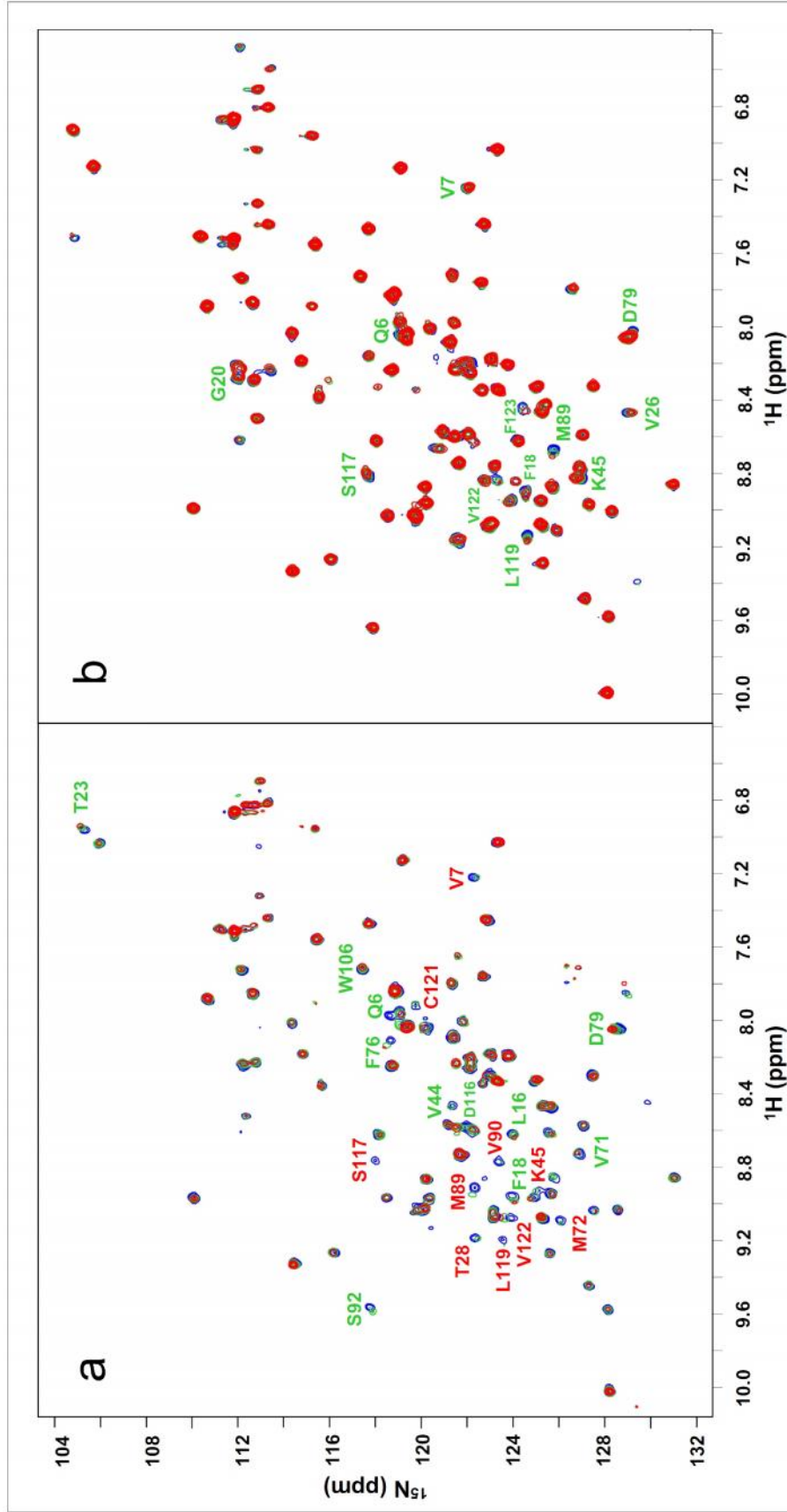
Figure 14. NMR titration of ^{15}N labeled wt-VAPB and VAPB (T46I) MSP domain with EphA4 receptor

a. 1H,15N HSQC spectra of wt-VAPB MSP domain in the presence of EphA4 with a molar ratio of 1:2 (Green) and 1:8 (Red) and in the absence of EphA4 (blue);
b. 1H,15N HSQC spectra of VAPB (T46I) MSP domain in the presence of EphA4 with a molar ratio of 1:2 (Green) and 1:8 (Red) and in the absence of EphA4 (blue). Residues that were significantly perturbed even before saturation were labeled. These residues included those which have disappeared (Red) or have shifted significantly (Green). The buffer used was 10mM phosphate pH8.0

59

has already provided clear evidences that the MSP domain of VAPB does not contribute to VAPB oligomerisation.

As shown in Figure 14a, introduction of unlabeled EphA4 ligand binding domain to ^{15}N labeled wt-VAPB MSP domain induced shifts of few HSQC resonance peaks and more significantly disappearance of several peaks. If the residues with significantly perturbed HSQC resonance peaks were mapped back to the MSP structure (PDB: 3IKK), it appears to be located on the E-F loop and several β-strands: C-strand carrying Thr46, F- and G-strands (Figure 15a). By contrast, addition of EphA4 to ^{15}N labeled VAPB (T46I) resulted in almost no disappearance of HSQC peaks with only peak shifts for some residues (Figures 14b and 15b). These results indicate that the T46I mutation dramatically disrupts the binding ability of the MSP domain to EphA4.
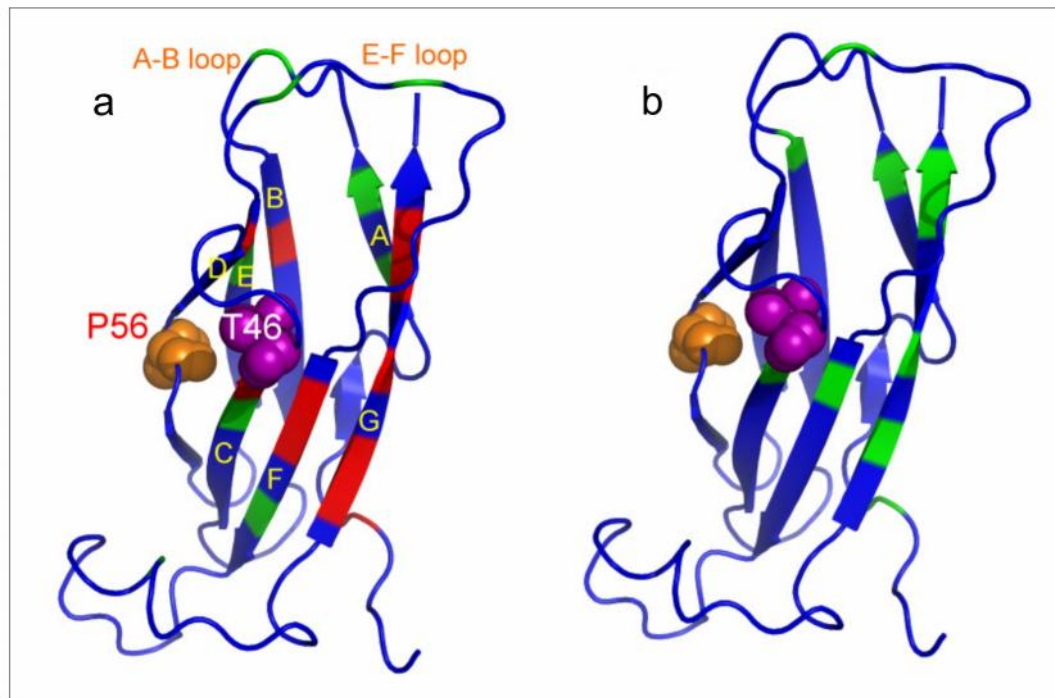
Figure 15. Interaction between the wt-VAPB- and VAPB(T46I) - MSP domains with EphA4 ligand binding domain.
The MSP structure with the perturbed residues mapped back for the interaction between wt-VAPB - (a), and VAPB (T46I) – MSP domain (b) with EphA4 ligand binding domain. Blue is to indicate residues with unperturbed HSQC peaks, while green and red for residues with shifted and disappeared peaks respectively.
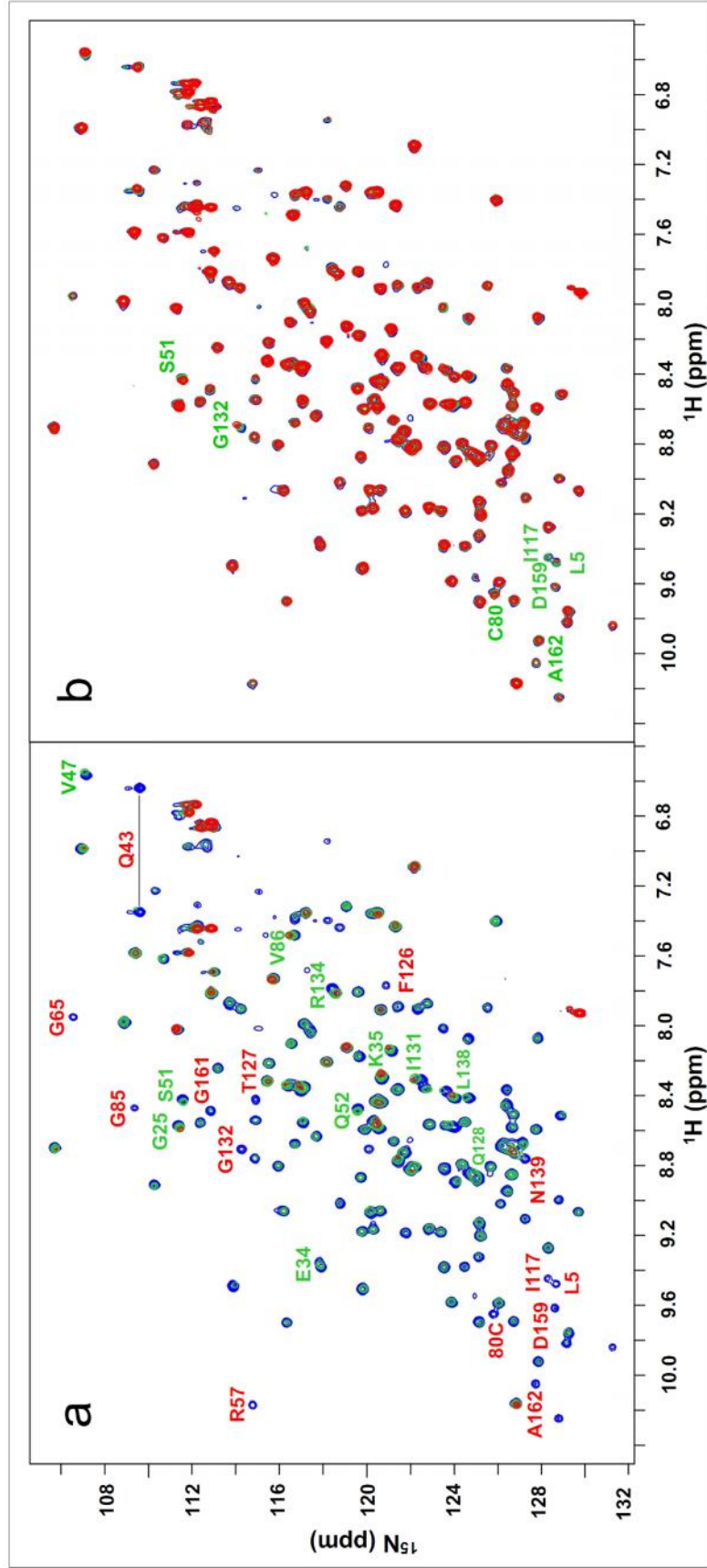
Figure 16. NMR titration of 15N labeled EphA4 receptor with the MSP domain of wt-VAPB and VAPB (T46I)
a. 1H,15N HSQC spectra of EphA4 receptor in the presence of the MSP domain of wt-VAPB with a molar ratio of 1:2 (Green) and 1:8 (Red) and in the absence of wt-VAPB (blue). b. 1H,15N HSQC spectra of EphA4 receptor in the presence of the MSP domain of VAPB (T46I) with a molar ratio of 1:2 (Green) and 1:8 (Red) and in the absence of VAPB (T46I) (blue). Residues that were significantly perturbed even before saturation were labeled. These residues included those which have disappeared (Red) or have shifted significantly (Green). The buffer used was 10mM phosphate pH8.0.

61

We further study the interaction by monitoring the HSQC spectra of ^{15}N labeled EphA4 ligand binding domain upon the gradual addition of unlabeled wt-VAPB or VAPB (T46I) MSP domain. As shown in Figure 16a, addition of the wt-VAPB MSP domain protein even at a ratio of 1:2 (EphA4/wt-VAPB) induced disappearance or intensity-reduction of several EphA4 HSQC resonance peaks, together with shifts of some peaks. If more wt-VAPB MSP domain protein was added, almost all EphA4 peaks disappeared at a ratio of 1:8. Again, when the residues with perturbed peaks were mapped back to the EphA4 structure, the D-E, G-H and J-K loops were observed to be involved in binding to the MSP domain (Figure 17a). These loops were also previously established by Qin *et al*., (2010) to directly contact its ephrins ligands. By a sharp contrast, addition of the VAPB (T46I) MSP domain caused almost no peak disappearance, but only shifts

Figure 17. Interaction between the EphA4 ligand binding domain with wt-VAPB- and VAPB(T46I) - MSP domains.
The EphA4 structure with the perturbed residues mapped back for the interaction between EphA4 ligand binding domain with wt-VAPB - (a), and VAPB (T46I) – MSP domain (b) Purple is to indicate residues with unperturbed HSQC peaks, while green and red for residues with shifted and disappeared peaks respectively.

of few peaks (Figures 16b and 17b). Together, these results indicated that the T46I mutation dramatically eliminates the binding capability of the MSP domain to EphA4.
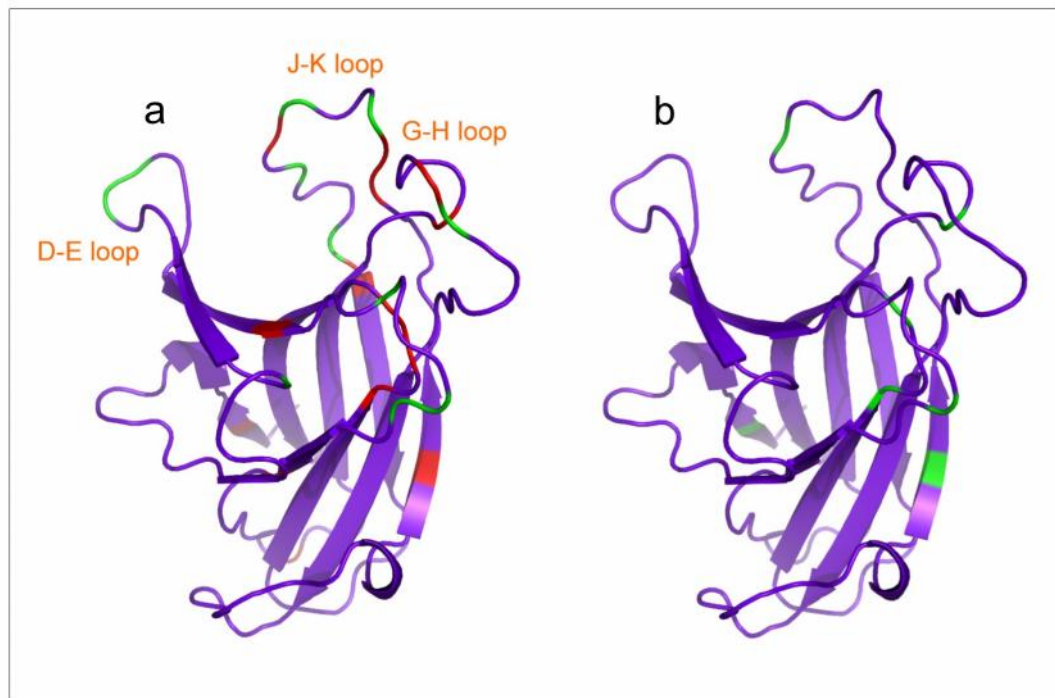
To understand the underlying mechanism for the significant disappearance of both MSP and EphA4 HSQC resonance peaks, we measured the radius of the EphA4 ligand binding domain by dynamic light scattering (DLS) in the presence of both wt-VAPB - and VAPB (T46I) - MSP domains at different molar ratios but no significant changes were observed. In addition, size exclusion chromatography of EphA4 and wt-VAPB mixed in a 1:1 ratio at high concentrations yielded only free proteins in their monomeric state. This implies that the binding triggers no formation of the tight EphA4-MSP complex and no significant oligomerization. As such, the disappearance of the MSP and EphA4 HSQC peaks is most likely to arise from the increase of conformational exchanges on the μs-ms time scale upon binding.

Next the binding of wt-VAPB MSP domain and EphA4 was tested to see if it can be interrupted by the presence of the FFAT motif containing Nir2 peptide. Intriguing as seen in figure 18b, unlike before where the addition of wt-VAPB could induce significant shift/disappearance of several EphA4 HSQC resonance peaks, only a small portion of EphA4 residues were perturbed in the presence of the Nir2 peptide. Also as seen in figure 18a, the addition of Nir2 peptide did not cause significant changes in the HSQC of EphA4. These observations strongly implied that the binding of the Nir2 peptide to the MSP domain would inhibit its binding to EphA4. This inhibition is most likely due to the fact that EphA4 and the Nir2 peptide may have overlapped binding interfaces on the MSP domain. It is unlikely that a structural change in the MSP domain could interrupt this binding because it had been demonstrated by Kaiser *et al*., (2005) that the MSP domain
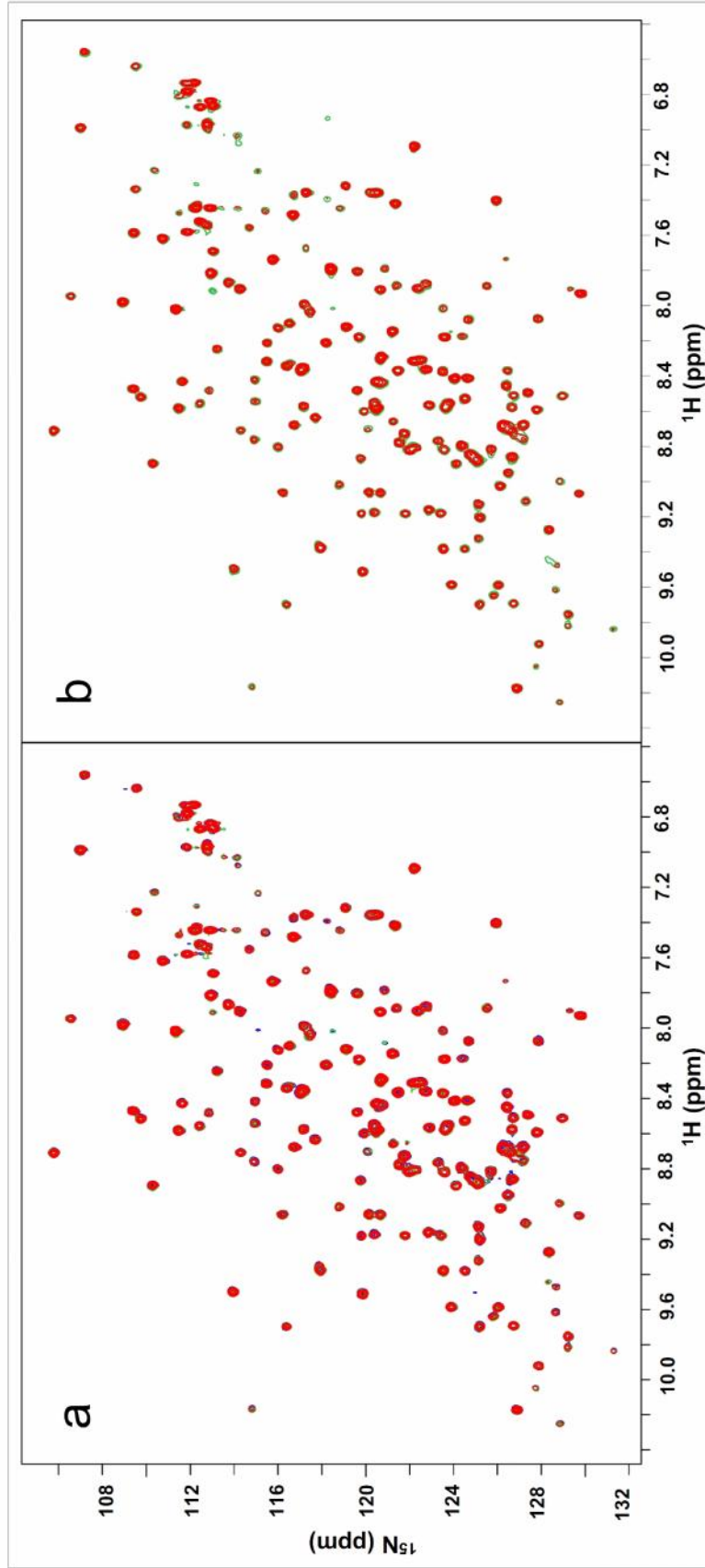
Figure 18. NMR titration of 15N labeled EphA4 receptor with the MSP domain of wt-VAPB in the presence of FFAT motif containing Nir2 peptide
a. 1H,15N HSQC spectra of EphA4 receptor in the presence of the FFAT containing Nir2 peptide with a molar ratio of 1:2 (Green) and 1:6 (Red) and in the absence of the FFAT containing Nir2 peptide (blue). b. 1H,15N HSQC spectra of FFAT saturated EphA4 receptor in the presence of the MSP domain of wt-VAPB with a molar ratio of 1:2 (Green) and 1:8 (Red) and in the absence of wt-VAPB (blue).

showed no significant change upon binding to ORP1, a FFAT-containing peptide.

3.4.   Discussion and conclusion

Two mis-sense point mutations in the human VAPB gene are associated with a familial form of motor neuron disease that has been classified as Amyotrophic Lateral Sclerosis type 8 (ALS8). The pathogenic mutations have been exhaustively studied by several groups and we now have a plethora of knowledge on the possible mechanisms responsible for the specific death of motor neurons in ALS8. However, so far, no study on the structure and stability of the wild-type MSP domain has been reported, and in particular, the structural consequences of this mutation remain completely unknown.

The wild-type hVAPB MSP domain is shown to be well-folded at neutral pH, with a three-dimensional structure highly similar to that of the rVAPA MSP domain. The wild-type MSP domain can undergo a reversible acid-induced unfolding, is fully functional in tightly binding to the FFAT-motif containing peptide derived from the Nir2 protein, with a K_d of 0.65 uM and has a moderately low stability free energy of 7.40 kcal/mol.

Our results also clearly demonstrate that the Pro56Ser mutant remains lacking of native structure under a variety of pH values and salt concentrations. This implies that the P56S mutation is able to eliminate the ability of the mutated sequence to fold into the native structure adopted by the wild-type MSP sequence. This is surprising as it is previously thought that the P56S mutation would only remove a kink between the stretches of ß-strand, changing the hydrogen bond pattern but not completely eliminate its structure. As seen in Figure 6c, Proline 56 is not only located at the central position of the hydrophobic core formed by the side chains of the hydrophobic residues but also in the characteristic S-shape loop, adopting the unusual cis-peptide bond conformation. As

such, the replacement of the hydrophobic Proline 56 by the polar Serine is anticipated to impose two effects. The first is to abolish the S-shape loop and significantly increase the backbone flexibility around Proline 56; and secondly is to destabilize the hydrophobic core upon introducing polar side chain of Serine. The importance of the two S-shape loops in maintaining the structural integrity of the MSP domain is further supported by our experimental results about the abolishment of its structure and solubility as triggered by the Pro12Ser mutation. Because the thermodynamic stability of the hVAPB MSP domain is also not very large, the two destabilizing effects appear sufficient to abolish the ability of the mutant sequence to form the native structure of the wild-type MSP domain.

The elimination of the tight tertiary structure in P12S and P56S results in the exposure of hydrophobic side chains. The exposed hydrophobic side chains have a large tendency to be clustered together to form aggregates, unless the attractive hydrophobic interaction can be suppressed by the intrinsic repulsive electrostatic interactions in salt-free water, with the solution pH several units away from the protein isoelectric point (pI). Indeed, the pI values of the P56S and P12S mutants were estimated to be ~7.5, thus explaining the observation that the Pro56Ser and Pro12Ser proteins would precipitate immediately after the solution pH was adjusted to neutral. Unsurprisingly, under the physiological condition, the pH is ~7.0 and the concentration of the salt ions is ~150 mM. As a result, under the physiological-relevant pH values, the repulsive electrostatic interactions are relatively small and also will be further screened out by the presence of ~150 mM salt. Consequently, in vivo the hydrophobic interaction will become dominant in the Pro56Ser mutant because of both neutral pH and high salt concentration, thus resulting in severe aggregation.

Unlike the Pro56Ser mutation, the Thr46Ile do not result in the elimination of the native structure of the MSP domain. This came as a surprise as it has been suggested by Chen *et al.*, 2010 that the theoretical pathogenicity of this mutation as calculated by the program PMut is greater than that of the VAPB (P56S). Despite this, the Thr46Ile mutation does abolish the cooperative urea-unfolding transition and reduce the thermodynamic stability of the MSP domain. The Thr46 residue lies in a loop that connects the D and E β-stand. The D β-stand harbors the Cys53 residues that formed an intermolecular disulphide bond with another MSP domain as shown in the structure (figure 6a). Pro56 lies immediately after this D β-stand and as discussed above is critical in maintaining a compact hydrophobic core. As such, replacement of the Threonine residue with a polar uncharged side chain to a hydrophobic side in isoleucine might have two effects. First, the long side chain of Isoleucine may disrupt the hydrophobic interaction network of the domain and consequently destabilize or decrease the overall compactness of the hydrophobic core resulting in the observed reduced thermodynamic stability. Secondly, the T46I mutation might also affect the ability of the S-shape loop created by Pro56 in maintaining structural integrity. The reduced stability of VAPB (T46I) allows the MSP domain to more easily access the partially- or/and highly-unfolded intermediates which are prone to aggregation (Li *et al.*, 2006 and Song *et al.*, 2009). Indeed, if compared to the wt-VAPB MSP domain, the VAPB (T46I) domain is much more prone to aggregation at high protein concentration and temperature.

We have also suggested that the segment of the MSP domain bearing the mutation could be more dynamic. The T46I mutation could also change the global dynamics of the MSP domain, inducing conformational changes that eventually lead to as exposure of

hydrophobic patches which becomes accessible to solvents. The exposed hydrophobic patches in turn, cause the mutated protein to be prone to aggregation at high concentration.

We have also demonstrated that the Thr46Ile mutation does not abolish the ability of VAPB (T46I) to interact with FFAT containing Nir2 peptide. Indeed, the T46I mutation merely causes a reduction in affinity by ~3 times as compared to wt-VAPB. Intriguingly, in other studies a VAPB mutant with Thr46Ala and Thr47Ala mutation was found to not to interact with FFAT containing proteins ORP2, ORP3, or ORP7 as demonstrated by Kaiser *et al*., (2005) and Loewen *et al*., (2005) using yeast cells and also by Suzuki *et al*., (2009) using pull-down analysis. In addition, Suzuki *et al*., (2009) has demonstrated that the VAPB (T46A, T47A) mutant showed proper ER localization and that their Triton X-100-soluble amounts were comparable to that of wt-VAPB. In contrast the T46I mutation in VAPB as shown by Chen *et al*., (2010) aggregates in cells and have increased insolubility in Triton X-100 buffers. Together the data presented here might have suggested that the mutation of Thr46 to Isoleucine or Alanine in the VCS of the MSP domain might cause the mutant domain to change its substrate specificity. Also such mutation produced striking differences in ER localization, thus implying that the VCS may be involved as well. Additionally, because the methyl side chain of Alanine is relatively small as compared to that isoleucine, the structural consequence of T46A or T47A mutation may not disrupt the hydrophobic core as much as an isoleucine mutation does.

Finally, evidences that the MSP domain of wt-VAPB interacts with EphA4 was also presented. This binding can be disrupted either by the pathogenic T46I mutation or in the

presence of FFAT containing peptide. In the co-crystal of ephA4 and ephrin-B2 binding, four loops (A-C, D-E, G-H, and J-K) have been demonstrated to undergo substantial movements. Interestingly, several residues such as E34 and K35 in the DE loop; 80C, G85 and V86 in the GH loop; F126, T127, Q128, I131, G132, R134, L138 and N139 in the JK loop of EphA4 have also been perturbed upon wt-VAPB binding, This thus implies that the MSP domain might bind to the same interface as Epherin-B2. Indeed, it has been demonstrated by Tsuda *et al.,* 2008 that epherin-B2 can block binding of MSP and EphA4. Together, these data suggest that the binding surface on MSP which interacts with EphA4 and FFAT may largely overlap with each other.

In conclusion, through this study, we have shown that mutation/modification on strategic positions may dramatically eliminate the ability of the mutant sequences to fold into the stable and well-folded structures adopted by the wild type sequences. As a consequence, the partially-folded or highly disordered mutants with many hydrophobic side chains exposed can only be dissolved in salt-free water but not in buffers mimicking the physiological condition. Additionally, we have also rationalize the previous observations *in vivo* and strongly imply the interplay of the signaling networks associated with Eph and FFAT-containing proteins may play a key role in ALS pathogenesis.

In future, it will be interesting to delineate the interaction of play between FFAT-motif containing proteins, EphA4 and MSP domain in *vivo* studies. Although crystallization trials have failed so far, continued efforts to screen using more diverse crystallization conditions might yield favorable results. It is also interesting to note that although the hanging drops consisted of EphA4 and VAPB MSP domain mixed in a 1:1 ratio at high concentration with homogenous purity, only EphA4 had aggregated into

crystals. It is worth to diffract this free EphA4 crystal grown in the presence of the MSP domain. In addition, we could also harness the information gathered form NMR titration experiments to construct a model of the EphA4-MSP complex using HADDOCK.

Chapter 4

Effects of Proline substitutions in VAPB (P56S)

As mentioned, other than Pro-63 in the VCS of VAPA MSP domain, two other prolines at position 13 and 97 were also substituted in wt-VAPB (Figure 19a). Here, the substitutions of Gln-13, Ala-63 and Thr-97 to a Proline residue were investigated to see if it would affect the structural characteristics of VAPB (P56S). To achieve this, recombinant VAPB (Q13P, P56S); VAPB (P56S, A63P); VAPB (Q13P , T97P); VAPB (Q13P , P56S, A63P,) and VAPA (P56S) MSP domain (1-125) was cloned, expressed and purified using a prokaryotic system under the native condition. Except for VAPA (P56S) which was highly soluble in the buffer systems (5mM phosphate 1mM DTT pH6.5) we used, all the other mutants were prone to aggregation at high concentration (~100uM) and temperature. CD and NMR spectroscopy was utilized to study its structural properties.

4.1. Effects of Proline substitutions on the structural characteristics of VAPB (P56S)

As shown in Figure 5a, at pH 6.5, the Far-UV CD spectroscopy of VAPB (P56S) showed a spectrum with a prominent single negative band at ~215nm but no positive signal at ~199nm. At this pH, the sample is heavily precipitated and light scattering which results from these particles causes anomalies in the circular dichroism spectra (Litman, 1972). Also no HSQC peaks could be detected at pH6.5. Henceforth we suggested that the CD spectra of VAPB (P56S) at pH 6.5 was probably an artifact of aggregated sample and hence was not used for comparison with the rest of the mutants.

In figure 19b, the Far-UV CD spectroscopy of VAPB (Q13P, P56S, A63P, T97P) showed a spectrum which clearly resembles that of wt-VAPB with the maximal negative signal at ~218 nm and positive signal at ~199 nm. The intensity of the positive signal at ~199 is also lower as compared to wt-VAPB. In contrast, the substitution of a single

Proline in the VAPB (Q13P, P56S); VAPB (P56S, A63P) and VAPB (Q13P, T97P)

mutants showed a spectra which is similar to each other but are distinctly different from

wt-VAPB and VAPB (Q13P, P56S, A63P, T97P). This implies that probably all 3 prolines

are required to be introduced back into VAPB (P56S) in order to recover its native

structure. Nevertheless, as indicated by a reduced positive signal at ~199nm, this

restoration of native structure is incomplete and the protein may still be unfolded to some

degree.
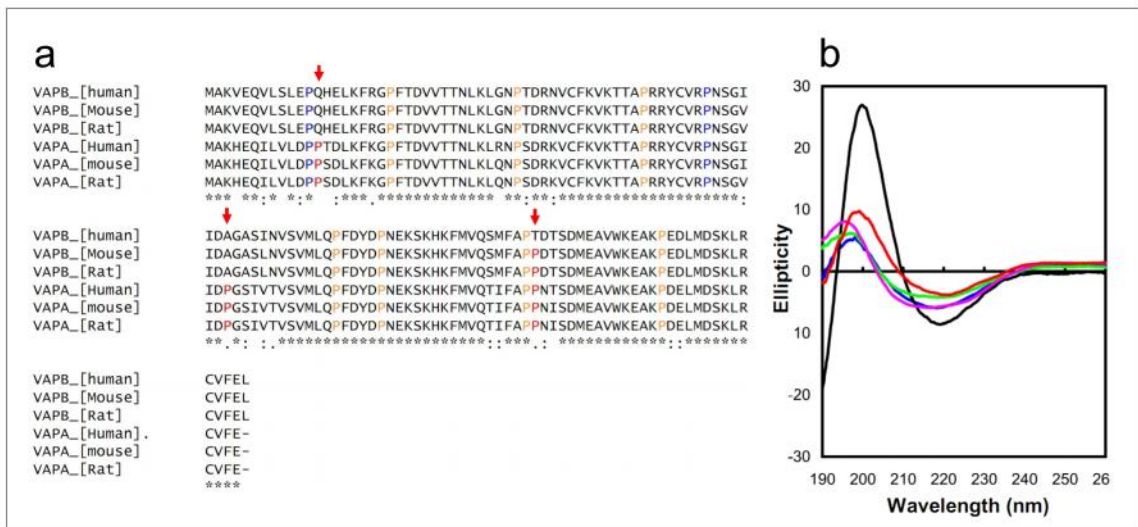
Figure 19. Structural characterization of the Proline mutants
a. Multiple sequence alignment of the MSP domain of VAPA and VAPB from mouse, rat and human. Red arrows are used to point to location on the MSP domain where a difference in Proline distribution is identified. Proline residues in Blue refer to those that contribute to the S-shape loop i.e. Pro12 and Pro56. Residues in orange refer to those which are conserved. b. Far UV CD spectra of the MSP domain mutants of wt-VAPB (Black); VAPB (Q13P, P56S) (Blue); VAPB (P56S, A63P) (Green)); VAPB (P56S, T97P) (Magenta) and VAPB (Q13P, P56S, A63P, T97P) (Red).

NMR spectroscopy was also utilized to study the effect of Proline substitution on

the structural characteristics of P56S-VAPB. As seen in figure 20a-d, the mutants have a

HSQC spectrum characteristic of a well folded protein with a wide dispersion over the ^{1}H

and ^{15}N dimensions. Interestingly, many HSQC peaks of the mutants are also

superimposable to those of wt-VAPB, implying that the mutants might have a

conformational ensemble similar to that of wt-VAPB. The numbers of peaks in the HSQC

spectrum of all the mutants were also greater than expected from the amino acid sequence of the MSP domain. In addition, obvious line-broadenings were also observed in all spectra.
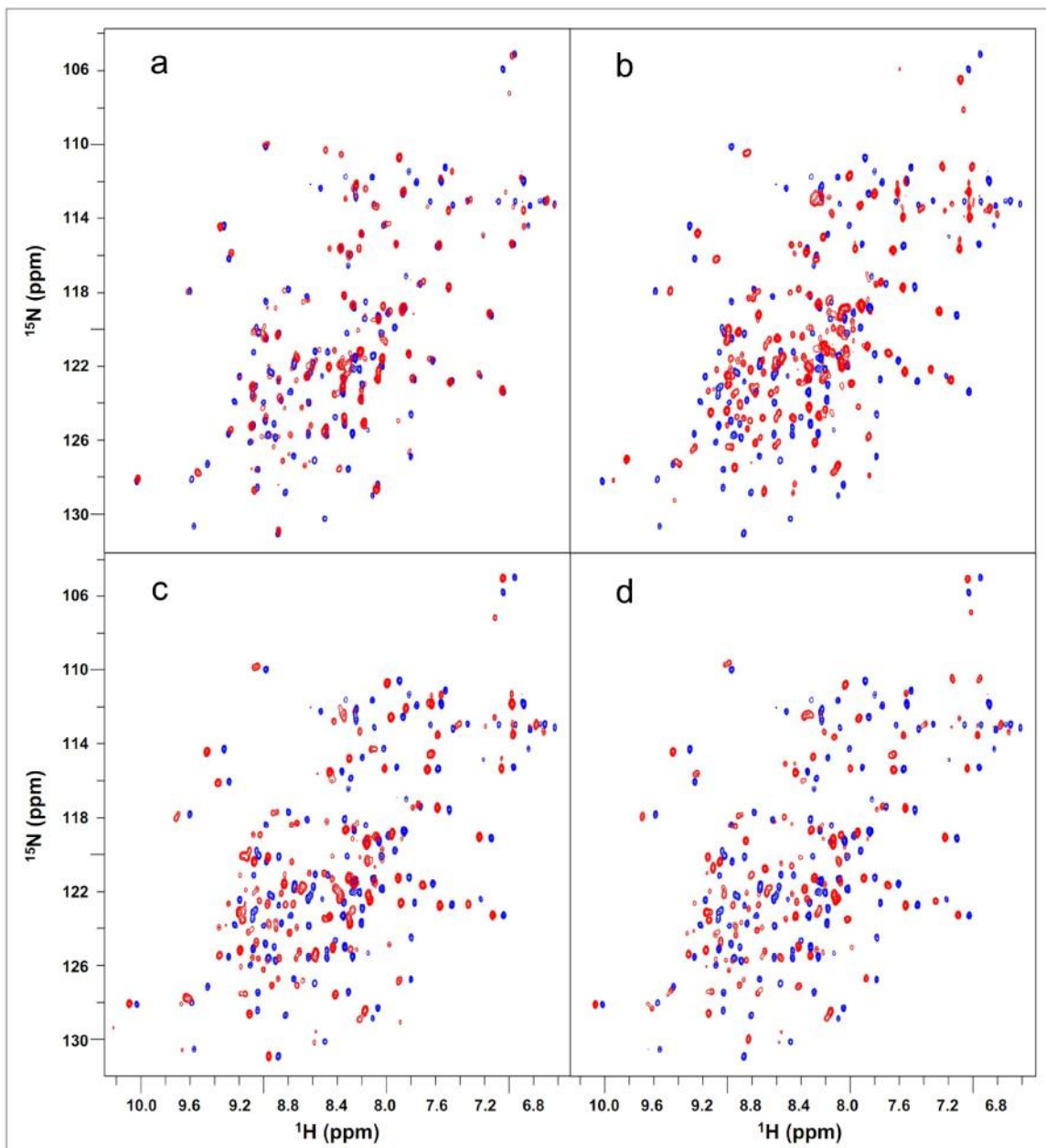
Figure 20. Structural consequence of introducing Proline residues to VAPB (P56S)
a. $^1H,^{15}N$ HSQC spectra of the MSP domain VAPB (Q13P, P56S) (red) and wt-VAPB (Blue). b. $^1H,^{15}N$ HSQC spectra of the MSP domain VAPB (P56S, A63P) (red) and wt-VAPB (Blue). c. $^1H,^{15}N$ HSQC spectra of the MSP domain VAPB (P56S, T97P) (red) and wt-VAPB (Blue). d. $^1H,^{15}N$ HSQC spectra of the MSP domain VAPB (Q13P, P56S, A63P, T97P) (red) and wt-VAPB (Blue)
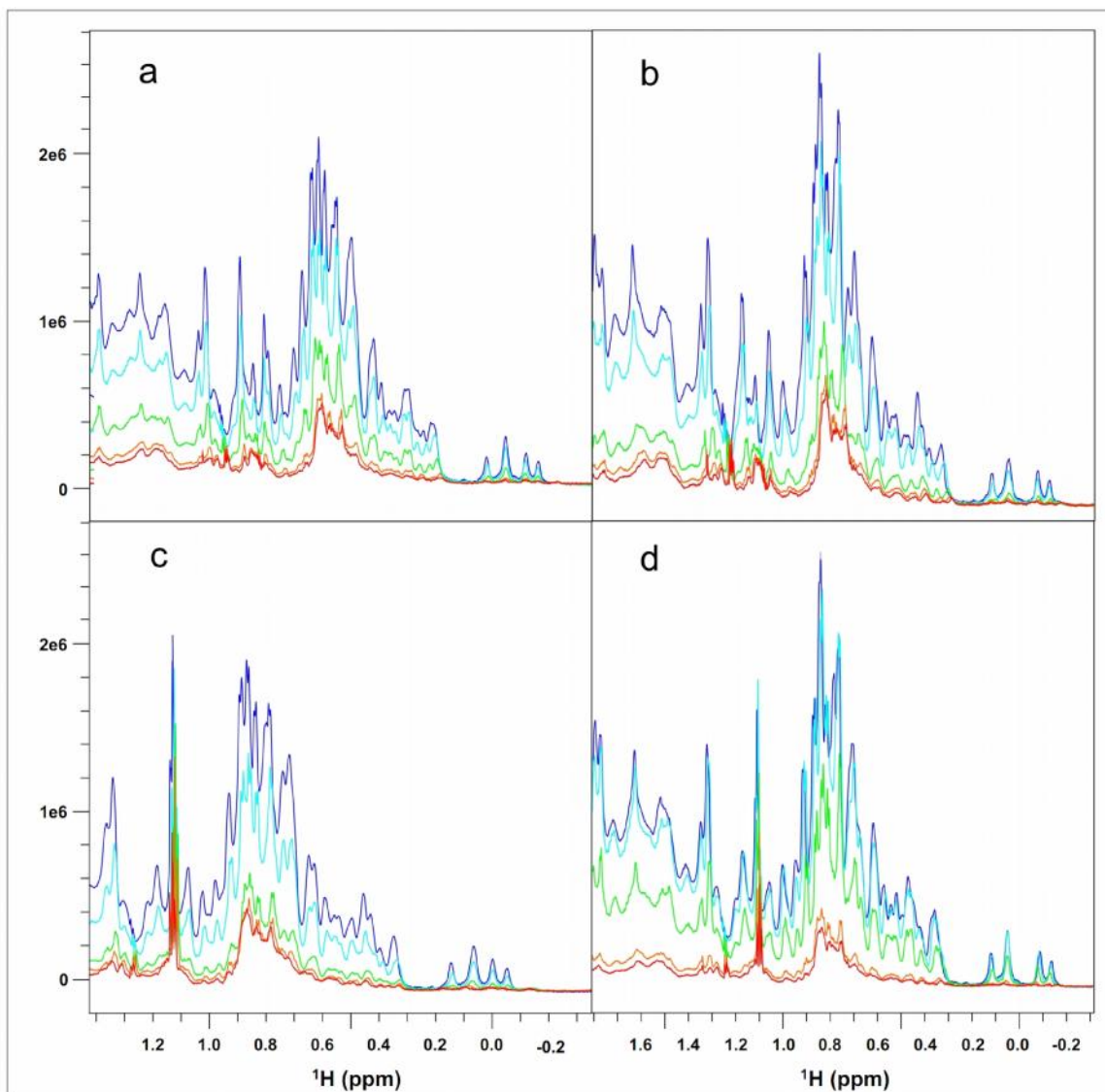
Figure 21. Thermodynamic stability of VAPB (T46I) MSP domain
a. Superimposition of the 1D spectrum of the VAPB (Q13P, P56S) at 25° (Blue) , 30°C (Cyan), 35°C (Green), 40°C (Orange) and 45°C (Red). b. Superimposition of the 1D spectrum of the VAPB (P56S, A63P) at 25° (Blue) , 30°C (Cyan), 35°C (Green), 40°C (Orange) and 45°C (Red). c. Superimposition of the 1D spectrum of the VAPB (P56S, T97P) at 25° (Blue) , 30°C (Cyan), 35°C (Green), 40°C (Orange) and 45°C (Red). d. Superimposition of the 1D spectrum of the VAPB (Q13P, P56S, A63P, T97P) at 25° (Blue) , 30°C (Cyan), 35°C (Green), 40°C (Orange) and 45°C (Red).

4.2. Effects of Proline substitution on the stability of VAPB (P56S)

Next, the effect of temperature on the stability of all the different mutants was explored. Strikingly, as shown in Figure 21a-d, the 1D spectrum showed drastic line broadening and intensity dipped starting at 30°C for the mutants with a single Proline substitution. On the other hand, VAPB (Q13P, P56S, A63P, T97P) starts to aggregate

75

only after 35°C and VAPA (P56S) at 40°C (figure 22). This indicates that although the substitution of Proline residues into VAPB (P56S) makes it more stable and tolerable to aggregation at high temperature, there are also certain other critical residues in VAPA which are more crucial in maintaining stability.
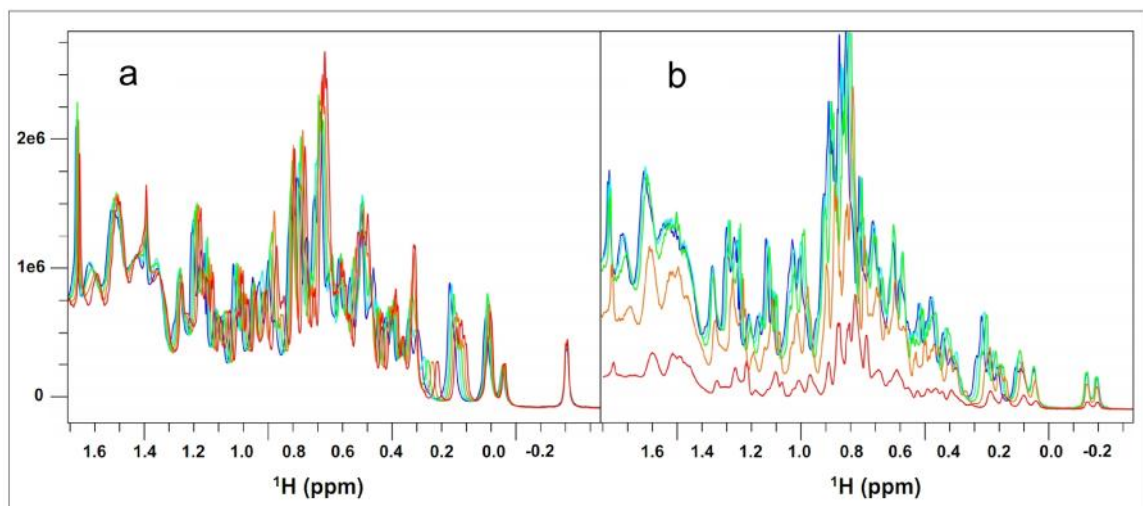
Figure 22. Thermodynamic stability of wt-VAPA and VAPA (P56S)
a. Superimposition of the 1D spectrum of the MSP domain of wt-VAPA at 25° (Blue) , 30°C (Cyan), 35°C (Green), 40°C (Orange) and 45°C (Red). b. Superimposition of the 1D spectrum of the VAPA (P56S) at 25° (Blue) , 30°C (Cyan), 35°C (Green), 40°C (Orange) and 45°C (Red).

4.3. Effects of Proline substitution on the binding ability of VAPB (P56S)

Since the introduction of additional Proline residues have prevented P56S from abolishing the native state of VAPB MSP domain, it is interesting to see if it had restored its ability to bind the FFAT motif containing Nir2 peptide as well. Hence the thermodynamic parameters for the binding between the various Proline mutants and the FFAT-containing motif of the Nir2 protein were measured by ITC (Figure 23). The VAPB (Q13P, P56S, A63P, T97P) mutant is able to bind the FFAT-motif containing Nir2 peptide, with a dissociation constant (K_D) of 1.75 µM. Additionally, VAPB (P56S, A63P) and VAPB (P56S, T97P) also bind but with weaker affinity at 4.27uM and 4.78uM respectively. Strangely, although we have suggested that a single Proline addition to

76
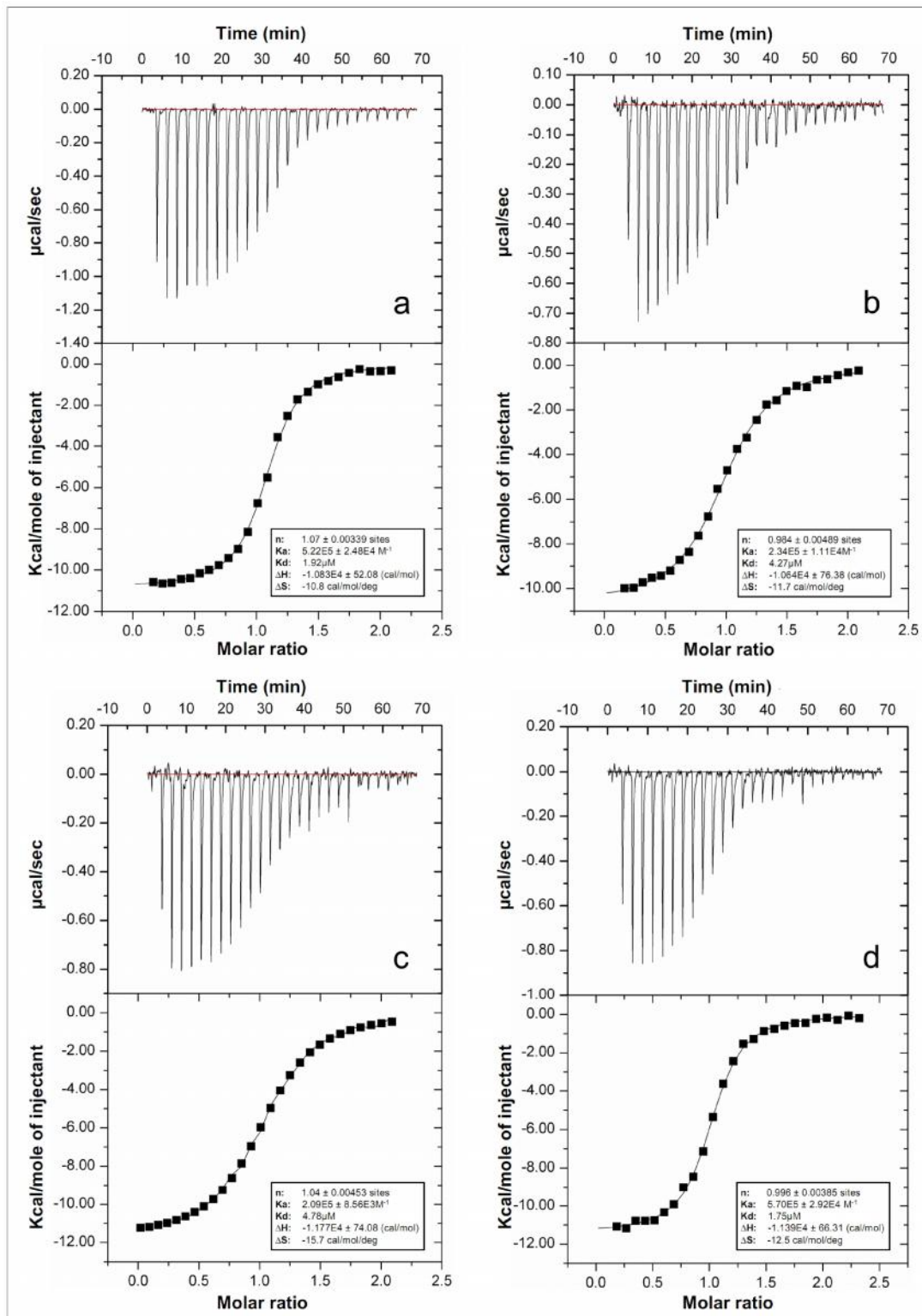
Figure 23. Activity of the Proline mutants

The ITC titration profiles of the binding reaction of (a) VAPB (Q13P, P56S); (b) VAPB (P56S, A63P); (c) VAPB (P56S, T97P) and (d) VAPB (Q13P, P56S, A63P, T97P) to the FFAT-motif containing peptide derived from Nir2 (upper panel); and integrated values for reaction heats with subtraction of the corresponding blank results normalized by the amount of ligand injected versus molar ratio of MSP/FFAT (lower panel). The thermodynamic binding parameters obtained from fitting the data are shown in the box.

77

VAPB (P56S) might not restore the native state of wt-VAPB MSP domain as much as an addition of 3 Proline residues would, VAPB (Q13P, P56S) binds with an affinity of 1.92uM which is comparable to that of VAPB (Q13P, P56S, A63P, T97P).

4.4. Discussions, conclusion and future directions

The mis-sense mutation of Proline-56 to Serine in the MSP domain of VAPB causes ALS8. In contrast, its isoform, VAPA is not significantly affected by the same mutation. Last year, Nakamichi *et al*., (2010) had demonstrated that it was the existence of Pro-63 that confers VAPA the resistance to the pathogenic Pro56Ser mutation. Intuitively, they went on to investigate if the addition of Pro-63 has the same effect on VAPB (P56S). However, they found that the localization of VAPB (P56S, A63P) was similar to that of VAPB (P56S) and different from that of VAPA (P56S). They thus suggested that another factor(s) other than Proline distribution in the VCS is required for proper localization of VAPB.

Through the alignment of the different isoforms of VAPA and VAPB (figure 19a), we realized that other than Pro-63 in the VCS of the MSP domain, two other prolines at position 13 and 97 were also substituted in wt-VAPB. We have demonstrated that although VAPB (P56S, A63P) has a native secondary and tertiary structure, it is still thermodynamically unstable. As compared to VAPB (T46I) and VAPA (P56S) which starts to precipitate at ~40°C, VAPB (P56S, A63P) precipitates at ~30°C as indicated by the change of the up field peaks in the one-dimensional NMR proton spectra (figure 12, 21b and 22b). This significantly reduce stability, consequently caused the VAPB (P56S, A63P) MSP domain to be prone to aggregation at high protein concentrations and temperatures in *vitro*, which may become more severe in cellular environments resulting

in improper localization as observed by Nakamichi *et al*., (2010). The effects are similar for VAPB (Q13P, P56S) and VAPB (P56S, T97P). Interestingly, the addition of three prolines in VAPB (Q13P, P56S, A63P, T97P) confers increased thermodynamic stability to the mutant MSP mutant as compared to those which had one additional Proline.

Our study also demonstrated for the first time that the addition of Prolines to VAPB (P56S) restored its ability to bind to FFAT-motif containing Nir2 peptide. Intriguingly, while the VAPB (P56S, A63P) - and VAPB (P56S, T97P) - MSP domain has a lower binding affinity to the FFAT-motif containing Nir2 peptide, VAPB (P56S, Q13P) bind to the Nir2 peptide as tightly as the MSP domain of VAPB (Q13P, P56S, T97P). Further studies have to be done to understand the underlying molecular mechanism. Probably, we could use molecular simulation to model the consequences of the different Proline mutants. Upon close examination of the HSQC of VAPB (P56S, Q13P), we also noticed that the occurrence of repeating resonance peaks were significantly lesser. In future, assignment of the HSQC peaks might also bring further insights.

In addition, it will be also interesting to investigate the localization of the Proline mutants in yeast models. We could also study the thermodynamic stability and binding ability of mutants which are systemically substituted to increase the identity of VAPB to VAPA. It is hope that the results gathered might further provide valuable insights into which residue is responsible for providing resistance to the P56S mutation and shed light into protein folding

REFERENCES

Anfinsen CB (1973). "Principles that govern the folding of protein chains". Science 181 (96): 223–230

Amos FF, Evans JS. (2009) "AP7, a partially disordered pseudo C-RING protein, is capable of forming stabilized aragonite in vitro". Biochemistry. 48, 1332-9

Armon C (2009) "Smoking may be considered an established risk factor for sporadic ALS". Neurology. 17;73(20):1693-8.

Amarilio, R., Ramachandran, S., Sabanay, H. & Lev, S. (2005) Differential regulation of endoplasmic reticulum structure through VAP-Nir protein interaction. J Biol Chem, 280, 5934-44.

Bruijn LI, Miller TM, Cleveland DW (2004). "Unraveling the mechanisms involved in motor neuron degeneration in ALS". Annu Rev Neurosci. 27:723-49.

Baker AM, Roberts TM, Stewart M. (2002) "2.6 A resolution crystal structure of helices of the motile major sperm protein (MSP) of Caenorhabditis elegans". J Mol Biol 319:491–499.

Borgese, N., Brambillasca, S., and Colombo, S. (2007) How tails guide tail-anchored proteins to their destinations. Curr. Opin. Cell Biol. 19, 368–375

Brosig B, Langosch D. (1998) "The dimerization motif of the glycophorin A transmembrane segment in membranes: importance of glycine residues". *Protein Sci.* **7**(4):1052–1056.

Bertolotti A, Zhang Y, Hendershot LM, Harding HP, Ron D. (2000) Dynamic interaction of BiP and ER stress transducers in the unfolded-protein response. Nat Cell Biol 2:326–332

Bartoszewski R, Rab A, Jurkuvenaite A, Mazur M, Wakefield J, Collawn JF, Bebok Z. (2008) :Activation of the unfolded protein response by F508 CFTR". Am J Respir Cell Mol Biol 39:448–457.

Chen HJ, Anagnostou G, Chai A, Withers J, Morris A, Adhikaree J, Pennetta G, de Belleroche JS (2010). "Characterization of the properties of a novel mutation in VAPB in familial amyotrophic lateral sclerosis". J Biol Chem. 285(51):40266-81.

Chen YZ, Bennett CL, Huynh HM, Blair IP, Puls I, Irobi J, Dierick I, Abel A, Kennerson ML, Rabin BA, Nicholson GA, Auer-Grumbach M, Wagner K, De Jonghe P, Griffin JW, Fischbeck KH, Timmerman V, Cornblath DR, Chance PF. (2004) "DNA/RNA helicase gene mutations in a form of juvenile amyotrophic lateral sclerosis (ALS4)". Am J Hum Genet. 74(6):1128-35.

Chai A, Withers J, Koh YH, Parry K, Bao H, Zhang B, Budnik V, Pennetta G. (2008) "hVAPB, the causative gene of a heterogeneous group of motor neuron diseases in humans, is functionally interchangeable with its Drosophila homologue DVAP-33A at the neuromuscular junction" Hum Mol Genet. 17(2):266-80.

Cheung, M. S., Maguire, M. L., Stevens, T. J., and Broadhurst, R. W. (2010) "DANGLE: A Bayesian inferential method for predicting protein backbone dihedral angles and secondary structure." J. Magn. Reson. 202, 223– 233

Calò L, Cinque C, Patanè M, Schillaci D, Battaglia G, Melchiorri D, Nicoletti F, Bruno V. (2006) "Interaction between ephrins/Eph receptors and excitatory amino acid receptors: possible relevance in the regulation of synaptic plasticity and in the pathophysiology of neuronal degeneration". J Neurochem. 98(1):1-10.

Carette, J. E., Verver, J., Martens, J., Van Kampen, T., Wellink, J. & Van Kammen, A. (2002) Characterization Of Plant Proteins That Interact With cowpea mosaic virus '60K' protein in the yeast two-hybrid system. J Gen Virol, 83, 885-93.

Delak K, Harcup C, Lakshminarayanan R, Sun Z, Fan Y, Moradian-Oldak J, Evans JS. (2009) "The Tooth Enamel Protein, Porcine Amelogenin, Is an Intrinsically Disordered Protein with an Extended Molecular Configuration in the Monomeric Form Biochemistry". 48, 2272-2281.

Delak K, Collino S, Evans JS (2009) "Polyelectrolyte Domains and Intrinsic Disorder within the Prismatic Asprich Protein Family" Biochemistry 48, 3669-3677.

Dupuis L, Corcia P, Fergani A, Gonzalez De Aguilar JL, Bonnefont-Rousselot D, Bittar R, Seilhean D, Hauw JJ, Lacomblez L, Loeffler JP, Meininger V. (2008) "Dyslipidemia is a protective factor in amyotrophic lateral sclerosis". Neurology. 70(13):1004-9.

Ellgaard L, Molinari M, Helenius A. (1999) Setting the standards: quality control in the secretory pathway. Science 286:1882–1888

Elena B. Pasquale (2010) "Eph receptors and ephrins in cancer: bidirectional signalling and beyond". Nature Reviews Cancer 10, 165-180

Ettayebi, K. & Hardy, M. E. (2003) "Norwalk virus nonstructural protein p48 forms a complex with the SNARE regulator VAP-A and prevents cell surface expression of vesicular stomatitis virus G protein". J Virol, 77, 11790-7.

Emmanouilidou E, Melachroinou K, Roumeliotis T, Garbis SD, Ntzouni M, Margaritis LH, Stefanis L, Vekrellis K. (2010) "Cell-produced alpha-synuclein is secreted in a calcium-dependent manner by exosomes and impacts neuronal survival". J Neurosci. 30(20):6838-51.

Foster LJ, Klip A. (2000) "Mechanism and regulation of GLUT-4 vesicle fusion in muscle and fat cells". Am J Physiol Cell Physiol. 279(4):C877-90.

Feldman DE, Chauhan V, Koong AC. (2005) "The unfolded protein response: a novel component of the hypoxic stress response in tumors". Mol Cancer Res 3:597–605

Furuita K., Jee J., Fukada H., Mishima M. and Kojima C. (2010) "Electrostatic interaction between oxysterol-binding protein and VAMP-associated protein A revealed by NMR and mutagenesis Studies". J. Biol. Chem. 285, 12961–12970.

Furby A, Beauvais K, Kolev I, Rivain JG, Sébille V. (2010) "Rural environment and risk factors of amyotrophic lateral sclerosis: a case-control study". J Neurol. 257(5):792-8.

Greenway MJ, (2004)Alexander MD, Ennis S, Traynor BJ, Corr B, Frost E, Green A, Hardiman O. "A novel candidate region for ALS on chromosome 14q11.2". Neurology. 63:1936–1938.

Greenway MJ, Andersen PM, Russ C, Ennis S, Cashman S, Donaghy C, Patterson V, Swingler R, Kieran D, Prehn J, et al. (2006) "ANG mutations segregate with familial and 'sporadic' amyotrophic lateral sclerosis". Nat Genet. 38:411–413.

Gass JN, Gifford NM, Brewer JW. (2002) "Activation of an unfolded protein response during differentiation of antibody-secreting B cells". J Biol Chem 277(50):49047-54.

Gkogkas C, Middleton S, Kremer AM, Wardrope C, Hannah M, Gillingwater TH, Skehel P. (2008) "VAPB interacts with and modulates the activity of ATF6". Hum Mol Genet. 17(11):1517-26.

Gupta, R., Yadav, S., and Ahmad, F. (1996) Protein stability: Urea-induced versus guanidine induced unfolding of metmyoglobin Biochemistry 35, 11925– 11930

Gong, Y., Lee, J. N., Brown, M. S., Goldstein, J. L. & Ye, J. (2006) Juxtamembranous aspartic acid in Insig-1 and Insig-2 is required for cholesterol homeostasis. Proc Natl Acad Sci U S A, 103, 6154-9.

Gougeon, P. Y. & Ngsee, J. K. (2005) Purification and functional properties of prenylated Rab acceptor 2. Methods Enzymol, 403, 799-807.

Gavin, A. C., Bosche, M., Krause, R., Grandi, P., Marzioch, M., Bauer, A., Schultz, J., Rick, J. M., Michon, A. M., Cruciat, C. M., Remor, M., Hofert, C., Schelder, M., Brajenovic, M., Ruffner, H., Merino, A., Klein, K., Hudak, M., Dickson, D., Rudi, T., Gnau, V., Bauch, A., Bastuck, S., Huhse, B., Leutwein, C., Heurtier, M. A., Copley, R. R., Edelmann, A., Querfurth, E., Rybin, V., Drewes, G., Raida, M., Bouwmeester, T., Bork, P., Seraphin, B., Kuster, B., Neubauer, G. & Superti-Furga, G. (2002) Functional organization of the yeast proteome by systematic analysis of protein complexes. Nature, 415, 141-7.

Hadano S, Hand CK, Osuga H, Yanagisawa Y, Otomo A, Devon RS, Miyamoto N, Showguchi-Miyata J, Okada Y, Singaraja R,Figlewicz DA, Kwiatkowski T, Hosler BA, Sagie T, Skaug J, Nasir J, Brown RH Jr, Scherer SW, Rouleau GA, Hayden MR, Ikeda JE. (2001) "A gene encoding a putative GTPase regulator is mutated in familial amyotrophic lateral sclerosis 2". Nat Genet. 29(2):166-73.

Hadano, S., Benn, S. C., Kakuta, S., Otomo, A., Sudo, K., Kunita, R., Suzuki-Utsunomiya, K., Mizumura, H., Shefner, J. M., Cox, G. A., Iwakura, Y., Brown, R. H., Jr., Ikeda, J.-E. (2006) "Mice deficient in the Rab5 guanine nucleotide exchange factor ALS2/alsin exhibit age-dependent neurological deficits and altered endosome trafficking. Hum". Molec. Genet. 15: 233-250

Hamamoto, I., Nishimura, Y., Okamoto, T., Aizaki, H., Liu, M., Mori, Y., Abe, T., Suzuki, T., Lai, M.M., Miyamura, T., Moriishi, K., Matsuura, Y. (2005) "Human VAP-B is involved in hepatitis C virus replication through interaction with NS5A and NS5B". J. Virol. 79(21):13473-82

Hoozemans JJ, Stieler J, van Haastert ES, Veerhuis R, Rozemuller AJ, Baas F, Eikelenboom P, Arendt T, Scheper W. (2006) "The unfolded protein response affects neuronal cell cycle protein expression: implicatios for Alzheimer's disease pathogenesis". Exp Gerontol. 41(4):380-6. Epub 2006 Mar 27.

Hirano M, Hung WY, Cole N, Azim AC, Deng HX, Siddique T. (2000) "Multiple transcripts of the human Cu,Zn superoxide dismutase gene". Biochem Biophys Res Commun. 276(1):52-6.

Honig LS, Chambliss DD, Bigio EH, Carroll SL, Elliott JL. (2000) "Glutamate transporter EAAT2 splice variants occur not only in ALS, but also in AD and controls" Neurology. 55(8):1082-8. 26

Haaf A, LeClaire L 3rd, Roberts G, Kent HM, Roberts TM, Stewart M, Neuhaus D. (1998) "Solution structure of the motile major sperm protein (MSP) of Ascaris suum – evidence for two manganese binding sites and the possible role of divalent cations in filament formation". J. Mol. Biol. 284, 1611–1624

Harding HP, Novoa I, Zhang Y, Zeng H, Wek R, Schapira M, Ron D. (2000) "Regulated translation initiation controls stress-induced gene expression in mammalian cells". Mol Cell 6:1099–1108

Harding HP, Zhang Y, Ron D. (1999) "Protein translation and folding are coupled by an endoplasmic-reticulum-resident kinase". Nature 397:271–274

Holthuis JC, Levine TP. (2005) Lipid traffic: floppy drives and a superhighway. Nat Rev Mol Cell Biol 6, 209 –220.

Hanada, K., Kumagai, K., Tomishige, N. & Kawano, M. (2007) CERT and intracellular trafficking of ceramide. Biochim Biophys Acta, 1771, 644-53.

Ito D, Suzuki N (2009) "Seipinopathy: a novel endoplasmic reticulum stress-associated disease". Brain 132(1):8–15

Isler JA, Skalet AH, Alwine JC. (2005) "Human cytomegalovirus infection activates and regulates the unfolded protein response". J Virol 79

Ilieva H., Polymenidou M., Cleveland D. W.(2009) "Non-cell autonomous toxicity in neurodegenerative disorders: ALS and beyond". J. Cell Biol. 187, 761–772

Litman BJ. (1972) "Effect of light scattering on the circular dichroism of biological membranes". Biochemistry. 15;11(17):3243-7. [37]

Iwamasa H, Ohta K, Yamada T, Ushijima K, Terasaki H, Tanaka H. (1999) "Expression of Eph receptor tyrosine kinases and their ligands in chick embryonic motor neurons and hindlimb muscles". Dev Growth Differ. 41(6):685-98.

Kwiatkowski TJ Jr, Bosco DA, Leclerc AL, Tamrazian E, Vanderburg CR, Russ C, Davis A, Gilchrist J, Kasarskis EJ, Munsat T, Valdmanis P, Rouleau GA, Hosler BA, Cortelli P, de Jong PJ, Yoshinaga Y, Haines JL, Pericak-Vance MA, Yan J, Ticozzi N, Siddique T, McKenna-Yasek D, Sapp PC, Horvitz HR, Landers JE, Brown RH Jr. (2009) "Mutations in the FUS/TLS gene on chromosome 16 cause familial amyotrophic lateral sclerosis". Science. 323(5918):1205-8.

Kabashi E, Valdmanis PN, Dion P, Spiegelman D, McConkey BJ, Velde C Vande, Bouchard JP, Lacomblez L, Pochigaeva K, Salachas F, et al. (2008) "TARDBP mutations in individuals with sporadic and familial amyotrophic lateral sclerosis". Nat Genet .40:572–574.

Kukihara H, Moriishi K, Taguwa S, Tani H, Abe T, Mori Y, Suzuki T, Fukuhara T, Taketomi A, Maehara Y, Matsuura Y. (2009) "Human VAP-C negatively regulates hepatitis C virus propagation". J Virol.83 (16):7959-69.

Kaiser SE, Brickner JH, Reilein AR, Fenn TD, Walter P, Brunger AT. (2005) Structural basis of FFAT motif mediated ER targeting. Structure 13:1035–1045.

Kim S, Leal SS, Ben Halevy D, Gomes CM, Lev S. (2010) "Structural requirements for VAP-B oligomerization and their implication in amyotrophic lateral sclerosis-associated VAP-B(P56S) neurotoxicity". J Biol Chem. 285(18):13839-49

Kohno K (2007) ""How transmembrane proteins sense endoplasmic reticulum stress". Antioxid Redox Signal 9:2295–2303

Kanekura K, Nishimoto I, Aiso S, Matsuoka M. (2006) Characterization of amyotrophic lateral sclerosis-linked P56S mutation of vesicle-associated membrane protein-associated protein B (VAPB/ALS8). J Biol Chem. 281(40):30223-33.

Kawano, M., Kumagai, K., Nishijima, M. & Hanada, K. (2006) Efficient trafficking of ceramide from the endoplasmic reticulum to the Golgi apparatus 180 requires a VAMP-associated protein-interacting FFAT motif of CERT. J Biol Chem, 281, 30279-88.

Levinthal, Cyrus (1968). "Are there pathways for protein folding?" *Journal de Chimie Physique et de Physico-Chimie Biologique* **65**: 44–45.

Lapierre LA, Tuma PL, Navarre J, Goldenring JR, Anderson JM. (1999) "VAP-33 localizes to both an intracellular vesicle population and with occludin at the tightjunction". J Cell Sci. 112 (Pt 21):3723-32.

Lipson KL, Fonseca SG, Ishigaki S, Nguyen LX, Foss E, Bortell R, Rossini AA, Urano F. (2006) "Regulation of insulin biosynthesis in pancreatic beta cells by an endoplasmic reticulum-resident protein kinase IRE1". Cell Metab 4:245–254

Lee AS (1992) Mammalian stress response: induction of the glucose-regulated protein family. Curr Opin Cell Biol 4:267–273

Lai KO, Ip FC, Cheung J, Fu AK, Ip NY.(2001) " Expression of Eph receptors in skeletal muscle and their localization at the neuromuscular junction". Mol Cell Neurosci. 17(6):1034-47.

Loewen, C. J. & Levine, T. P. (2005) A highly conserved binding site in vesicle associated membrane protein-associated protein (VAP) for the FFAT motif of lipid-binding proteins. J Biol Chem, 280, 14097-104.

Loewen, C. J., Roy, A. & Levine, T. P. (2003) A conserved ER targeting motif in three families of lipid binding proteins and in Opi1p binds VAP. Embo J, 22, 2025-35.

Lev, S., Ben Halevy, D., Peretti, D. & Dahan, N. (2008) The VAP protein family: from cellular functions to motor neuron disease. Trends Cell Biol, 18, 282-90.

Levine T, Loewen C (2006) Inter-organelle membrane contact sites: through a glass, darkly. Curr Opin Cell Biol 18, 371–378.

Meininger V (2011). "ALS, what new 144 years after Charcot?" Arch Ital Biol. (1):29-37.

Momeni, P., Rogaeva, E., Van Deerlin, V., Yuan, W., Grafman, J., Tierney, M., Huey, E., Bell, J., Morris, C. M., Kalaria, R. N., van Rensburg, S. J., Niehaus, D., Potocnik, F., Kawarai, T., Salehi-Rad, S., Sato, C., St. George-Hyslop, P., Hardy, J. (2006) "Genetic variability in CHMP2B and frontotemporal dementia". Neurodegener. Dis. 3: 129-133.

Munch C, Sedlmeier R, Meyer T, Homberg V, Sperfeld AD, Kurt A, Prudlo J, Peraus G, Hanemann CO, Stumm G, Ludolph AC.(2004) "Point mutations of the p150 subunit of dynactin (DCTN1) gene in ALS". Neurology. 63:724–726.

Magal E, Holash JA, Toso RJ, Chang D, Lindberg RA, Pasquale EB. (1996) "B61, a ligand for the Eck receptor protein-tyrosine kinase, exhibits neurotrophic activity in cultures of rat spinal cord neurons". J Neurosci Res 43(6):735-44.

Mitne-Neto M, Machado-Costa M, Marchetto MC, Bengtson MH, Joazeiro CA, Tsuda H, Bellen HJ, Silva HC, Oliveira AS, Lazar M, Muotri AR, Zatz M. "Downregulation of VAPB expression in motor neurons derived from induced pluripotent stem cells of ALS8 patients". Hum Mol Genet. [Epub ahead of print]

Marques VD, Barreira AA, Davis MB, Abou-Sleiman PM, Silva WA Jr, Zago MA, Sobreira C, Fazan V, Marques W Jr. (2006) "Expanding the phenotypes of the Pro56Ser VAPB mutation: proximal SMA with dysautonomia". Muscle Nerve. 34(6):731-9.

Nassif M, Matus S, Castillo K, Hetz C (2010). Amyotrophic lateral sclerosis pathogenesis: a journey through the secretory pathway. Antioxid Redox Signal. (12):1955-89.

Nishimura AL, Mitne-Neto M, Silva HC, Richieri-Costa A, Middleton S, Cascio D, Kok F, Oliveira JR, Gillingwater T, Webb J,Skehel P, Zatz M. (2004) "A mutation in the vesicle-trafficking protein VAPB causes late-onset spinal muscular atrophy and amyotrophic lateral sclerosis". Am J Hum Genet. 75(5):822-31.

Nishimura AL, Al-Chalabi A, Zatz M (2005) "A common founder for amyotrophic lateral sclerosis type 8 (ALS8) in the Brazilian population". Hum. Genet. 118,499–500

Nishimura Y, Hayashi M, Inada H, Tanaka T.. (1999) "Molecular cloning and characterization of mammalian homologues of vesicle-associated membrane protein associated (VAMP-associated) proteins". Biochem. Biophys. Res. Commun. 254, 21–26

Nachreiner T, Esser M, Tenten V, Troost D, Weis J, Krüttgen A. (2010) "Novel splice variants of the amyotrophic lateral sclerosis-associated gene VAPB expressedin human tissues" . Biochem Biophys Res Commun.   394(3):703-8.

Nakamichi S, Yamanaka K, Suzuki M, Watanabe T, Kagiwada S. (2011) "Human VAPA and the yeast VAP Scs2p with an altered proline distribution can phenocopyamyotrophic lateral sclerosis-associated VAPB(P56S)". Biochem Biophys Res Commun. 404(2):605-9

Oyadomari S, Mori M (2004) Roles of CHOP/GADD153 in endoplasmic reticulum stress. Cell Death Diff 11:381–389

Olkkonen VM. (2004) Oxysterol binding protein and its homologues: new regulatory factors involved in lipid metabolism. Curr Opin Lipidol. 15, 321–327.

Pasinelli P, Brown RH. (2006) "Molecular biology of amyotrophic lateral sclerosis: insights from genetics". Nat Rev Neurosci. 7(9):710-23. 1.

Parkinson, N., Ince, P. G., Smith, M. O., Highley, R., Skibinski, G., Andersen, P. M., Morrison, K. E., Pall, H. S., Hardiman, O., Collinge, J., Shaw, P. J., Disher, E. M. C., MRC Proteomics in ALS Study and the FReJA Consortium (2006) "ALS phenotypes with mutations in CHMP2B (charged multivesicular body protein 2B)". Neurology 67: 1074-1077.

Puls I, Jonnakuty C, LaMonte BH, Holzbaur EL, Tokito M, Mann E, Floeter MK, Bidus K, Drayna D, Oh SJ, et al. (2003) "Mutant dynactin in motor neuron disease". Nat Genet. 33:455–456

Pennetta G, Hiesinger PR, Fabian-Fine R, Meinertzhagen IA, Bellen HJ. (2002) "Drosophila VAP-33A directs bouton formation at neuromuscular junctions in a dosage-dependent manner". Neuron. 35(2):291-306.

Perry RJ, Ridgway ND. (2006) Oxysterol-binding protein and vesicleassociated membrane protein-associated protein are required for steroldependent activation of the ceramide transport protein. Mol Biol Cell 17, 2604 –2616.

Prosser DC, Tran D, Gougeon PY, Verly C, Ngsee JK. (2008) FFAT rescues VAPA-mediated inhibition of ER-to-Golgi transport and VAPB-mediated ER aggregation. J Cell Sci. 121(Pt 18):3052-61.

Qin H, Noberini R, Huan X, Shi J, Pasquale EB, Song J. (2010) "Structural characterization of the EphA4-Ephrin-B2 complex reveals new features enabling Eph-ephrin binding promiscuity". J Biol Chem. 285(1):644-54

Rosen DR, Siddique T, Patterson D, Figlewicz DA, Sapp P, Hentati A, Donaldson D, Goto J, O'Regan JP, Deng HX, et al. (1993). "Mutations in Cu/Zn superoxide dismutase gene are associated with familial amyotrophic lateral sclerosis". Nature 362(6415):59-62.

Russ, W. P. & Engelman, D. M. (2000). "The GxxxG motif: a framework for transmembrane helix-helix association". J. Mol. Biol. 296, 911–919

Ricard J, Salinas J, Garcia L, Liebl DJ. (2006) "EphrinB3 regulates cell proliferation and survival in adult neurogenesis". Mol Cell Neurosci 31(4):713-22.

Shaw PJ. (2005). "Molecular and cellular pathways of neurodegeneration in motor neurone disease". J Neurol Neurosurg Psychiatry. 76(8):1046-57.

Sreedharan J, Blair IP, Tripathi VB, Hu X, Vance C, Rogelj B, Ackerley S, Durnall JC, Williams KL, Buratti E, et al. (2008) "TDP-43 mutations in familial and sporadic amyotrophic lateral sclerosis". Science. 319:1668–1672.

Skehel, P., Martin, K., Kandel, E. and Bartsch, D. (1995) "A VAMP binding protein from Aplysia required for neurotransmitter release". Science, 269, 1580–1583

Skehel PA, Fabian-Fine R, Kandel ER. (2000) "Mouse VAP33 is associated with the endoplasmic reticulum and microtubules". Proc Natl Acad Sci U S A. 97(3):1101-6.

Soussan L, Burakov D, Daniels MP, Toister-Achituv M, Porat A, Yarden Y, Elazar Z. (1999) "ERG30, a VAP-33-related protein, functions in protein transport mediated by COPI vesicles". J Cell Biol. 146(2):301-11.

Senes A, Engel DE & DeGrado WF. (2004). "Folding of helical membrane proteins: the role of polar, GxxxG-like and proline motifs". Curr Opin Struct Biol 14, 465-79.

Schubert U, Antón LC, Gibbs J, Norbury CC, Yewdell JW, Bennink JR. (2000) Rapid degradation of a large fraction of newly synthesized proteins by proteasomes. Nature 404:770–774

Suzuki H, Kanekura K, Levine TP, Kohno K, Olkkonen VM, Aiso S, Matsuoka M. (2009) "ALS-linked P56S-VAPB, an aggregated loss-of-function mutant of VAPB, predisposes motor neurons to ER stress-related death by inducing aggregation of co-expressed wild-type VAPB"
J Neurochem 108(4):973-985.

Sutedja NA, Veldink JH, Fischer K, Kromhout H, Heederik D, Huisman MH, Wokke JH, van den Berg LH. (2009) "Exposure to chemicals and metals and risk of amyotrophic lateral sclerosis: a systematic review". Amyotroph Lateral Scler. 10(5-6):302-9.

Saito, S., Matsui, H., Kawano, M., Kumagai, K., Tomishige, N., Hanada, K., Echigo, S., Tamura, S. & Kobayashi, T. (2008) Protein phosphatase 2Cepsilon is an endoplasmic reticulum integral membrane protein that dephosphorylates the ceramide transport protein CERT to enhance its association with organelle membranes. J Biol Chem, 283, 6584-93.

Song J . (2009) Insight into "insoluble proteins" with pure water. FEBS Lett. 18; 583(6):953-9.

Teuling E, Ahmed S, Haasdijk E, Demmers J, Steinmetz MO, Akhmanova A, Jaarsma D, Hoogenraad CC. (2007) "Motor neuron disease-associated mutant vesicle-associated membrane protein-associatedprotein (VAP) B recruits wild-type VAPs into endoplasmic reticulum-derived tubularaggregates". J Neurosci. 27(36):9801-15.

Tsuda H, Han SM, Yang Y, Tong C, Lin YQ, Mohan K, Haueter C, Zoghbi A, Harati Y, Kwan J, Miller MA, Bellen HJ. (2008) "The amyotrophic lateral sclerosis 8 protein VAPB is cleaved, secreted, and acts as a ligand for Eph receptors". Cell. 133(6):963-77.

Tu, H., Gao, L., Shi, S. T., Taylor, D. R., Yang, T., Mircheff, A. K., Wen, Y., Gorbalenya, A. E., Hwang, S. B. & Lai, M. M. (1999) "Hepatitis C virus RNA polymerase and NS5A complex with a SNARE-like protein". Virology, 263, 30-41.

Urano F, Wang X, Bertolotti A, Zhang Y, Chung P, Harding HP, Ron D. (2000) Coupling of stress in the ER to activation of JNK protein kinases by transmembrane protein kinase IRE1. Science 287:664–666

Vance C, Rogelj B, Hortobágyi T, De Vos KJ, Nishimura AL, Sreedharan J, Hu X, Smith B, Ruddy D, Wright P, Ganesalingam J, Williams KL, Tripathi V, Al-Saraj S, Al-Chalabi A, Leigh PN, Blair IP, Nicholson G, de Belleroche J, Gallo JM, Miller CC, Shaw CE. (2009) "Mutations in **FUS**, an RNA processing protein, cause familial amyotrophic lateral sclerosis type 6". Science. 323(5918):1208-11.

Vattem KM and Wek RC. (2004) "Reinitiation involving upstream ORFs regulates ATF4 mRNA translation in mammalian cells". Proc Natl Acad Sci 101:11269–11274

Vranken, W. F., Boucher, W., Stevens, T. J., Fogh, R. H., Pajon, A., Llinas, M., Ulrich, E. L., Markley, J. L., Ionides, J., and Laue, E. D. (2005) "The CCPN data model for NMR spectroscopy: Development of a software pipeline" Proteins 59, 687– 696

Werner ED, Brodsky JL, McCracken AA. (1996) "Proteasome-dependent endoplasmic reticulum-associated protein degradation: an unconventional route to a familiar fate". Proc Natl Acad Sci USA 93:13797–13801

Weir ML, Klip A, Trimble WS. (1998) "Identification of a human homologue of the vesicle-associated membrane protein (VAMP)-associated protein of 33 kDa (VAP-33): a broadly expressed protein that binds to VAMP". Biochem J. 333 (Pt 2):247-51.

WEIR, M. L., XIE, H., KLIP, A. & TRIMBLE, W. S. (2001) "VAP-A binds promiscuously to both v- and tSNAREs". Biochem Biophys Res Commun, 286,616-21.

Wishart, D. S., Bigam, C. G., Yao, J., Abildgaard, F., Dyson, H. J., Oldfield, E., Markley, J. L., and Sykes, B. D. (1995) "1H, 13C and 15N chemical shift referencing in biomolecular NMR" J. Biomol. NMR 6, 135– 140

Wyles, J. P., Mcmaster, C. R. & Ridgway, N. D. (2002) Vesicle-associated membrane protein-associated protein-A (VAP-A) interacts with the oxysterol binding protein to modify export from the endoplasmic reticulum. J Biol Chem, 277, 29908-18.

Wyles, J. P. & Ridgway, N. D. (2004) VAMP-associated protein-A regulates partitioning of oxysterol-binding protein-related protein-9 between the endoplasmic reticulum and Golgi apparatus. Exp Cell Res, 297, 533-47.

Yang Y, Hentati A, Deng HX, Dabbagh O, Sasaki T, Hirano M, Hung WY, Ouahchi K, Yan J, Azim AC, Cole N, Gascon G, Yagmour A, Ben-Hamida M, Pericak-Vance M, Hentati F, Siddique T.(2001) "The gene encoding alsin, a protein with three guanine-nucleotide exchange factor domains, is mutated in a form of recessive amyotrophic lateral sclerosis". Nat Genet. 29(2):160-5.

Yokoseki A, Shiga A, Tan CF, Tagawa A, Kaneko H, Koyama A, Eguchi H, Tsujino A, Ikeuchi T, Kakita A, et al. (2008) "TDP-43 mutation in familial amyotrophic lateral sclerosis". Ann Neurol. 63:538–542.

Ye J, Rawson RB, Komuro R, Chen X, Davé UP, Prywes R, Brown MS, Goldstein JL. (2000) ER stress induces cleavage of membrane-bound ATF6 by the same proteases that process SREBPs. Mol Cell 6:1355–1364

Zinszner H, Kuroda M, Wang X, Batchvarova N, Lightfoot RT, Remotti H, Stevens JL, Ron D. (1998) "CHOP is implicated in programmed cell death in response to impaired function of the endoplasmic reticulum". Genes Dev 12:982–995

Table S1
Primers used for cloning

Primer ID	Sequence 5' to 3'
VAPB	CGCGGATCCATGGCGAAGGTGGAGC
VAPB_ANTI	CCGCTCGAGCAATTCAAACACACATCTAAG
VAPA	CGCGGATCCATGGCGAAGCACGAGCAGATC
VAPA_ANTI	CCGCTCGAGTTATTCATTGGGCATTTCAAATAC
P12A	CTGAGCCTCGAGGCGCAGCACGAGC
P12A_ANTI	GCTCGTGCTGCGCCTCGAGGCTCAG
P56S	GTAGGTACTGTGTGAGGAGCAACAGCGGAATCATCG
P56S_ANTI	CGATGATTCCGCTGTTGCTCCTCACACAGTACCTAC
P12S	CTGAGCCTCGAGTCGCAGCACGAGC
P12S_ANTI	GCTCGTGCTGCGACTCGAGGCTCAG
B_T46I	GTGTGTTTTAAGGTGAAGATTACAGCACCACGTAGGTAC
B_T46I_ANTI	GTACCTACGTGGTGCTGTAATCTTCACCTTAAAACACAC
VAPB_Q13P	GCCTCGAGCCGCCGCACGAGCTCAA
VAPB_Q13P_ANTI	TTGAGCTCGTGCGGCGGCTCGAGGC
VAPB_A63P	CAACAGCGGAATCATCGATCCAGGGGCCTCAATTAATG
VAPB_A63P_ANTI	CATTAATTGAGGCCCCTGGATCGATGATTCCGCTGTTG
VAPB_T97P	CAGTCTATGTTTGCTCCACCTGACACTTCAGATATGG
VAPB_T97P_ANTI	CCATATCTGAAGTGTCAGGTGGAGCAAACATAGACTG

Table S2
Primers used for site directed mutagenesis

Primer ID	Sequence 5' to 3'
B_P12A	CTGAGCCTCGAGGCGCAGCACGAGC
B_P12A_anti	GCTCGTGCTGCGCCTCGAGGCTCAG
B_P12S	CTGAGCCTCGAGTCGCAGCACGAGC
B_P12S_anti	GCTCGTGCTGCGACTCGAGGCTCAG
B_P56S	GTAGGTACTGTGTGAGGAGCAACAGCGGAATCATCG
B_P56S_anti	CGATGATTCCGCTGTTGCTCCTCACACAGTACCTAC
A_P56S	CGCCGGTACTGTGTGAGGAGCAACAGTGGAATTATTGA
A_P56S_anti	TCAATAATTCCACTGTTGCTCCTCACACAGTACCGGCG
B_T46I	GTGTGTTTTAAGGTGAAGATTACAGCACCACGTAGGTAC
B_T46I_ANTI	GTACCTACGTGGTGCTGTAATCTTCACCTTAAAACACAC
B_Q13P	GCCTCGAGCCGCCGCACGAGCTCAA
B_Q13P_ANTI	TTGAGCTCGTGCGGCGGCTCGAGGC
B_T97P	CAGTCTATGTTTGCTCCACCTGACACTTCAGATATGG
B_T97P_ANTI	CCATATCTGAAGTGTCAGGTGGAGCAAACATAGACTG
B_A63P	CAACAGCGGAATCATCGATCCAGGGGCCTCAATTAATG
B_A63P_ANTI	CATTAATTGAGGCCCCTGGATCGATGATTCCGCTGTTG

PUBLICATIONS

Shi J, **<u>Lua S</u>**, Tong JS, Song J. (2010) Elimination of the native structure and solubility of the hVAPB MSP domain by the Pro56Ser mutation that causes amyotrophic lateral sclerosis. Biochemistry. 49(18):3887-97.